Bacteria and Virus Control by Electrochemical Coagulation and Microfiltration

A Dissertation

Presented to

The Faculty of the Department of Civil and Environmental Engineering

In Partial Fulfillment

Of the Requirements for the Degree

Doctor of Philosophy

In Environmental Engineering

By

Charan Tej Tanneru

May 2014

Bacteria and Virus Control by Electrochemical Coagulation and Microfiltration

_____

Charan Tej Tanneru

Approved:

_____

Chair of the Committee
S. Chellam, Professor,
Civil and Environmental Engineering
Chemical and Biomolecular Engineering

Committee Members:

_____

W. G. Rixey, Associate Professor,
Civil and Environmental Engineering

_____

J. D. Rimer, Assistant Professor,
Chemical and Biomolecular Engineering

_____

J. C. Conrad, Assistant Professor,
Chemical and Biomolecular Engineering

_____

R. E. Baltus, Professor,
Chemical and Biomolecular Engineering,
Clarkson University

_____

Suresh K. Khator, Associate Dean,
Cullen College of Engineering

_____

Hanadi S. Rifai, Professor,
Civil and Environmental Engineering
Director, Environmental Engineering
Graduate Program

Acknowledgements

I would like to thank Dr. Shankar Chellam for giving me this opportunity to work in his research group. Numerous conversations I had with him will help me to face different challenges in life. I would like to express my gratitude for training me and teaching me different aspects of my work throughout my doctoral study.

I would like to acknowledge National Science Foundation and United States Bureau of Reclamation for providing support and funding my research work at University of Houston. I would like to thank all my committee members for their invaluable suggestions during my doctoral work. I thank Raju and Vidya for training me with microbiological techniques. I would like to thank my parents, brother, Pavani, Bindu, Khushi, Harish and Sankeerth for continuously encouraging me. Finally, I would like to thank Vijay, Ayu, Nick, Neranga, Pratik and Apeksha for making my doctoral study fun and enjoyable.

Bacteria and Virus Control by Electrochemical Coagulation and Microfiltration

An Abstract

Presented to

The Faculty of the Department of Civil and Environmental Engineering

In Partial Fulfillment

Of the Requirements for the Degree

Doctor of Philosophy

In Environmental Engineering

By

Charan Tej Tanneru

May 2014

Abstract

Bench-scale experiments were performed to evaluate microorganism control by electrochemical coagulation and membrane microfiltration. Natural organic matter (NOM) present in natural waters appears to reduce the effectiveness of iron electrocoagulation pretreatment to microfiltration for MS2 virus control by complexing ferrous ions generated at the sacrificial anode during electrolysis. This inhibits (i) Fe^{2+} oxidation, precipitation, and virus destabilization and (ii) virus inactivation through reactive oxygen species intermediates or by direct interactions with Fe^{2+} ions. In contrast, higher reductions in MS2 virus concentrations were obtained when aluminum was electrochemically added to surface water. Sweep flocculation was the primary virus destabilization mechanism with secondary contributions from charge neutralization. Direct evidence for virus enmeshment in flocs was provided by two independent methods: quantitative elution using beef extract at elevated pH and quantitating fluorescence from labeled viruses. Monotonically increasing adhesion force between viruses immobilized on AFM tips and floc surfaces with increasing electrocoagulant dosage was measured by atomic force microscopy, which was accompanied by decreasing magnitude of the zeta potential ($\rightarrow 0$) and increasing NOM removal. Hence, virus uptake mechanisms also include charge neutralization and hydrophobic interactions with NOM on floc surfaces. Evidence for virus inactivation was also obtained during iron and aluminum electrocoagulation of synthetic water spiked with viruses. Free chlorine was produced during aluminum electrolysis of saline solutions via oxidation of chloride ions, which inactivated MS2 viruses. Capsid protein modifications probed using Fourier transform infrared spectroscopy (FTIR) revealed significant oxidative modification in amide I and II (1700-1500 cm^{-1}) region. Evidence for genome damage was obtained using quantitative real time polymerase chain reaction (q-RT-PCR). Hence,

alterations of capsid proteins and loss of genome structural integrity both contributed to inactivation.

Separate experiments were performed to examine the rejection of spherical silica colloids and viruses as well as capsule-shaped bacteria by clean microfiltration membranes. Modeling efforts (performed by Prof. Ruth Baltus' group at Clarkson University) focused on incorporating the convective hindrance factor for a capsule shaped particle in a cylindrical pore into predictions of the rejection coefficient. Short-term MF experiments were performed at the University of Houston to measure rejection of three Gram negative bacteria, two spherical viruses, and several spherical silica particles by a number of track-etched membranes with near cylindrical pore geometry in a stirred cell before the onset of fouling. Experimental rejections of spherical viruses, and particulate silica and several rod-shaped Gram negative bacteria with aspect ratio from 2 to 5 by clean track-etched membranes were in general agreement with theoretical predictions.

Table of Contents

List of Figures

List of Tables

Chapter 1. Background and Research Objectives

1.1 Background

This research focuses on microorganism control by electrochemical treatment and microfiltration (MF). It has two specific parts: (i) elucidating mechanisms that facilitate virus control during electrocoagulation and electroflotation and (ii) investigating microorganism (bacteria and viruses) retention by clean microfilters before the onset of fouling.

The first part of the dissertation focuses on virus control by an integrated electrochemical-microfiltration process at the bench scale. In contrast to the substantial database available on natural organic matter (NOM)/disinfection by-product (DBP) precursor removal by coagulation, much less information is available on its ability to control viruses and therefore requires further study. It should be noted that this work rigorously elucidates virus destabilization mechanisms rather than simply optimizing coagulation conditions to maximize virus removals. Detailed understanding of sweep flocculation was obtained by dissolving flocs and attaching a fluorescent label to viruses. Atomic force microscopy was used to directly measure adhesion forces between viruses and flocs. The biochemical basis of virus inactivation during electrochemical coagulation was investigated using Fourier Transform Infra-red spectroscopy (FTIR) and quantitative reverse transcription polymerase chain reaction (q-RT-PCR). Two peer-reviewed journal articles have already been published based on this aspect of my work (Tanneru and Chellam 2012, Tanneru et al. 2013) and a third one is currently in preparation. The first two chapters of this dissertation are the same as published journal articles and the third chapter is the manuscript that is being written.

The second part of my research is ongoing collaborative work with Basavaraju Agasanapura, a graduate student of Dr. Ruth E. Baltus at Clarkson University. They are

developing comprehensive models for convective transport of a rigid particle in a cylindrical pore using Computational Fluid Dynamic (CFD) calculations. We at the University of Houston are performing short term microfiltration experiments to measure the rejection of viruses and bacteria by track-etched membranes of different pore sizes. We have jointly published one journal article (Agasanapura et al. 2013) and a second one is being prepared for submission. Theoretical work performed at Clarkson University considers hydrodynamic particle-wall interactions and was quantitatively compared to experiments performed with *Brevundimonas diminuta*, *Serratia marcescens*, and *Escherichia coli* (rod shaped bacteria), MS2 and PRD1 (spherical viruses), and inorganic silica particles.

1.2 Research goals and Objectives

The overall goals of this research are (i) to elucidate virus reduction mechanisms (both removal and inactivation) during electrocoagulation and microfiltration, (ii) to generate experimental data on the rejection of microorganisms (bacteria and viruses) by clean microfilters to validate theoretical transport models incorporating convective hindrance.

Specific objectives of my doctoral research include:

1. To determine mechanisms of virus control from natural surface water in a hybrid iron electrocoagulation – MF process
2. To empirically demonstrate enhanced virus removals from surface water in a hybrid aluminum electrochemical − MF process and to systematically elucidate underlying destabilization/removal mechanisms
3. To elucidate virus inactivation during aluminum electrolysis with emphasis on factors affecting disinfection including the role of solids, pH, ionic strength, and aluminum concentration

4. To complete short-term MF experiments with rod shaped bacteria (*E. coli, B. diminuta* and *S. marcescens*) and spherical viruses (MS2 and PRD1) and different pore-sized membranes in support of numerical calculations performed at Clarkson University.

1.3 Dissertation organization

The main body of this dissertation is composed of four principal chapters; the first two chapters are already published journal articles, the third chapter will be soon submitted peer-review, and the fourth chapter is a subsection of another published paper. This features only the experimental data because the hindered convection model was developed by our collaborators and is an integral component of Basavaraju Agasanapura's dissertation.

Chapter 2 summarizes mechanisms of virus control from natural surface water by a combined iron electrocoagulation – microfiltration process. Comparisons were also made with experimental results using synthetic water and conventional chemical coagulation (with $FeCl_3$) to empirically demonstrate the role of NOM in inhibiting virus control during iron electrocoagulation. These findings are available in "Tanneru, C. T.; Chellam, S., Mechanisms of Virus Control during Iron Electrocoagulation - Microfiltration of Surface Water. *Water Research* **2012,** *46* (7), 2111-2120."

Chapter 3 specifically demonstrates enhanced virus removals from surface water in a hybrid electrochemical – MF process and systematically elucidates underlying destabilization and removal mechanisms. Since we have recently reported poor virus control by iron electrocoagulation in NOM-laden waters due to generation of soluble ferrous ions in Chapter 2, only aluminum is considered herein. These findings can be found in "Tanneru, C. T.; Rimer, J. D.; Chellam, S., Sweep Flocculation and Adsorption of Viruses on Aluminum Flocs during Electrochemical Treatment Prior to Surface Water Microfiltration. *Environmental Science & Technology* **2013,** *47* (9), 4612-4618."

Chapter 4 discusses mechanisms of virus inactivation during electrolysis of saline solutions with emphasis on factors effecting disinfection including coagulation/aggregation and presence of solids, pH, ionic strength and aluminum concentration. This work will be submitted for peer-review soon.

Chapter 5 only shows short-term laboratory measurements of the removal of three rod-shaped bacteria *B. diminuta, S. marcescens,* and *E. coli*), two spherical viruses (MS2 and PRD1), and multiple spherical silica colloids by a number of track-etched membranes with near cylindrical pore geometry. These findings have already been published "Agasanapura, B.; Baltus, R. E.; Tanneru, C.; Chellam, S., Membrane Rejection of Nonspherical Particles: Modeling and Experiment. *AIChE Journal* **2013,** *59* (10), 3863-3873."

Chapter 2. Mechanisms of Virus Control during Iron Electrocoagulation – Microfiltration of Surface Water

2.1 Introduction

Disinfection of contaminated waters to reduce enteric diseases continues to be one of the most important aspects of drinking water purification (Madaeni 1999). Enteric viruses have been identified as causative agents for over 40% of childhood diarrhea in developing countries (Ramani and Kang 2009). It has also been suggested that viruses are the etiologic agents responsible for the majority of unidentified outbreaks since they are typically more difficult to analyze than bacterial pathogens (USEPA 2006). While microfiltration alone is highly efficient for the control of pathogenic protozoa and bacteria, it is not well-suited for removing viruses since they are substantially smaller than membrane pore sizes (Jacangelo et al. 1995, Madaeni et al. 1995, Mi et al. 2005, Pontius et al. 2009, Urase et al. 1996) Although sorption onto microfilters can transiently increase virus removal (Madaeni 1999, van Voorthuizen et al. 2001), hydrophobic, electrostatic, and other non-specific interactions leading to their attachment onto the membrane material cannot reliably remove viruses during water purification especially during long-term (pseudo steady-state) operation. However, virus removal by microfiltration can be significantly improved by chemical coagulation pretreatment, with several studies demonstrating > 99.99% or 4-log removals (as required under the Surface Water Treatment Rule) using alum or iron salts e.g., (Fiksdal and Leiknes 2006, Shirasaki et al. 2009, Zhu et al. 2005a, b). Alternately, electrocoagulation can also be employed for micro- and ultrafiltration pretreatment.

Electrocoagulation is a process in which metal-ion coagulants are directly added to the feed water by *in situ* electrochemical dissolution of an anode. The burgeoning interest in applying it for water and wastewater treatment can be attributed to its many potential advantages such as (i) portability, (ii) reduced use of corrosive chemicals, (iii) availability of

optimized module configurations that have decreased energy consumption and increased capacity, (iv) suitability for use in predesigned packaged plants, and so on (Cañizares et al. 2007, Mollah et al. 2004, Moreno C et al. 2009).

Electrocoagulation alone has been shown to be effective in removing oil and grease, chemical oxygen demand (COD), dyes, heavy metals, turbidity, and bacteria from drinking water and wastewaters (Bayat et al. 2006, Cañizares et al. 2007, Chen et al. 2002, Durante et al. 2011, Jiang et al. 2002, Lakshmanan et al. 2010, Ricordel et al. 2010, Wan et al. 2011). Electrocoagulation has also been combined with microfiltration and shown to be highly effective for *synthetic waters*, achieving ~ 90% energy savings, ~ 99% removals of heavy metals (Se, Pb, Zn, Cu, Cd, and As) and > 99.999% removal of viruses (Ben Sasson and Adin 2010, Mavrov et al. 2006, Zhu et al. 2005a). In contrast, iron electrocoagulation appears to be less promising for pretreating *natural waters* prior to low-pressure membrane filtration since chemical coagulation with $FeCl_3$ has consistently out-performed it. For example, significantly greater fluxes were obtained following conventional chemical coagulation compared with iron electrocoagulation during seawater ultrafiltration (Timmes et al. 2010) as well as microfiltration of surface water from an inland lake (Bagga et al. 2008). Hence, it appears that experiments using synthetic waters cannot be directly used to extrapolate and predict electrocoagulation system performance for fouling control under real-world conditions. Therefore, a study was undertaken to determine whether the excellent (> 5-log) removal of viruses measured from waters devoid of NOM by iron electrocoagulation – microfiltration (Zhu et al. 2005a) could be extended to surface water containing NOM.

The icosahedral F-specific ssRNA coliphage MS2 was employed to facilitate comparisons with earlier results of virus removals by low-pressure membranes e.g., (Jacangelo et al. 1995, Mi et al. 2005, Shirasaki et al. 2009, van Voorthuizen et al. 2001, Zhu et al. 2005a, b). Its small size

(approx. 30 nm) and low isoelectric point (3.9) reduce steric interactions and adsorption allowing a conservative estimate of virus removal by microfilters. Further, it has been shown to be a conservative surrogate for the treatability of human viruses such as coxsackievirus and echovirus by coagulation (Mayer et al. 2008). Since MS2 specifically infects the gastrointestinal bacterium *Escherichia coli*, it also captures similarities of origin and release of human enteric viruses into the aquatic environment. Additionally, being similar in size, shape, and nucleic acid composition to hepatitis A and polio virus, MS2 is an excellent surrogate for pathogenic human enteric viruses (Grabow 2007, Havelaar et al. 1993, Mayer et al. 2008). Finally, bacteriophages facilitate experimentation since they are not hazardous to humans, avoid the need for animal cell lines, and are relatively easy to cultivate and dispose.

The objective of this study is to determine mechanisms of virus control from natural surface water by a combined iron electrocoagulation – microfiltration process. Comparisons were also made with experimental results using synthetic water and conventional iron chemical coagulation (with $FeCl_3$) to empirically demonstrate the role of natural organic matter (NOM) in inhibiting virus control during electrocoagulation. Virus removals were evaluated in a range of iron dosages (0 – 13 mg/L) and at pH 6.4 and 7.5. Results reported herein are part of our larger effort aimed at evaluating novel surface water treatment processes to meet the increased demands of a growing population in the greater Houston, Texas area and combating land subsidence associated with groundwater extraction.

2.2 Experimental Work

2.2.1. Virus

The double-top agar layer technique was employed for MS2 (ATCC 15597-B1) propagation using *E. coli* (ATCC 15597) as the host. *E. coli* was first cultured overnight (18-24h) in

Tryptic Soy Broth (TSB; Difco, Detroit, MI) at 37 °C and later cultured TSB was added to a fresh TSB and grown to a mid-log phase for 3-6 hours also at 37 °C. MS2 stock was serially diluted in Phosphate Buffered Saline (PBS; composition 137 mM NaCl, 2.7 mM KCl, 4.3 mM $Na_2HPO_4.7H_2O$, and 1.4mM KH_2PO_4; pH 7.5). Next *E. coli* suspension (0.9 mL) and phage dilution (0.1 mL) were mixed in 3 mL 0.5% soft overlay agar and poured onto pre-solidified Trypticase Soy Agar plates (TSA 1.5%, Difco, Detroit, MI). The plates were incubated at 37 °C for 24 h. Plaques numbering from 20 to 300 were counted and MS2 concentrations are reported as plaque forming units/mL (PFU/mL). For filtration experiments, 1 mL of purified virus stock was added to 450 mL of feed surface water to obtain a feed concentration of $O(10^7\text{-}10^8)$ PFU/mL. All the natural water samples were centrifuged at 5,000 g for 20 minutes to remove any debris before plating and propagation.

Recently, quantitative real-time PCR (q-RT-PCR) is gaining prominence for virus enumeration to calculate log-removals associated with water treatment unit processes to reduce potential issues associated with virus aggregation e.g.(Kim et al. 2011, Langlet et al. 2009, Shirasaki et al. 2009). In our experiments MS2 concentrations in feed waters measured using the plaque assay were very close to the calculated value based on the stock titer suggesting limited phage aggregation (see Figure 2.4). Additionally, since the plaque assay continues to be routinely employed in environmental engineering e.g., (Anders and Chrysikopoulos 2006, Mayer et al. 2008, Shen et al. 2008), it was used in this research as well.

2.2.2 Source waters

The natural water sample was obtained from Lake Houston, which had a pH close to 7.5, total hardness of 60 mg/L as $CaCO_3$, conductivity of 288 µS/cm, dissolved organic carbon (DOC) concentration of 4.9 mg/L, absorbance at 254 nm and one cm path length of 0.165 cm^{-1}, alkalinity of 57 mg/L as $CaCO_3$, and 8 NTU turbidity. Experiments were also conducted with

synthetic water, prepared by adding 3 mM $NaHCO_3$ and 1 mM $CaCl_2$ to deionized water (and in some cases Suwanee River Humic Acid was also added).

2.2.3. Electrocoagulation and chemical coagulation

Electrocoagulation was performed in batch mode using a 450 mL bench-scale unit fitted with a high purity (99.9965%) iron anode and porous stainless steel cathode. The desired iron dosage was obtained by controlling the current passage time according to Faraday's law. All experiments were performed by vigorously stirring the cell contents during electrolysis (to simulate rapid mixing) and under open atmospheric conditions with dissolved oxygen content near saturation (~ 9 mg/L). The entire suspension was then slowly mixed for 2 minutes to flocculate the destabilized particles. To maintain reproducible iron dissolution, the anode was gently scrubbed with a silicon paper sanding sheet before each experiment(Bagga et al. 2008, Lakshmanan et al. 2009).

A programmable jar tester (Phipps & Bird Inc., Richmond, VA) was used for chemical coagulation. The target iron concentration was achieved by adding $FeCl_3$ to 1 L water in square Gator jars. Rapid mixing was performed by mixing at G = 495 s^{-1} for 1 minute, which was followed by 30 minutes of flocculation at G = 32 s^{-1}. Both electro- and chemical coagulation experiments were performed at pH 6.4 (adjusted using HCl) and 7.5 with a precision of ± 0.2 pH units. NaOH was added as necessary to maintain the pH at its target value during chemical coagulation to neutralize the Brønsted acid behavior of $FeCl_3$.

2.2.4. Microfiltration

Hydrophilic modified PVDF membranes nominally rated at 0.22 µm (Durapore, GVWP02500, Millipore) were used. Pretreated waters were batch-transferred to a plexiglass feed tank, which was connected to a compressed air cylinder to perform experiments at 14 kPa.

The suspension was kept gently stirred in the tank to avoid settling of the flocs. Dead-end filtration was performed without stirring using a commercially available cell with 4.1 cm^2 effective area (Millipore, Bedford, MA). A fresh membrane disc was used for each experiment, which was first washed by passing 100 mL of ultrapure water at 25 kPa before filtering the feed suspension.

2.2.5. Iron measurement

Total iron was measured using atomic absorption spectroscopy (AAnalyst 300, Perkin-Elmer Corp., CT) after acidifying the samples to pH < 2 using HNO_3. Ferrous iron in electrocoagulated waters was determined by chelating it to 1, 10 phenanthroline after adding HCl to bring the pH to 4 and buffering with acetate. The resulting reddish-orange complex was quantified by light absorption at 510 nm using a spectrophotometer (Hach Co., Loveland, CO). The difference between total iron and ferrous iron concentrations gave the ferric iron concentration.

2.2.6. Zeta potential

The electrophoretic mobility of colloids in natural and synthetic waters was measured using the electrophoretic light scattering technique over a wide range of iron dosages (Nicomp 380 ZLS, Particle Sizing Systems, Santa Barbara, CA). A He-Ne laser of 632.8 nm wavelength, 0.4 cm electrode spacing, and 10 V/cm field strength were employed for all measurements. The Smoluchowski equation was used to convert electrophoretic mobility to zeta potential. Each sample was run in triplicate each for 60 s duration.

2.3. Results and Discussion

2.3.1. General statement of experimental reproducibility

Approximately 15% of the experiments at different pH values and coagulant dosages were repeated. Paired t-tests conducted on virus reduction values from duplicate experiments showed no statistical differences at the 95% confidence level. These experimental results demonstrate that all our laboratory protocols related to electrocoagulation, flocculation, microfiltration and virus enumeration were consistent and reproducible.

2.3.2. Electrocoagulation generated ferrous iron at nearly 100% efficiency

Iron dissolution was monitored over a range of current densities by varying the current and electrocoagulant generation times and summarized in Figure 2.1.

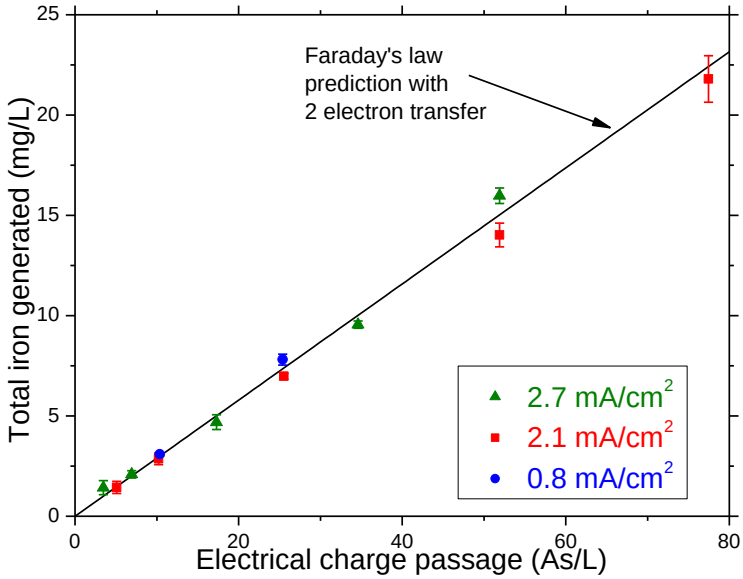

Figure 2.1. Experimental evidence for ferrous iron generation during electrocoagulation at different current densities.

Figure 2.1 demonstrates that iron concentrations in the electrochemical cell increased linearly with total charge passed and agreed quantitatively with Faraday's law predictions for two electron transfer. Therefore, the only anodic process in our experiments was the oxidation of iron metal to soluble Fe^{2+} in accordance with other recent reports (Ben Sasson et al. 2009,

Lakshmanan et al. 2009). In contrast, not cleaning the anode can result in passivation, chemical dissolution, or pitting which can either increase or decrease iron concentrations in the cell compared with Faraday's law especially during longer-term operation (Ben Sasson and Adin 2010, Cañizares et al. 2007, Lakshmanan et al. 2009). Substantial ferrous iron concentrations were directly measured in the cell after 2 minutes of rapid mixing especially at pH 6.4 providing additional evidence for Fe^{+2} dissolution (see Figure 2.2). The fraction of Fe^{2+} decreased significantly when the pH was increased. For example with 6 s electrolysis, more than half the total iron was present as Fe^{2+} at pH 6.4 whereas only 6% Fe^{2+} was measured at pH 7.5. This was caused by the strong (inverse second order) influence of pH on the Fe^{2+} oxidation rate since electrocoagulation was initiated under open atmospheric conditions (Ben Sasson et al. 2009, Morgan and Lahav 2007, Stumm and Morgan 1996) in the absence of NOM.

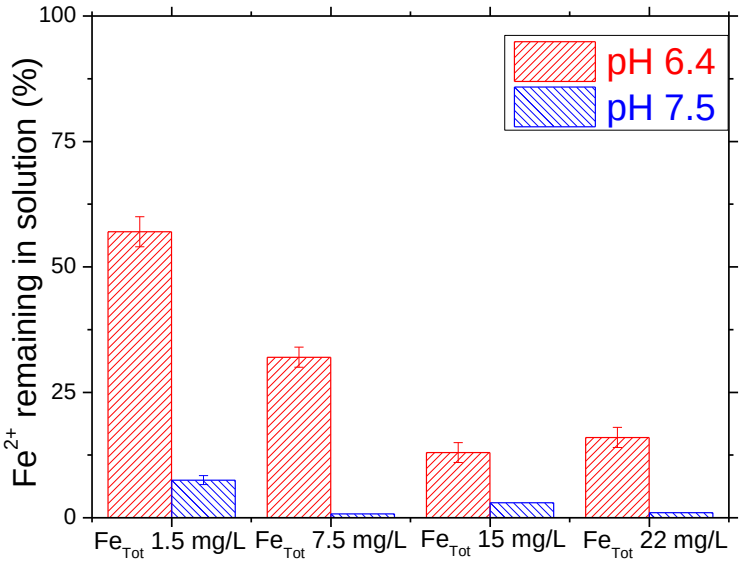

Figure 2.2. Ferrous iron concentrations as a percentage of total iron for different electrolysis durations at pH 6.4 and 7.5.

Based on the above evidence, $Fe(OH)_3$ precipitation in our experiments is expected to occur predominantly through dissolved oxygen mediated oxidation of electrochemically generated Fe^{2+}:

Anode: $Fe^0(s) = Fe^{2+} + 2e^-$

Oxidation: $4Fe^{2+} + O_2 + 4H^+ = 4Fe^{3+} + 2H_2O$

Hydrolysis: $Fe^{3+} + 3H_2O = Fe(OH)_3 + 3H^+$

Cathode: $2H_2O + 2e^- = 2OH^- + H_2(g)$

Overall: $4Fe^0(s) + 10H_2O + O_2 = 4Fe(OH)_3\ (s) + 4H_2(g)$

Bubbles were formed in the electrochemical cell as predicted by the above reactions. Also, cathodic production of hydroxyl ions transiently increased the bulk pH of the low buffering capacity (alkalinity) Lake Houston water during electrolysis by approximately 0.5 units, which later decreased to approximately the original value. Since these pH changes are expected to depend on feed water alkalinity, current density, and residence time (iron dosage), it is recommended that the pH be monitored closely during electrocoagulation.

2.3.3. Virus reductions in electrocoagulated and chemically coagulated and microfiltered waters

Figure 2.3 summarizes reductions in MS2 virus concentrations in microfiltered synthetic and natural waters after electro- and chemical coagulation pretreatment. In the absence of any pretreatment, microfiltration alone removed only < 0.5-log of viruses demonstrating negligible sieving as was expected from the low ratio of virus size to membrane pore diameter (0.14). Pretreatment with chemical coagulation for Lake Houston water and electrocoagulation for synthetic water increased virus removals monotonically with coagulant dosage (Shirasaki et al. 2009, Zhu et al. 2005a, b), attaining the 4-log removal/inactivation criterion under the Surface Water Treatment Rule at relatively low iron dosages (< 4 mg/L). In contrast, electrocoagulation was ineffective for virus control in natural water achieving a maximum of only 1.5-log (97%) reduction at pH 6.4 even at a relatively high iron dosage of 13 mg/L. In comparison, electrocoagulation-microfiltration achieved 6.5-log (99.99997%) virus reduction from synthetic water at pH 6.4 at a similar iron dosage. Similar trends were obtained at pH 7.5 where again

electrocoagulation-microfiltration was more effective in controlling viruses from synthetic water that was devoid of NOM compared with natural water that contained moderate DOC concentrations (4.5mg/L). It is hypothesized that the poor performance of iron electrocoagulation pretreatment in terms of virus removals from Lake Houston water was caused by the presence of NOM (discussed later in § 2.3.8).

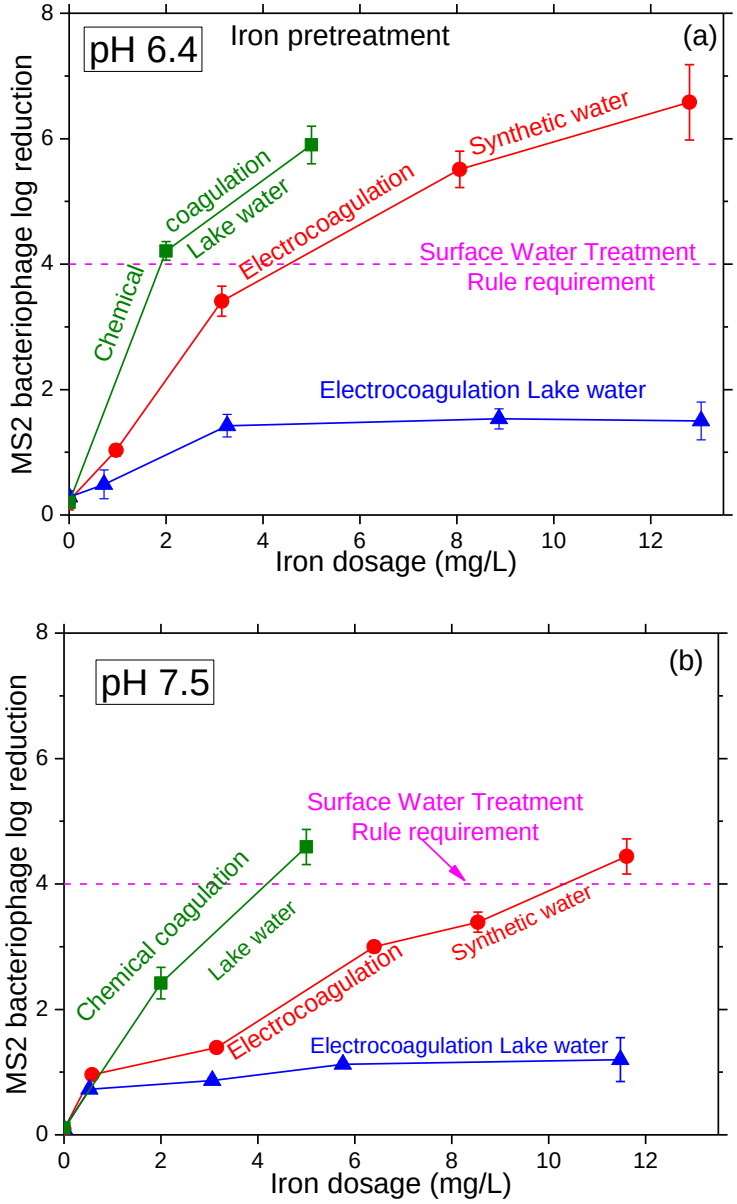

Figure 2.3. Comparison of virus removals by microfiltration with different pretreatment processes and feed waters at pH 6.4 and 7.5.

Also as seen in Figure 2.3, conventional chemical coagulation outperformed electrocoagulation pretreatment for virus control from Lake Houston water at both pH values investigated. Low virus reductions by electrocoagulation were due to electrochemical generation of soluble Fe^{2+} (which was oxidized to insoluble Fe^{3+} *in situ* as described in § 2.3.2). Whereas, insoluble Fe^{3+} was directly added in chemical coagulation, which precipitated and encapsulated viruses, removing them over the course of the experiment. Viruses were controlled more effectively by adding more and more Fe^{3+} due to availability of a greater number of sites for virus sorption and superior virus enmeshment by increasing mass of $Fe(OH)_3$ precipitates (Mayer et al. 2008, Zhu et al. 2005a).

Figure 2.3 further depicts better virus control at pH 6.4 compared with pH 7.5 from natural water by chemical coagulation and synthetic water by electrocoagulation. Hence, it appears that increased charge neutralization and greater degree of electrochemical inactivation at pH 6.4 (as described in § 2.3.5 and 2.3.6) were more important than decreased $Fe(OH)_3$ precipitation in controlling viruses in these experiments. However, virus reductions were poor and similar during electrocoagulation of natural water at both pH values investigated, which is attributed to Fe^{2+} complexation by NOM and resulting weak destabilization.

2.3.4. Direct evidence for virus sorption onto iron flocs

Virus concentrations in seeded feed waters were measured after adding 1 mL stock solution ($O(10^{10})$ PFU/mL) to 450 mL test suspension to be electrocoagulated resulting in feed concentrations of $O(10^{8})$ PFU/mL. After selected electrocoagulation experiments (before microfiltration), iron flocs were separated by centrifugation (10,000 g for 20 minutes) and dissolved in 6% beef extract (after elevating the pH to 9.5) to quantify sorption of MS2 phages onto the precipitated coagulant (Matsui et al. 2003, Shirasaki et al. 2009).

As seen in Figure 2.4, nearly all the seeded viruses ($O(10^8)$) were recovered from synthetic water demonstrating that the vast majority of the viruses were sorbed onto the iron hydroxide precipitates. In contrast, only a very small fraction of the seeded viruses (1.3%) were associated with the precipitates for natural water. These measurements confirm the negligible removals by sweep flocculation from NOM-containing surface water whereas excellent removals were possible in the absence of NOM (from synthetic water) shown in Figure 2.3.

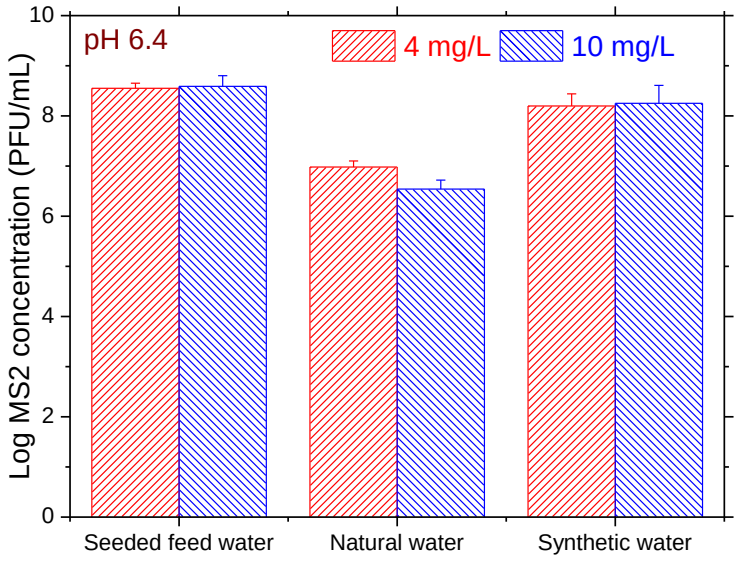

Figure 2.4. Virus recoveries by dissolving electrocoagulated flocs from natural and synthetic waters. The bars labeled "seeded feed water" refer to measurements made immediately after adding virus stock to the test water.

2.3.5. Evidence for virus inactivation in the electrochemical cell

Figure 2.3 also depicts that a lower pH enhanced virus control during electrocoagulation-microfiltration of synthetic waters and chemical coagulation-microfiltration of Lake Houston water. For example, at an electrocoagulant dose of ~ 8 mg/L, MS2 concentrations were reduced by 5.5-log (99.9997%) at pH 6.4 but only by 3.4-log (99.96%) at pH 7.5 from synthetic water. To better understand the differences in virus reductions during electrocoagulation between pH 6.4 and 7.5, more control experiments were performed. Viruses

were added to natural and synthetic water after pH adjustment and electrocoagulated at a dose of 10 mg/L as Fe. After electrochemical iron dosing, the water was then slowly mixed for a period of 5 hours (duration of a typical experiment) and viruses in the supernatant and flocs were enumerated every hour. Viruses associated with the flocs were enumerated following dissolution in beef extract at pH 9.5 as explained in the previous section. Inactivation values reported in Figure 2.5 were calculated using virus concentrations in both supernatant and the flocs (Matsui et al. 2003, Shirasaki et al. 2009).

As seen in Figure 2.5 for synthetic waters, virus concentrations monotonically decreased over time reaching 2.2-log at pH 6.4 and 1.2-log at pH 7.5 after 5 hours. Hence, MS2 viruses appear to be inactivated during electrocoagulation of synthetic waters in the absence of NOM, which can be partially attributed to electrochemically generated oxidants such as $^{\bullet}OH$, O_3, H_2O_2, free chlorine and ClO_2 simply due to current passage (Drees et al. 2003, Jeong et al. 2006, Liu et al. 1997).

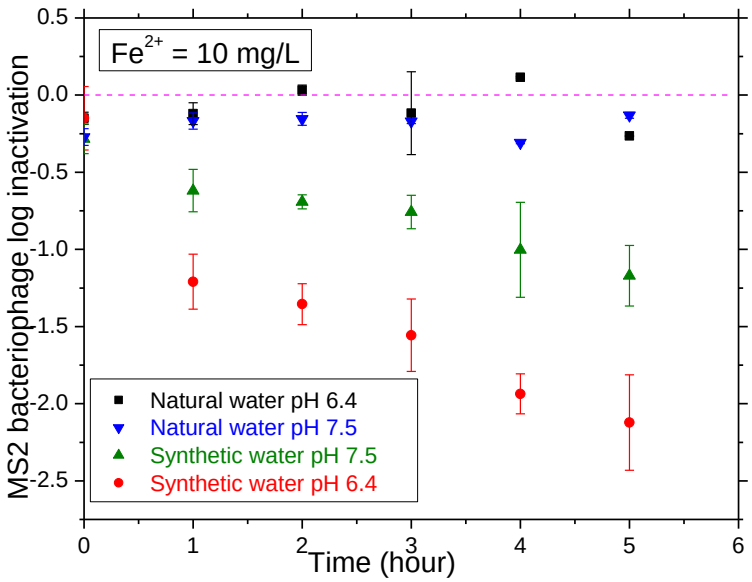

Figure 2.5. Ferrous iron inactivates MS2 coliphage in synthetic waters only when no NOM is present.

Additionally, similar to Fe^{2+} produced by dissolution of nanoparticulate zerovalent iron (Kim et al. 2011), hydroxyl radicals and superoxide anions may also be formed following anodic

dissolution of metallic iron, which are capable of inactivating MS2 viruses. In any case, the measured reductions in MS2 concentrations in synthetic waters are attributed to oxidative modifications of the proteinaceous capsid by exogenous reactive oxygen species (ROS) or alterations to the capsid proteins' secondary structures following sorption on to the flocs (Hotze et al. 2009, Kim et al. 2011, Shirasaki et al. 2009). In contrast, only 0.2-log reductions in MS2 concentrations were measured at 5 hours for natural waters. This suggests that NOM potentially acted as a sink for electrochemically produced ROS, reduced ROS generation rate, and/or decreased direct Fe^{2+} - virus interactions via complexation (Kim et al. 2011, Lindsey and Tarr 2000, Theis and Singer 1974).

2.3.6. Virus destabilization mechanisms

As summarized in Figure 2.6, the ζ potential of MS2 viruses in synthetic water in the absence of any coagulant was approx. -35 mV, which is consistent with literature reports e.g (Choi and Dempsey 2004, Holt et al. 2002) The magnitude of the ζ potential decreased in natural water (~ -17 mV) potentially due to adsorption of NOM and divalent cations. The less negative zeta potentials for colloids suspended in natural water at pH 6.4 were attributed to more protonation of adsorbed NOM (reduced degree of dissociation and lower negative charge) in acidic waters and to the higher concentrations of positively charged $Fe(OH)^{2+}$ and $Fe(OH)_2^{+}$. Whereas at pH 7.5, the dominant species are $Fe(OH)_3^{0}$, $Fe(OH)_2^{+}$ and $Fe(OH)_4^{-}$, which as a first approximation can be assumed to be adsorbing onto flocs (O'Melia 1972). Since the MS2 virus was negatively charged in all the experiments, the electrostatic barrier was decreased at lower pH allowing greater removals by adsorption. The ζ potential of electrocoagulated virus suspensions increased ($\rightarrow$ 0) with iron dose for a given pH in both surface water and synthetic water as measured by other researchers e.g., (Choi and Dempsey 2004, Holt et al. 2005).

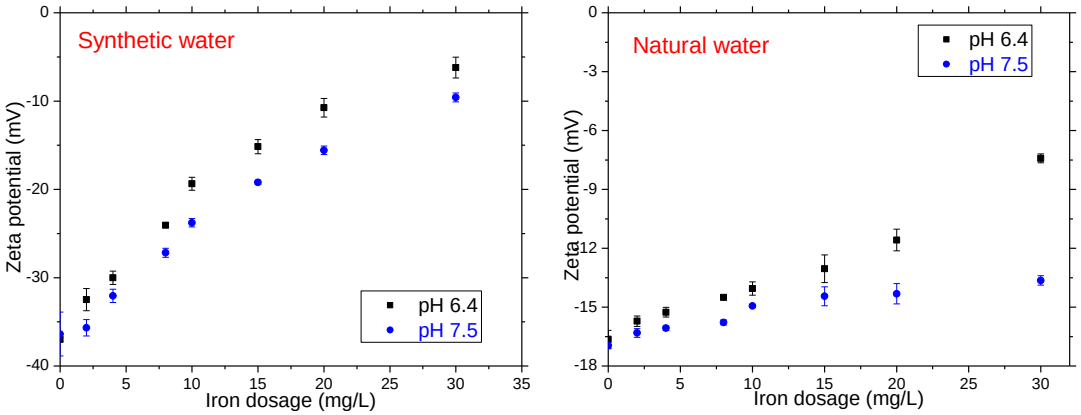

Figure 2.6. Effect of electrochemical iron addition on zeta potential in synthetic and natural waters at pH 6.4 and 7.5.

Sweep flocculation was the dominant virus destabilization mechanism since significantly negative ζ potentials (approx. -15 mV) were measured even at the highest iron concentration employed in removal experiments (see Figure 2.3). This suggests the secondary role of adsorption of positively charged iron species onto viruses and associated charge neutralization.

2.3.7. Virus removals increased as a cake layer was formed for natural water

A monotonic trend of increasing removals was observed for natural waters as filtration progressed (Figure 2.7).

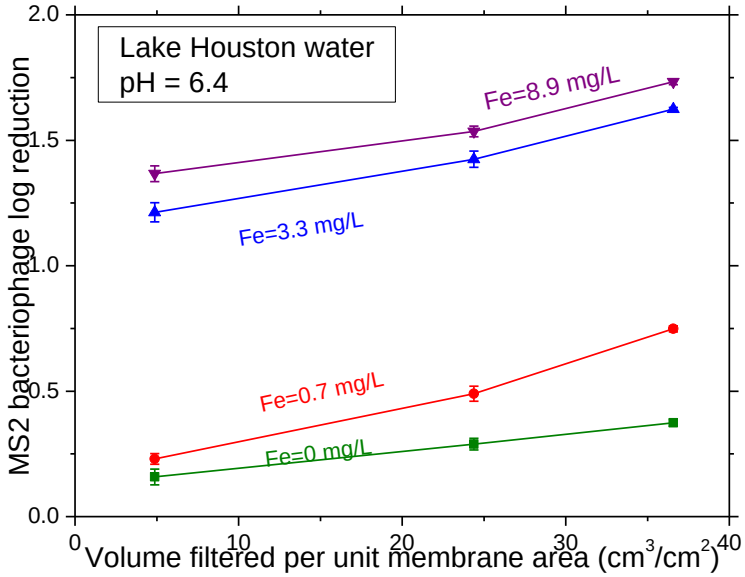

Figure 2.7. Effects of coagulant dose and cumulative volume filtered on virus control. MS2 concentrations in the permeate decreased as a cake was formed during microfiltration of natural water.

In other words, the cake layer appears to have reduced the effective membrane pore size and also served as a “dynamic membrane” contributing a secondary filtration effect for viruses in the presence of colloidal materials (Jacangelo et al. 1995, Madaeni et al. 1995). Additionally, since the isoelectric point of $Fe(OH)_3$ is close to 8.0, it tends to be positively charged in the pH range of our experiments and can therefore adsorb negatively charged MS2 viruses, thus contributing to additional removal by the cake layer. These effects are similar to increases in dissolved solute rejection due to the presence of a foulant layer, which has been attributed to sieving or specific interactions (Bellona et al. 2010, Schafer et al. 2001). Since virus concentrations in the filtered water decreased over time, the average of three samples (taken near the beginning, middle, and end of filtration after 5, 24, and 37 cm^3 filtered/cm^2 membrane area respectively) was used to calculate log virus reductions reported in Figure 2.3. After filtration, the membranes were dried overnight in an oven at 60 °C, sputter coated with a thin conductive (gold) layer and observed under a field emission scanning electron microscope (LEO 1525, Carl Zeiss).

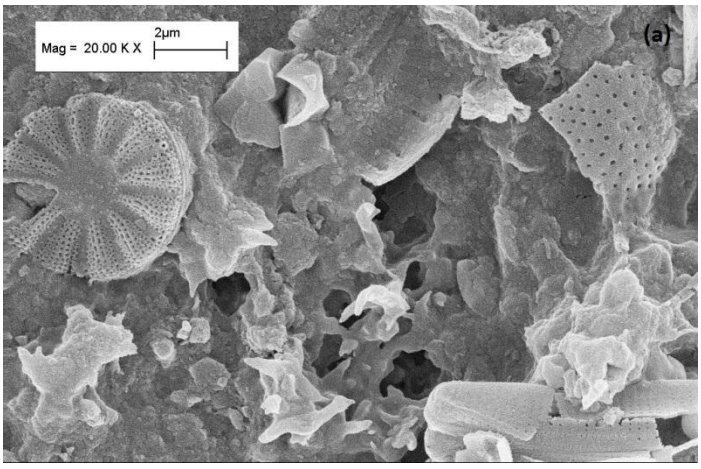

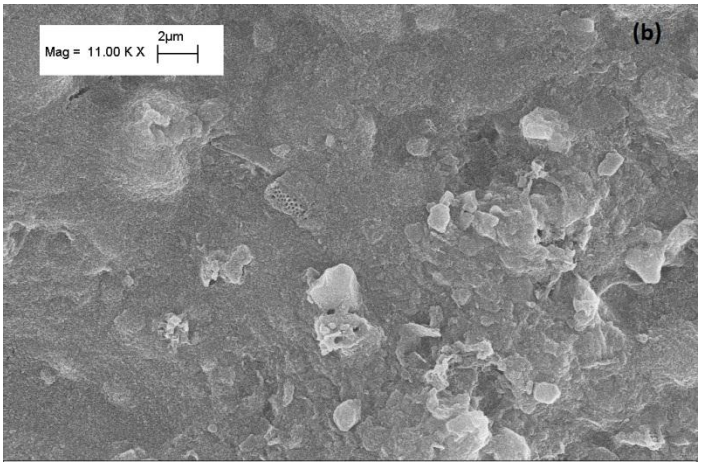

Figure 2.8. Scanning electron micrographs of natural colloidal materials visualized after filtering raw water (top). An image of the cake formed after filtration of 150 mL of electrocoagulated water at pH 6.4 and 10 mg Fe/L is shown in the (bottom).

Figure 2.8a depicts the heterogeneous nature of natural colloidal materials present in surface water. Morphology of the cake in Figure 2.8b also suggests that amorphous Fe oxyhydroxides were present. Natural colloids can be seen to be interspersed with flocs for electrocoagulated samples, which is consistent with *in situ* oxidation of Fe^{2+} to form insoluble Fe^{3+} species as summarized in § 2.3.2 (and explaining poor electrocoagulation performance in Figure 2.3).

2.3.8. NOM worsens virus removals

To empirically demonstrate the deleterious role of NOM on virus removals during iron electrocoagulation, 5 mg/L of Suwannee River Humic Acid (SRHA) was also added to synthetic waters. Virus removals from these feed waters were evaluated by electrocoagulation – microfiltration at an iron dosage of 10 mg/L at pH 6.4 and 7.5. Separate chemical coagulation experiments were also performed where soluble $FeSO_4$ was added (10 mg/L as Fe^{2+}), rapid mixed for 1-minute at 495 s^{-1}, flocculated for 30 minutes at 32 s^{-1} and immediately filtered using a 0.22 µm syringe filter (09-719A MCE sterile, Fisher Scientific). As summarized in Figure 2.9, the presence of NOM worsened virus removals by ~ 4-log at pH 6.4 and ~ 2-log at pH 7.5 following electrocoagulation – microfiltration. Also, virus removals by $FeSO_4$ coagulation – microfiltration

deteriorated by ~ 1.5-log at both pH values. This indicates competition between NOM and viruses to interact with hydrolysis species such as Fe^{3+}, $Fe(OH)_2^+$, $FeOH^{2+}$, $Fe(OH)_4^-$, which would decrease viruses sorption onto iron flocs instead resulting in Fe^{2+}-NOM complexes. Humic acids can also interfere with the kinetics of ROS production in the electrochemical cell if carboxyl groups complex Fe^{2+} or alternately by initiating, promoting, or inhibiting ROS transformations (Lindsey and Tarr 2000, Staehelin and Hoigne 1985). Hence, NOM appears to inhibit virus control by (i) complexing with Fe^{2+} and slowing its rate of oxidation to insoluble Fe^{3+} thereby interfering with sweep flocculation (Singer and Reckhow 1999, Theis and Singer 1974), (ii) reducing direct interactions between Fe^{2+} and capsid amino acids due to complexation (Kim et al. 2010) (iii) scavenging ROS and decreasing their concentration, or (iv) decreasing ROS generation rate (Lindsey and Tarr 2000). Similar results have also been reported during filtration with carbon nanotubes, where virus removals decreased upon NOM addition (Brady-Estevez et al. 2010).

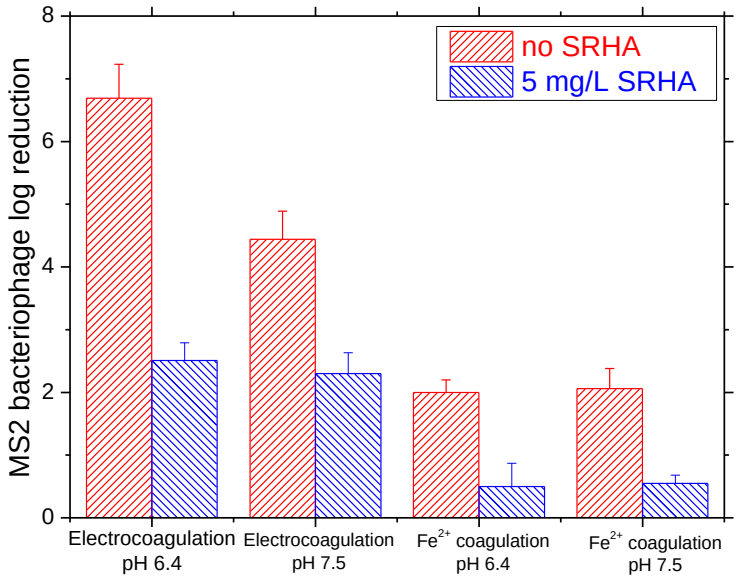

Figure 2.9. Lower virus removals from synthetic water to which 5 mg/L Suwanee River Humic Acid (SRHA) had been added. Electrocoagulation at 10 mg/L iron was used as pretreatment for microfiltration. $FeSO_4$ was employed as the chemical coagulant.

2.4. Conclusions

Ineffective virus control from surface water with iron electrocoagulation pretreatment for microfiltration is attributed to NOM complexation of electrochemically generated Fe^{2+}, which interferes with sweep flocculation, charge neutralization, as well as ROS-mediated inactivation. Floc flotation was observed at higher electrocoagulant dosages due to cathodic release of hydrogen gas. It is noted that aluminum, the other common metal-ion coagulant exists predominantly in the insoluble trivalent oxidation state (unlike a transition metal such as iron that exists in soluble and insoluble forms). Hence, current experiments are focused on evaluating aluminum for electrocoagulation and electroflotation pretreatment of natural water before microfiltration.

Significantly better virus reductions were measured in the absence of NOM compared with surface water containing moderate NOM concentrations. Importantly, mechanisms of virus control in synthetic water included both removal and inactivation whereas negligible inactivation was measured in surface water. Hence, NOM appears to inhibit inactivation by decreasing the ROS generation rate, scavenging ROS, and complexing with Fe^{2+} thereby reducing its interactions with capsid amino acids. Direct measurements of ROS need to be made to provide more conclusive evidence for inactivation mechanisms in the electrocoagulation cell. In any case, experimentation using synthetic water alone is insufficient and virus removal/inactivation should be quantified directly with natural water before implementing electrocoagulation for drinking water treatment.

Chapter 3. Sweep flocculation and adsorption of viruses on aluminum flocs during electrochemical treatment prior to surface water microfiltration

3.1 Introduction

A combined coagulation – microfiltration (MF) process is capable of removing protozoa, bacteria, turbidity, as well as a portion of natural organic matter (NOM) and disinfection by-product (DBP) precursors from surface water while maintaining relatively high flux (Choi and Dempsey 2005, Lahoussine-Turcaud et al. 1990, Laine et al. 1990) allowing cost-effective compliance with the Microbial-Disinfectants/ Disinfection by-products (M-DBP) cluster of regulations. Waterborne pathogens also include viruses which cause severe respiratory and gastrointestinal illnesses, hepatitis A and E, and are even linked to many unidentified outbreaks (Grabow 2007, Ramani and Kang 2009). Several viruses have also been included in the Environmental Protection Agency's (EPA's) Contaminant Candidate List since they are etiologic agents for emerging infectious diseases.

Viruses are poorly removed by MF alone in the absence of any pretreatment (Jacangelo et al. 1995, Madaeni et al. 1995, Meyn et al. 2012, Shirasaki et al. 2009, Zhu et al. 2005a), whereas alum coagulation followed by media filtration removes 2 – 4 log of influent viruses (Harrington et al. 2003, Hendricks et al. 2005) and enhanced coagulation with $FeCl_3$ has been shown to remove 1.75 – 3.0 log of animal viruses. These examples suggest virus removals by MF can also be increased by incorporating coagulation pretreatment. Indeed, incorporating aluminum and iron coagulation prior to MF has been shown to remove > 4-logs of viruses from the feed water (Meyn et al. 2012, Shirasaki et al. 2009, Zhu et al. 2005a). In contrast to the substantial database available on NOM/DBP precursor removal by coagulation, much less information is available on its ability to control viruses. It is noted that previous work on this topic has largely focused on optimizing coagulation conditions to maximize virus removals and to evaluate bacteriophage surrogates for human viruses rather than rigorously elucidate virus

destabilization mechanisms.

An alternative to conventional chemical coagulation is the electrochemical dissolution of a sacrificial anode to directly release metal ion coagulant precursors (Chen 2004). Hydrogen gas evolution at the cathode induces floc-flotation, especially for higher current passage times (Chen et al. 2002, Gamage et al. 2012). Electrocoagulation and electroflotation units are compact and skid-mountable, and can be fully automated to reduce labor costs. Moreover, they reduce handling of corrosive chemicals, thus alleviating safety concerns, and have been shown to remove physical, inorganic, and organic contaminants (Cañizares et al. 2006, Chen 2004, Holt et al. 2005, Mansouri et al. 2012). In addition to enhancing filtered water quality, membrane fouling is also reduced by electrocoagulation/electroflotation pretreatment making an integrated electrochemical – MF process particularly attractive for small drinking water treatment plants (Gamage et al. 2012, Timmes et al. 2010). However, very limited information is available on their ability to remove viruses.

The objectives of this manuscript are to empirically demonstrate enhanced virus removals from surface water in a hybrid electrochemical – MF process and to systematically elucidate underlying destabilization/removal mechanisms. Since we have recently reported poor virus control by iron electrocoagulation in NOM-laden waters due to generation of soluble ferrous ions (Tanneru and Chellam 2012), only aluminum is considered herein. Atomic force microscopy (AFM) was used to quantify the adhesion forces between viruses covalently immobilized on AFM tips and surfaces of electrochemically generated flocs at different aluminum dosages. Direct evidence of virus enmeshment and sweep flocculation is presented using fluorescence microscopy and quantitative elution from flocs at high pH. The MS2 coliphage was used since it is a conservative surrogate for the removal of human viruses by coagulation (Mayer et al. 2008) and is commonly employed in environmental studies

(Abbaszadegan et al. 2007, Attinti et al. 2010, Zhu et al. 2005a).

3.2 Experimental Work

3.2.1 Source water

A sample from Lake Houston was employed in all experiments. Its pH, total hardness, calcium hardness, conductivity, dissolved organic carbon (DOC) concentration, absorbance at 254 nm and one cm path length, alkalinity, and turbidity were 7.7 ± 0.2, 53 ± 3 mg/L as $CaCO_3$, 47 ± 3 mg/L as $CaCO_3$, 322 ± 13 µS/cm, 5.2 ± 0.6 mg C/L, 0.145 ± 0.005 cm^{-1}, 70 ± 3 mg/L as $CaCO_3$, and 15 ± 2 NTU, respectively.

3.2.2 Electrocoagulation, electroflotation, and conventional chemical coagulation

Batch electrolysis was performed in a 450 mL plexiglass cylindrical cell with a 15 cm aluminum anode (Puratronic grade 99.9965% as Al, Alfa Aesar) and 316-stainless steel cathode. Electrolysis generated trivalent aluminum at nearly 100% efficiency demonstrated by quantitative agreement with 3-electron transfer in Faraday's law (See Appendix Figure 7.2A). Electrocoagulant dosages in the range 2-30 mg/L were obtained by adjusting the current passage time as given by Faraday's law at a fixed charge density of 20 mA/cm^2. Passivation was avoided by mechanically scrubbing the electrode before each experiment and periodic cleaning with HCl. Substantial flotation occurred for longer electrolysis durations (i.e. > 5 mg/L). For electrocoagulation experiments the entire cell contents were gently mixed and transferred to MF (direct filtration). In contrast, for electroflotation pretreatment, the MF feed water was obtained from near the bottom of the cell avoiding the carryover of floating flocs reducing the total mass of colloids sent to downstream MF. Chemical coagulation was performed by adding reagent grade aluminum sulfate to 1 L water in a programmable jar tester (Phipps & Bird). Flash mixing was performed at 495 s^{-1} for 1 minute and flocculation was performed at 32 s^{-1} for 30

minutes. Similar to electrocoagulation, no sedimentation was allowed and the entire suspension was microfiltered. All experiments were performed at pH 6.4 ± 0.2 since we have shown effective coagulation and flux enhancement at this value (Gamage and Chellam 2011, Gamage et al. 2012), and this pH is close to the point of minimum aluminum solubility at room temperature (O'Melia 1972).

3.2.3 Microfiltration

Unstirred, normal flow, dead-end MF was performed at 14 kPa using hydrophilic modified PVDF membranes (0.22 μm Durapore, GVWP02500, Millipore). Pretreated water was batch transferred to a pressurized feed tank and gently stirred to avoid floc settling. Membranes were first washed by passing 100 mL of PBS solution before filtering 150 mL of the feed suspension. Permeate water samples were collected after filtering 10, 50, and 150 mL of feed suspension across 4.1 cm^2 disc membranes to measure virus removal over the course of MF.

3.2.4 Virus propagation, purification, and enumeration

MS2 (ATCC 15597-B1; host *Escherichia coli* ATCC 15597) was propagated using the double-top agar layer technique. Organic carbon carryover was minimized and stock titer was increased to $O(10^{11})$ plaque forming units (PFU)/mL by successively precipitating with polyethylene glycol (PEG) and extracting with chloroform (Mayer et al. 2008). MS2 suspension was mixed with 9 % 8000 Da PEG and 1 M NaCl and stirred overnight at 4 °C. Following centrifugation (8000 g for 45 minutes), equal amounts of resuspended pellet (in 4 mL PBS) and chloroform were mixed and centrifuged (5000 g for 45 minutes). The purified stock was collected from the supernatant and prepared freshly before each experiment. The average hydrodynamic diameter of MS2 viruses was measured using dynamic light scattering to be 27 ± 3 nm and shown to be highly monodisperse by cumulant analysis (see Appendix Figure 7.3A).

3.2.5 Optical fluorescence microscopy and fluorescent tagging of viruses

Fluorescein isothiocyanate isomer 1 (FITC) was conjugated to phages by mixing 1.2 mL of MS2 stock in 0.1 M borate buffer (pH 9.2) with 21 mg FITC and 5 mL dimethylformamide and allowed to react overnight at 4 °C (Johnson and Spence 2010). The resulting mixture was then dialyzed for 5 days using a 12 kDa membrane against frequent changes of PBS solution. The greenish yellow tinge of the dialysate progressively reduced in intensity over time, demonstrating effective removal of excess/free dye from the labeled virus suspension. The dialysis end product was further purified by successive PEG precipitation and chloroform extraction. The number of FITC labels attached to each MS2 capsid was calculated to be approximately 3.8 on average, which is similar to that reported for the pp7 bacteriophage (Bakhshayeshi et al. 2011). Following electrolysis of Lake Houston water spiked with fluorescently labeled viruses, 25 µL of suspension was placed on a glass slide and imaged (Olympus BX51) at 100x magnification. Both bright field and fluorescence images (excitation at 494 nm and emission at 518 nm after 250 ms exposure) were obtained to interpret virus capture mechanisms.

3.2.6 Surface charge

The electrophoretic mobility of colloids was measured over a range of aluminum dosages by the electrophoretic light scattering technique using a He-Ne laser of 632.8 nm wavelength (Nicomp 380 ZLS, Particle Sizing Systems). Each sample was run in triplicate with an electrode spacing of 0.4 cm and field strength of 10 V/cm. The Smoluchowski equation was used to calculate the zeta potential.

3.2.7 Atomic force microscopy

Force spectroscopy measurements were performed using Si_3N_4 TR400PSA probes

(Olympus) with covalently immobilized viruses. The adhesion force between freshly prepared AFM tips modified with virus and the surfaces of flocs were measured in contact mode using a MFP-3D-SA instrument (Asylum Research, Santa Barbara). A previously reported protocol was used to immobilize viruses on AFM tips (Attinti et al. 2010, Vinckier et al. 1998). Prior to modification, the surface of AFM tips were cleaned by exposure to UV irradiation for 1 h. The probes were immediately placed in a solution of 3-aminopropyl-triethoxysilane (APTES, 5 %) in 95 % ethanol for 30 minutes, washed with 95 % ethanol/5 % water, and dried at 100 °C for 5 minutes (Attinti et al. 2010). Probes were coated with viruses by placing them in a 1:1 suspension of 2.5 % glutaraldehyde and MS2 stock for 1 hour during which time surface amino groups were covalently bonded to the tip (Vinckier et al. 1998). The cantilever spring constants were measured after functionalization by thermal tuning and found to be close to manufacturer reported values (ca. 0.02 N/m).

The virus(tip)-floc adhesion force was measured in solutions of varying aluminum dosage using a liquid sample holder to simulate the localized environment during electrocoagulation. Flocs were deposited on a membrane surface and placed in the fluid cell. Changes in solution chemistry with aluminum dosage during electrolysis were reproduced during AFM assays by adding 1-2 mL of permeate water obtained after MF of the corresponding suspension and equilibrating with the virus modified tip for 1 h. Hence, interaction forces between individual virions and flocs present at the end of electrolysis were accurately measured over a range of aluminum dosages by ensuring identical composition of intervening fluid during instrumental measurement and electrochemical pretreatment. The standard deviation reported for each adhesion force was calculated from two separate measurements (each comprising 1,500 pull-off curves at 6 different locations on the floc surface using different probes and floc samples for robust statistical sampling). Instrument settings included a 1 Hz scan rate, 1 µm/s

approach/retraction velocity, and 500 pN trigger point. A 1 s dwell time (i.e. tip-substrate contact time) was used to ensure adequate time for viruses immobilized on the AFM tip to bind to the floc surface.

3.3. Results and Discussion

3.3.1 Virus reductions in treated waters

As shown earlier (Madaeni et al. 1995, Tanneru and Chellam 2012, Zhu et al. 2005a), when no coagulant was added, virus reductions were only approximately 0.2-log demonstrating negligible sieving of the 27 nm virus by the microfilter nominally rated at 220 nm as seen in Figure 3.1.

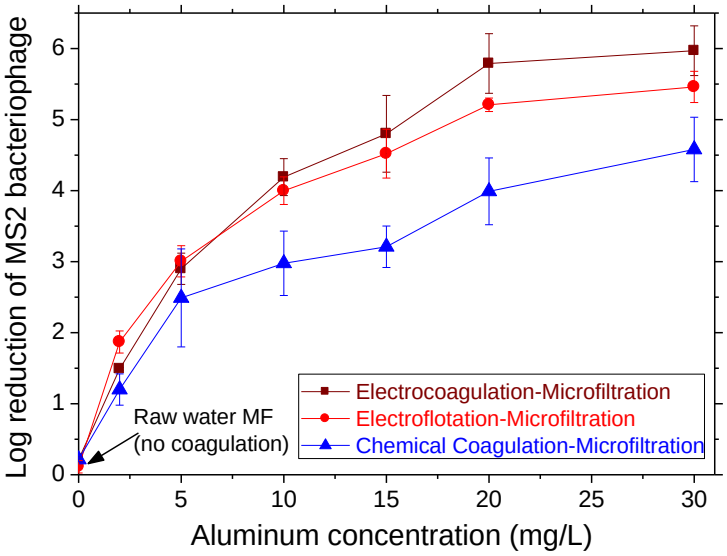

Figure 3.1. Virus control by combined coagulation pretreatment and MF. Data points are the average of 2 or 3 replicate experiments and error bars correspond to standard deviations of 6 – 9 plaque assays.

Coagulation pretreatment reduced virus passage, resulting in 2.5 – 3.0 log removal at an intermediate dosage of 5 mg/L. Separate control experiments demonstrated viruses were not inactivated by aluminum electrolysis and aluminum sulfate addition (see Appendix Figure 7.4A), unlike prehydrolyzed aluminum salts (Matsui et al. 2003, Matsushita et al. 2011). This also suggests negligible net production of chemical disinfectants/oxidants. Therefore, measured

reductions in virus concentrations in all our experiments were solely attributed to their removal and not their inactivation.Electrocoagulation and electroflotation pretreatment removed 5.5 – 6.0 logs of viruses at highest dosages evaluated compared with only 4.0 – 4.5 logs by chemical coagulation. Even at lower dosages, electrochemical treatment outperformed chemical coagulation. Enhanced virus control by electrochemical pretreatment is attributed to electrophoresis of negatively-charged phages that would have increased their concentrations in the proximity of the anode (note that the isoelectric point of MS2 is 3.9 and solution pH was 6.4; also see Figure 3.5c). Simultaneously, fresh aluminum precipitates are continually generated in this microenvironment by anodic dissolution. Additionally, hydrolysis of electrochemically generated Al^{3+} ions decreases the local pH, shifting the equilibrium towards other surface active dissolved monomers and polymers such as $AlOH^{2+}$, $Al(OH)_2^{+}$, $Al_2(OH)_2^{4+}$, $Al_3(OH)_4^{5+}$, etc (Baes and Mesmer 1976, O'Melia 1972). that can adsorb readily onto viruses. It is reasonable to suggest that the intermingling of locally high concentrations of viruses, dissolved hydrolysis products, and solid precipitates in the vicinity of the anode during electrolysis promoted destabilization, consequently increasing phage removal compared with conventional alum coagulation where concentrations are more uniform. Additionally, electrocoagulation was slightly more effective than electroflotation – notably at 20 and 30 mg/L dosages as seen in Figure 3.1. Insights into this observation were gleaned by monitoring viruses in the permeate water after filtering 2.4, 12.2, and 36.7 cm^3/cm^2 of pretreated waters per unit membrane area. Virus control by electrocoagulation–MF tended to improve with continued filtration of the suspension (Figure 3.2a), whereas it remained relatively constant following electroflotation–MF (Figure 3.2b). Therefore, the thicker cake layer formed during MF of electrocoagulated water appears to act as a dynamic membrane removing additional viruses as filtration progresses. Similar trends in virus removal have also been reported due to accumulation of bacteria or colloidal foulants on

microfilters (Madaeni et al. 1995, Shirasaki et al. 2008, Tanneru and Chellam 2012). As may be expected, this effect was more prominent at higher coagulant dosages corresponding to greater mass of precipitates (thicker cake and lower flux). Lower mass loading on the membrane following electroflotation resulted in the formation of thinner cakes making this effect less pronounced and allowing virus removal to be relatively constant over the duration of MF.

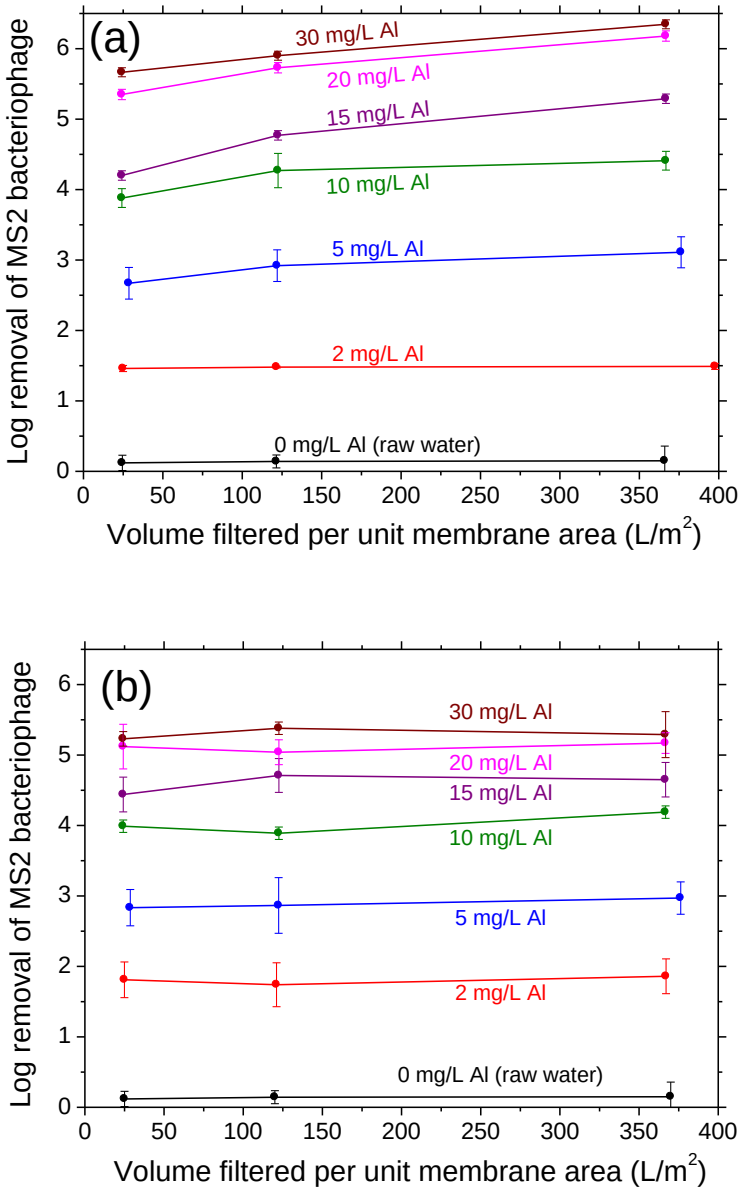

Figure 3.2. Virus removal over the course of MF following electrocoagulation pretreatment (a) and electroflotation pretreatment (b) at different dosages in the range 0 – 30 mg/L Al.

3.3.2 Enmeshment of viruses in aluminum precipitates

Direct evidence of virus enmeshment in precipitates was first obtained by epifluorescence microscopy. Figure 3.3 depicts corresponding bright field and fluorescence images of the raw water and electrocoagulated flocs in the range 0 – 30 mg/L incorporating FITC-labeled viruses.

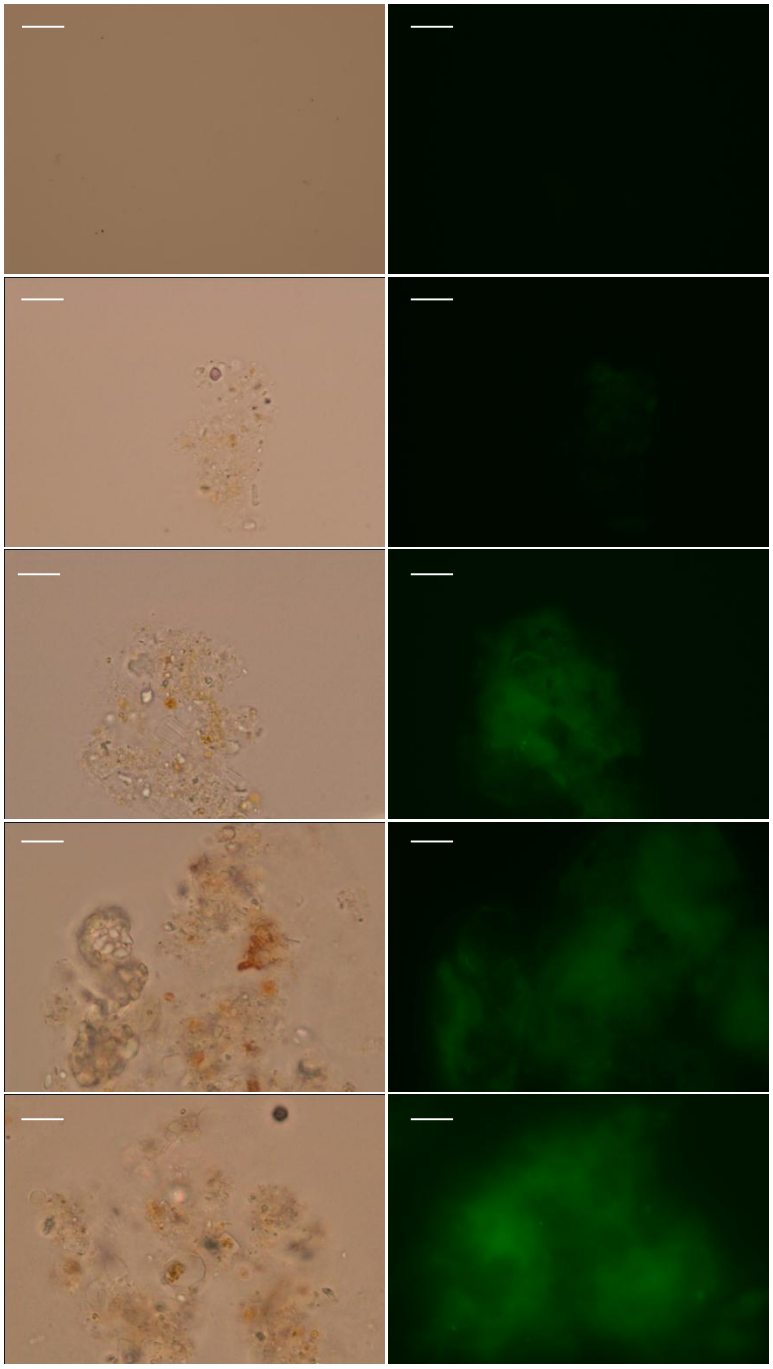

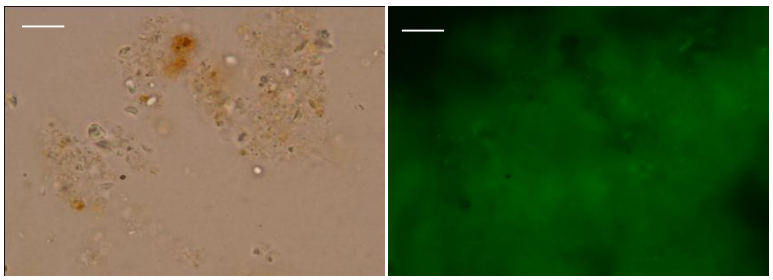

Figure 3.3. Bright field (left column) and corresponding epifluorescence images (right column) of electrocoagulated flocs incorporating FITC labeled viruses. Electrocoagulant dosages from top to bottom are 0, 2, 5, 10, 20 and 30 mg/L Al, respectively.

As seen qualitatively in Figure 3.3, the intensity increased with aluminum dosage. This was quantitatively shown by calculating the average fluorescence intensity over the entire floc area for 3 different images using Image J software (see Appendix Figure 7.12A). Hence, more viruses were captured with increasing dosage consistent with results summarized in Figure 3.1. X-ray diffractometry has shown that our experiments generate gelatinous and *fluffy* $Al(OH)_3$ polymorphs during electrocoagulation of surface water (Gamage and Chellam 2011). These amorphous precipitates could be initiated around virus nuclei. Additionally, floc growth during slow mixing sweeps out viruses from suspension, while more efficient virus capture occurs through the formation of bigger flocs at higher Al dosages (seen qualitatively in Figure 3.3) and reported quantitatively in our previous work (Gamage and Chellam 2011). As such, sweep flocculation of viruses onto $Al(OH)_3$ aggregates larger than the membrane pore size that are subsequently removed during MF are the dominant destabilization and removal mechanisms.

Secondly, after selected experiments, flocs were separated by centrifugation (10,000 g for 20 minutes) and the pellet dissolved in 6% beef extract after elevating the pH to 9.5 using NaOH (Clesceri et al. 2005, Tanneru and Chellam 2012). Flocs were visually observed to be completely dissolved at this pH, thereby releasing the captured viruses that were later enumerated along with the centrifuged supernatant. Representative results are summarized in Figure 3.4 for a relatively low (5 mg/L) and high (20 mg/L) dosage. Phage concentrations measured soon after adding MS2 stock suspension to the feed water are labeled “seeded feed”

water. The supernatant, which corresponds to uncoagulated or free viruses, contained significantly lower concentrations (e.g., 2.0 – 5.5 logs) than initial values representing only a very small fraction (< 0.7%) of the seed. Complementarily, nearly all the seeded viruses were present within the solid matrix (i.e., compare the 1st and 3rd bars in Figure 3.4), which confirmed that sweep flocculation was the dominant virus destabilization mechanism. The quantitative recovery of MS2 by elution using beef extract at alkaline pH demonstrates negligible inactivation as well as completely reversible attachment of viruses onto amorphous $Al(OH)_3$ precipitates during electro- and chemical coagulation. These results provide a mechanistic basis for the "Standard Method" SM 9510D for virus concentration by Al coagulation (Clesceri et al. 2005) and simultaneously demonstrate the superiority of electrochemical treatment over alum addition for such purposes (since it achieved higher removals as seen in Figure 3.1).

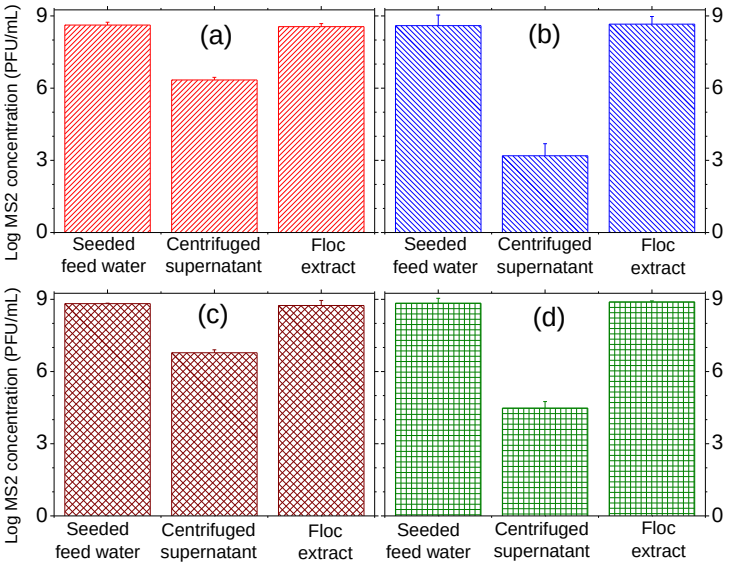

Figure 3.4. Quantitative recoveries of seeded viruses from flocs. Representative results for electrocoagulation (a and b) and chemical coagulation (c and d) are shown for 5 and 20 mg/L dosages, respectively. The error bars correspond to one standard deviation.

3.3.3 Evidence for virus adsorption onto flocs

Figure 3.5a depicts representative AFM force pull-off curves generated from the vertical retraction of virus-modified AFM tips from a contacting surface (i.e., floc interface) for a range of

aluminum dosages. The adhesion (or unbinding) force was calculated as a product of the maximum AFM tip deflection in the pull-off curve and the cantilever spring constant. Negligible virus(tip)-colloid interactions were observed for the raw water and lowest dosage investigated (2 mg/L), but adhesion forces progressively increased with electrocoagulant dosage. Pull-off curves at dosages > 5 mg/L exhibited multiple peaks during tip retraction from the floc surface, which is a characteristic trait when macromolecules (e.g. proteins, DNA, polymers, etc.) are used as functional moieties on AFM tips (Engel and Muller 2000, Lee et al. 1994, Oroudjev et al. 2002). These peaks correspond to multiple pull-off events that occur between protein segments on the virus that are bound to the surface of the floc (i.e., NOM and heterogeneous precipitates) as well as unbinding events pertaining to intraprotein bond formation and breakage as the virus is pulled (and stretched) during tip retraction. Multiple unbinding events have also been reported for rotavirus-NOM interactions (Gutierrez and Nguyen 2012) and may arise when virus-NOM bonds or calcium/aluminum bridges between virus and NOM are broken. This is indicative of covalent bonding between viruses and functionalized tips. Higher interaction forces also corresponded to unbinding events at greater tip-surface separation distances, presumably due to enhanced proximal binding of protein segments to the substrate. Experimental adhesion forces followed a log normal distribution in many, but not all cases. Representative histograms at various aluminum concentrations fitted with the log normal distribution are shown in Figure 7.5A a-d in appendix. In addition Table 7.1A directly compares the arithmetic mean and log normal distribution calculations of the average adhesion force (and standard deviation). The trend of increasing adhesion force with electrocoagulant dosage is consistent in both approaches (independent of the model) and we show the arithmetic mean.

The virus(tip)-floc adhesion force (Figure 3.5b) was calculated at different aluminum dosages by averaging a total of 3,000 individual pull-off curves taken from two separate

measurements at 12 different locations on the floc surface for each dosage. Low adhesion forces were measured between the virus-coated AFM tip and colloids in the raw water (0 mg/L) as well as flocs formed at 2 mg/L Al dosage (Figure 3.5b). This is attributed to repulsion between viruses and flocs, which are both negatively charged under these conditions as shown in Figure 3.5c. Progressive charge neutralization with increasing Al dosage was consistent with adsorption of $Al(OH)_2^+$, the predominant hydrolysis product at pH 6.4 during our experiments. The ζ potential (or approximate surface charge) of viruses and flocs effectively approached 0 near 10 mg/L and did not increase substantially even as more Al was electrolyzed (i.e., limited restabilization even upon overdosing). Hence, electrostatic interactions appear to explain the monotonic increase in adhesion forces between viruses and flocs as more and more electrocoagulant was added.

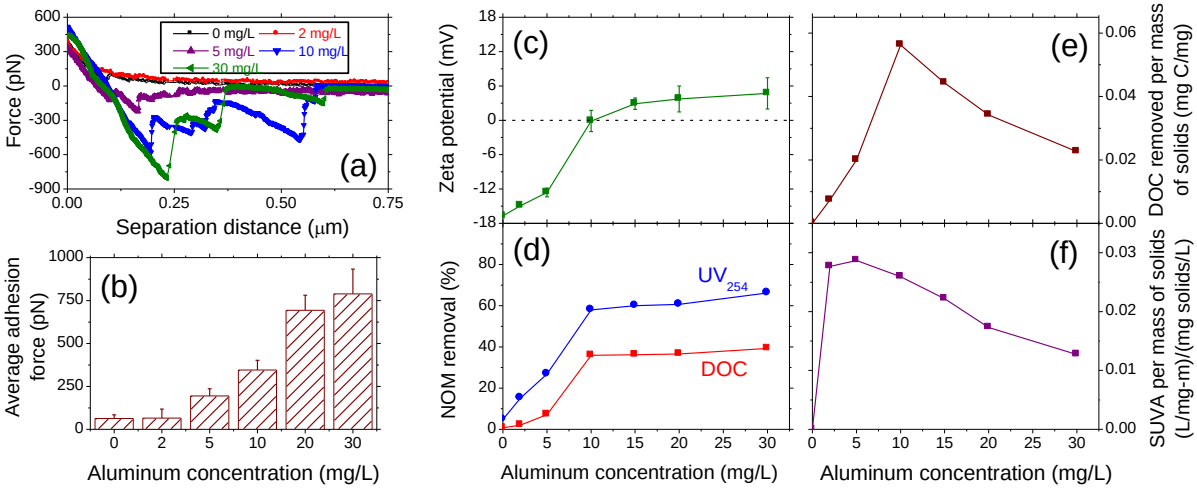

Figure 3.5. (a) Representative AFM pull-off curves (b) Average adhesion forces between viruses and surface of flocs (c) Progressive neutralization (d) UV254 absorbing substances compared with DOC. (e) NOM removal (f) Changes in relative hydrophobicity of flocs.

Concurrent with increasing virus removal, NOM uptake by the flocs and the mass of solids precipitated also increased with electrocoagulant dosage. As shown in Figure 3.5d, similar to alum coagulation, electrocoagulation preferentially removed humic substances and higher molecular weight components of NOM, as evidenced by the higher removal of UV absorbing

substances than DOC. Even though NOM concentration in the permeate water decreased progressively as more and more aluminum was added, a maximum in NOM removal was observed at 10 mg/L Al (Figure 3.5e). Here we express the amount of NOM adsorbed onto the flocs normalized to cake mass measured after filtering 367 L/m^2 pretreated water. This was due to DOC removal reaching the point of diminishing returns (White et al. 1997) at an electrocoagulant dosage of 10 mg/L (see Figure 3.5d) whereas the mass of solids precipitated continued to increase with dosage (Gamage and Chellam 2011). Effective removal of aromatic (i.e., humics) NOM moieties was verified by the specific UV absorbance (SUVA, absorbance at 254 nm for 1 m path length divided by the DOC concentration expressed in mg/L). Figure 3.5f depicts the SUVA of NOM captured by the flocs normalized to cake mass measured at the end of the experiment (cumulative filtration of 367 L/m^2), which peaked at an intermediate Al concentration (ca. 5 mg/L). These observations are consistent with floc surfaces becoming more hydrophobic at low dosages, which decreased as more coagulant was added, but were always more hydrophobic than raw water colloids. NOM-coated flocs can more strongly interact with viruses mediated by calcium ions present in the source water or hydrolyzed aluminum species following electrolysis. Therefore, hydrophobic interactions (Lee et al. 2008) would also have contributed to changes in virus adhesion force with Al dosage, potentially due to formation of Ca/Al inner sphere complexes with COO^- groups located on the MS2 capsid surface (primarily Asp and Glu amino acids).

Higher average adhesion forces measured for dosages ≥ 5 mg/L during electrocoagulation pretreatment are also consistent with the observed dynamic membrane effect (Figure 3.2a). In brief, freely suspended and uncoagulated viruses appear to have interacted more strongly with the relatively thick cake as more and more solids were deposited on the microfilter, which ultimately increased their removal as filtration progressed.

3.4 Implications for water treatment

Unlike iron (Tanneru and Chellam 2012), aluminum electrocoagulation and electroflotation outperformed conventional alum coagulation as a highly effective and facile method to remove viruses. These pretreatment processes also significantly reduce microfilter fouling (Gamage and Chellam 2011, Gamage et al. 2012) and remove a host of other contaminants, which include (but are not limited to) suspended solids, bacteria, organic compounds, algae, and metals, from municipal and industrial wastewaters (Cañizares et al. 2006, Chen 2004). Since coagulant dosage can be adjusted by simply changing the current density, rapid fluctuations in feed water quality can be easily handled. Their operational advantages coupled with their compactness make integrated electrochemical – MF processes very well suited for many practical applications, including treatment in small-scale drinking water plants, portable units to supply potable water during emergencies, and water and wastewater treatment in military forward operating bases (Holt et al. 2005). However, larger-scale testing and engineering cost comparisons are necessary before electrochemical processes can be recommended over conventional chemical coagulation for full-scale applications.

Two important advantages of electroflotation over electrocoagulation are that it inherently comprises an additional microbial barrier (floc flotation) without adding a separate unit process and it achieves higher MF flux (Gamage et al. 2012). Therefore, on-going work is focused towards optimizing bubble number and size to collectively increase collision frequency and solids removal. We are also working to simultaneously maximize removal of turbidity, microorganisms, as well as NOM and DBP precursors (similar to “enhanced coagulation”). An important impediment to widespread implementation of these technologies is passivation, which reduces Faradaic coagulant dissolution due to the accumulation of corrosion products and macromolecules on electrode surfaces or formation of an oxide film (Mouedhen et al.

2008). On the other hand, pitting can lead to super Faradaic dissolution. In either case, unreliable coagulant dissolution is detrimental to electrochemical cell performance and necessitates system downtime for periodic electrode cleaning. Further, the kinetics of these phenomena cannot be predicted *a priori* during treatment of natural waters, which necessitates long-term site-specific evaluations.

Chapter 4. Simultaneous inactivation and coagulation of viruses during aluminum electrochemical treatment

4.1 Background

This research is a collaborative effort between the Centers for Disease Control and Prevention (CDC) and University of Houston. In this work, we rigorously analyzed inactivation mechanisms of viruses during aluminum electrocoagulation of virus laden saline waters. All experiments were performed at University of Houston and our collaborator, Dr. Jothikumar Narayanan analyzed RNA degradation using the quantitative reverse transcription polymerase chain reaction (q-RT-PCR).

4.2 Introduction

Electrocoagulation, the *in situ* addition of metal-ion coagulants by anodic dissolution, has been gaining interest for small-scale water and wastewater treatment because it can be automated, is portable, and reduces handling of corrosive chemicals (Cañizares et al. 2007, Moreno C et al. 2009). Although a large body of literature has documented its capability to remove physical and chemical constituents of the feed water (Chen 2004, Dubrawski and Mohseni 2013, Li et al. 2012), very little information is availability on its ability to control viruses. Iron electrocoagulation can chemically inactivate viruses but its efficacy of virus control is poor because soluble ferrous iron is Faradaically generated rather than insoluble ferric iron necessary for effective coagulation (Tanneru and Chellam 2012). In contrast, aluminum electrocoagulation effectively destabilizes viruses in surface waters by a combination of sweep flocculation and charge neutralization even achieving 5.3logs (99.9995%) removal at a dosage of 20mg/L with no measurable inactivation (Tanneru et al. 2013). Electrolysis using inert (non-sacrificial) anodes has been shown to generate oxidants such as reactive oxygen species and chlorine, which can disinfect bacteria (Bensalah and Abdel-Wahab 2013, Jeong et al. 2009) and viruses (Drees et al.

2003) in the absence of coagulation. To our knowledge, the simultaneous inactivation and electrocoagulation has not yet been rigorously investigated even though it is expected to enhance virus control compared with either inactivation or coagulation alone.

The objectives of this work are to empirically demonstrate virus inactivation during electrocoagulation using a sacrificial aluminum anode and to elucidate associated inactivation mechanisms. Loss of infectivity of the F-specific ssRNA coliphage MS2 was monitored in model NaCl solutions by the plaque assay and compared with genomic damage measured by the quantitative reverse transcription polymerase chain reaction (q-RT-PCR). Free chlorine is shown to be generated during electrolysis and evidence for oxidative capsid modifications is provided using attenuated total reflectance – Fourier transform infrared spectroscopy (ATR-FTIR). Coagulation is shown to slow down disinfection kinetics due to a combination of aggregation and shielding by aluminum flocs.

4.3 Experimental Methodology

4.3.1 Electrocoagulation

Batch electrolysis was performed in a 450mL cylindrical Plexiglass cell with an annular electrode configuration; 15cm aluminum anode (Puratronic grade 99.9965% as Al, Alfa Aesar) surrounded by a perforated 316-stainless steel cathode. Prior to electrolysis, the cell was soaked overnight in free chlorine (≥ 5mg/L), rinsed 5-times with nanopure water, and thoroughly air dried to remove any chlorine demand. Aluminum in the range 0-30 mg/L was dosed at a charge density of 20mA/cm^2 by adjusting the current passage time according to Faraday's law. The anode was mechanically scrubbed before each experiment and periodically cleaned with HCl to avoid passivation. Most experiments were performed at pH 6.2±0.2 with selected few at 8.2±0.2. Electrolysis did not appreciably increase the pH, which remained within 0.2 units of the

initial value.

4.3.2 Disinfection protocol

Appropriate concentrations of ACS grade NaCl (1mM, 10mM, and 100mM) and $NaHCO_3$ were dissolved in nanopure water. Glassware was made to be chlorine demand free by overnight soaking in free chlorine (≥ 5mg/L), rinsing 5-times with nanopure water, wrapping in aluminum foil and baking at 400°C for 3h. Free chlorine was measured using N,N-diethyl-*p*-phenylenediamine (DPD) colorimetric method using a DR-4000 spectrophotometer (Hach company) (Cromeans et al. 2010, Gao et al. 2010, Kitajima et al. 2010, Sano et al. 2010). A sample was collected after seeding (spiking) the feed water with virus stock and before electrolysis that served as the initial concentration. Electrolysis was performed for a predetermined duration (using Faraday's law) to dose the appropriate amount of aluminum. The entire cell contents were then stirred slowly in the dark for 5h and hourly samples were collected. Sodium thiosulfate (50mg/L) was added to each sample to quench free chlorine and halt disinfection. Viruses associated with the flocs were separated by centrifugation (10,000g for 20 minutes) and dissolved in 6% beef extract (after elevating the pH to 9.5). Virus concentrations in supernatant and flocs were enumerated. Inactivation values reported were calculated using virus concentrations in both supernatant and the flocs.

4.3.3 Virus propagation, purification, and enumeration

MS2 (ATCC 15597-B1; host *Escherichia coli* ATCC 15597) was propagated using the double-top agar layer technique. Its genome is 3569 nucleotides long having 180 copies of the coat protein and only one copy of the A-protein. MS2 was selected because it is similar in size, shape, and nucleic acid composition to hepatitis A and polio virus and is commonly employed in environmental studies. Organic carbon carryover was minimized and stock titer was increased to

$O(10^{11})$ plaque forming units (PFU)/mL by successively precipitating with polyethylene glycol and extracting with chloroform (Mayer et al. 2008). MS2 suspension was mixed with 9% 8,000Da polyethylene glycol and 1M NaCl and stirred overnight at 4 °C. Following centrifugation (8,000g for 45min), equal amounts of resuspended pellet (in 4mL PBS) and chloroform were mixed and centrifuged (5,000g for 45min). The purified stock was collected from the supernatant and prepared freshly before each experiment.

4.3.4 Extraction of viral RNA and q-RT-PCR protocol

Quantitative real time PCR was performed by Dr. Narayanan of CDC on native viruses and on inactivated viruses to determine the amount of intact viral RNA. To avoid RNA degradation, equal volumes (400µl) of sample and UNEX lysis buffer (Hill et al. 2007) were mixed thoroughly and stored at room temperature until extraction. A sample volume of 700 µl was passed through a silica spin column (Omega Biotek, Norcross) by centrifugation (10,000 g for 1 min). The silica column was washed twice (once with 500 µl of 100% ethanol and then with 500 µl 70% ethanol). The column was centrifuged at 10,000 g for 1 min after each wash and followed by one final centrifugation again to remove any excess ethanol. The column was then transferred to a clean microfuge tube. Nucleic acid was eluted by adding 70µl Tris-EDTA (TE) buffer and centrifugation (10,000 g for 1min).

MS2 RNA was detected by a one-step q-RT-PCR assay. This assay reported earlier enables sensitive detection of MS2 (O'Connell et al. 2006). Following are the primers and probe sequences required. The TaqMan assay amplified a 77 bp fragment with a forward primer 632F, GTCGCGGTAATTGGCGC, reverse primer 708R, GGCCACGTGTTTTGATCGA and a fluorescent labeled probe 650P, 5'-AGGCGCTCCGCTACCTTGCCCT-3', labeled on the 5' end with FAM (6-carboxy-fluorescein) and 3' end with the black hole quencher (BHQ). A 20µl TaqMan reaction mixture for the assay consists of 5 µL of 4X TaqMan Fast Virus 1-Step Mastermix (Life

Technologies, Carlsbad, CA), 0.8µL primers (250nM), 1µL probe (100nM), 10.4 µL of nuclease free water and a 2µL of sample RNA. All q-RT-PCR reactions were performed on an ABI 7500 system (Applied Biosystems) with slight modification to PCR amplification protocol. Initially reverse transcription step was performed at 50°C for 5min, denaturation at 95°C for 20sec to obtain complementary DNA (cDNA). PCR amplification was performed on cDNA and it consists of 45 cycles of denaturation at 95°C for 5sec, followed by annealing and fluorescence acquisition at 60°C for 30 sec. Cycle threshold (C_T) values were collected at the end of each run and cycle threshold (C_T) values >45 were classified as undetectable. Two replicates of each sample extract (2 µL) were assayed by q-RT-PCR. All q-RT-PCR runs included a MS2 RNA positive control and a negative control (no-template negative control). The negative control did not show any amplification demonstrating high specificity. The C_T values, the fractional cycle number reported by real-time PCR instruments indicates the point at which the fluorescence associated with a positive DNA amplification reaction increases beyond the threshold fluorescence associated with negative reactions.

The sensitivity of TaqMan assays was evaluated using 10 fold serial dilutions of RNA extracted from MS2. A sample of known concentration was used to construct the standard curve. By running standards of varying concentrations, the standard curve is plotted and the results are extrapolated for unknown samples. A 2 µl RNA per 20 µl reaction was added to express in PFU/mL. For reproducibility, duplicate samples were tested at each dilution. The detection limit was established based on the highest dilution with a positive signal.

4.3.5 ATR-FTIR spectroscopy

ATR-FTIR spectra of native and inactivated viruses were collected by placing them on the transmissive Ge window of a Nicolet iS10 spectrometer equipped with an Ever-Glo MIR source, DTGS detector, KBr beam splitter and Omnic 8.5 software. Spectra reported herein are averages

of six measurements from 512 co-added scans collected from 650 to 4,000cm^{-1} at 4cm^{-1} resolution and a zero filling factor of 1 using a Happ-Genzel apodization and Mertz phase correction. The resolution in the amide I and II regions (1700-1500cm^{-1}) was enhanced by taking the second derivative of the original spectra after nine-point Savitzky-Golay smoothing to deconvolute overlapping peaks. Maximum absorption intensity, band frequency, and bandwidth, obtained from the second derivative spectra, were used to curve-fit the original spectra by assuming a Gaussian-Lorentzian shape for the amide I band and for each peak. This procedure gave insights into secondary structures of capsid proteins.

4.4 Results and Discussion

4.4.1 Virus reductions (removal and inactivation)

Since aluminum dissolution quantitatively obeyed Faraday's law, electrolysis was performed for the requisite time necessary to generate the desired coagulant dosage (193s, 386s, and 579s, respectively for 10mg/L, 20mg/L, and 30mg/L) (Gamage and Chellam 2011, Tanneru et al. 2013). The entire suspension was then flocculated for 5h and 40mL samples were collected at hourly intervals starting immediately after electrolysis, which were centrifuged (10,000g for 20min) to separate the solids.

The pellet was dissolved in 6% beef extract at a pH of 9.5 to measure plaque counts, i.e. infective viruses sorbed onto flocs during electrochemical treatment. Plaques were also measured in the supernatant corresponding to the infective viruses remaining in the water column. Results from these and two control experiments are summarized in Figure 4.1 where within each sub-figure one set of bars on the left hand side correspond to viruses sorbed onto the flocs and the second set of bars on the right hand side correspond to viruses in the water column. Other controls are depicted in the appendix (See Appendix Figure 7.15A). The

horizontal dashed lines are the measured range (1-standard deviation) of initial virus concentrations in the feed water ($O(10^{8.5})$).

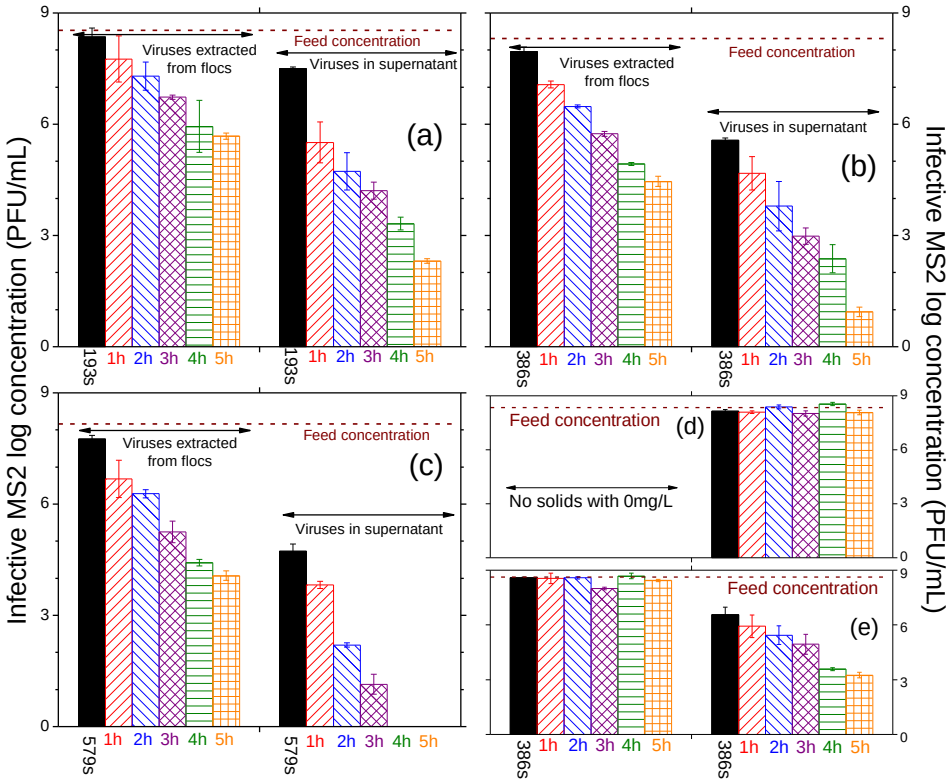

Figure 4.1. Infective viruses extracted from the flocs and in the supernatant after centrifugation at different aluminum dosages; (a) 10mg/L (b) 20mg/L (c) 30mg/L (d) no electrolysis (0mg/L) negative control (e) control with 20mg/L and thiosulfate quenching.

Figure 4.1 a, b, and c correspond to electrocoagulant dosages of 10mg/L, 20mg/L, and 30mg/L respectively from which two important trends can be discerned. First, for all three doses at each time point, virus concentrations in extracted flocs were higher than the corresponding supernatant by several orders of magnitude demonstrating highly effective electrocoagulation of viruses, i.e. uptake of viruses onto $Al(OH)_{3(s)}$ precipitates (Tanneru et al. 2013). Second, for any given dosage, i.e. duration of electrolysis, the number of infective viruses in the flocs and the supernatant decreased monotonically over time suggesting inactivation. Note that Figure 4.1d demonstrates that viruses were not lost on the electrochemical cell components since in the absence of electrolysis viruses were quantitatively recovered from the aqueous phase for

the entire 5h duration of experimentation. Figure 4.1e is another control experiment where a chlorine quenching agent (sodium thiosulfate) was initially added along with viruses to the feed water prior to electrochemically adding 20mg/L of aluminum. Corresponding data for pH 8.2 is shown in Figure 7.16A. In all cases, the spiked viruses were quantitatively recovered at each time point (constant magnitude of the left set of bars in Figure 4.1d over time equaling the feed concentration) demonstrating highly effective uptake of viruses by $Al(OH)_{3(s)}$ and that our extraction and plating protocols were accurate and reproducible. Therefore, the reducing concentration of infective viruses in the solid phase in Figure 4.1a, b, and c over time can be attributed to inactivation by free chlorine (discussed in more detail later). The monotonic decrease in supernatant concentrations in Figure 4.1e signifies progressive uptake of viruses on flocs over the duration of our experiments and is not the focus of this manuscript.

Supernatant concentrations from Figure 4.1a, b, and c were normalized by initial concentrations in the feed water to calculate combined removal and inactivation of viruses and shown in Figure 4.2a. As expected, cumulative virus control increased with dosage even reaching > 8-log removal/inactivation for 30mg/L at ≥ 4h contact time. As reported recently by us, virus removal during aluminum electrocoagulation is primarily due to sweep flocculation (Tanneru et al. 2013). Adsorption of hydrolyzed aluminum species and charge neutralization contributed secondarily as evidenced by decreasing zeta potential of viruses as more and more aluminum was added (see Appendix Figure 7.18A).

The sum of viruses extracted from the flocs (by high pH dissolution onto beef extract) and in the supernatant represents the total number concentration of infective viruses in each sample. Note that in all cases, viruses sorbed on the solids overwhelmed free viruses in the aqueous phase due to highly effective electrocoagulation.

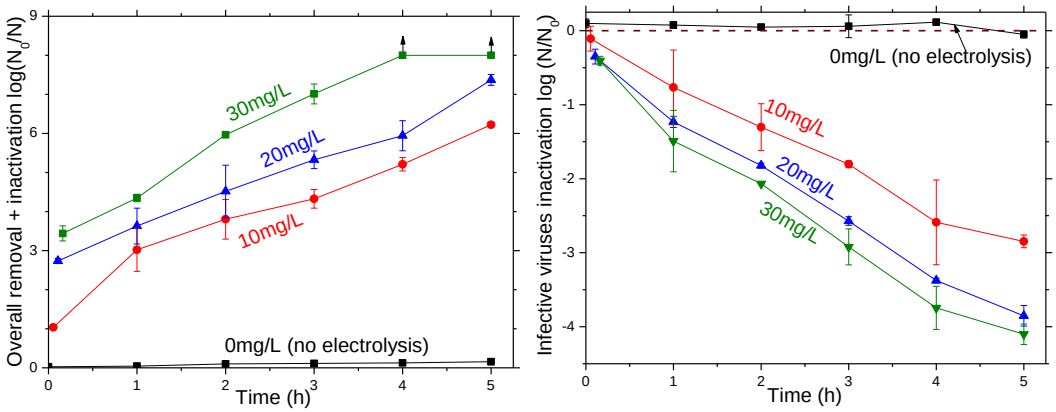

Figure 4.2. (a) Cumulative virus reductions (i.e., removal + inactivation) by electrocoagulation. Points are the average of 2 or 3 replicates (b) Inactivation of viruses during electrocoagulation representing free viruses and those encapsulated in aluminum flocs.

Nevertheless, strictly speaking the total number of infective virions is obtained by adding the solid and liquid phase concentrations. This was normalized by the measured initial concentrations (before starting electrolysis) to calculate virus inactivation as shown in Figure 4.2b. Infective virus concentrations quantified by the plaque assay decreased monotonically over time reaching 2.5-log inactivation for the experiment corresponding to 193s electrolysis time (10mg/L aluminum dosage) after flocculation for 5h. Higher levels of inactivation were measured for prolonged durations of electrolysis (i.e., higher electrocoagulant concentrations).

4.4.2 Further evidence of chlorine-induced virus inactivation during electrocoagulation

As discussed earlier and shown in Figure 4.3, infective virus concentrations remained unchanged over the entire duration of experimentation when thiosulfate, a chlorine quenching agent, was added before initiating electrolysis (black line). Similar results were obtained when electrolysis was performed in the absence of chloride ions, i.e., only using buffer (green line). Additionally, inactivation was halted when thiosulfate was added after 1h of flocculation (red line). Inactivation was also monitored by externally adding free chlorine to viruses electrocoagulated with buffer only and no NaCl (purple line) at 20mg/L dose. Adding free chlorine at a concentration similar to what was electrochemically generated (~0.06mg/L)

resulted in very similar inactivation profiles and rates to what was observed during electrochemical treatment (blue line). These controls provide additional evidence for the role of chlorine in inactivating viruses during electrocoagulation of saline waters.

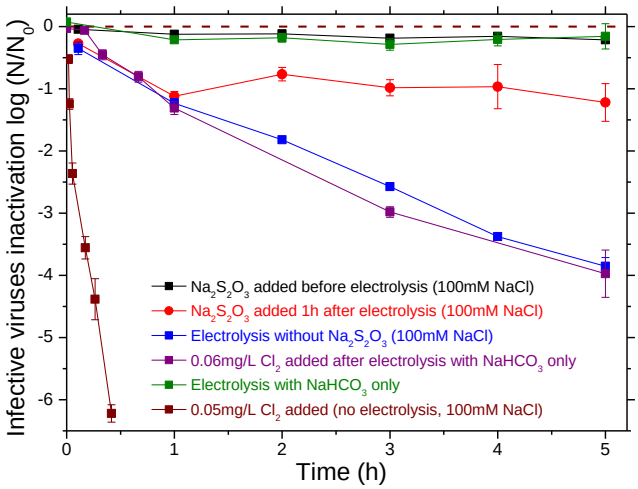

Figure 4.3. Evidence of chlorine-induced inactivation. Results from numerous control experiments are shown along with data from electrocoagulation at 20mg/L.

Table 4.1 summarizes average free chlorine concentrations and inactivation rate constants measured under different NaCl concentrations and electrolysis durations (Al concentrations) at pH 6.2. Limited experiments were also performed at pH 8.2. Chlorine consumption was <30% over 5h in all cases and was mainly attributed to losses arising from surface reactions during diffusion within the floc network (Boardman and Sproul 1977, Cromeans et al. 2010, Dietrich et al. 2003). In the absence of electrolysis and in the absence of NaCl, chlorine was not generated and viruses were not inactivated. For a fixed electrolysis time of 193s, increasing amounts of chlorine were generated for more saline solutions resulting in faster inactivation kinetics (See Appendix Figure 7.17A). Increasing electrolysis time for a fixed NaCl concentration also generated more chlorine and enhanced virus inactivation rates. As seen, free chlorine in the range 0.010 – 0.086mg/L was directly measured in electrolyzed suspensions confirming its role in virus inactivation during electrocoagulation at pH 6.2. Changing the pH from 6.2 to 8.2 did not impact free chlorine generated but significantly reduced inactivation

rates demonstrating that the hypochlorite anion is a very weak disinfectant compared to hypochlorous acid (White 2010).

Table 4.1. Free chlorine concentrations and corresponding first inactivation rate constants under different electrolysis conditions.

Electrolysis time (s)	NaCl conc. (mM)	pH	Al conc. (mg/L)	Chlorine conc. (mg/L)	First order inactivation rate constant (h^{-1})
0	100	6.2	<0.1	<0.010	Control, no inactivation
386	0	6.2	20.74±0.68	<0.010	Control, no inactivation
193	1	6.2	11.15±0.42	0.010±0.000	0.041±0.029
193	10	6.2	10.61±0.25	0.013±0.005	0.388±0.060
193	100	6.2	10.55±0.43	0.025±0.005	0.565±0.029
386	100	6.2	20.33±0.92	0.065±0.007	0.715±0.030
579	100	6.2	31.17±1.48	0.086±0.013	0.760±0.054
193	100	8.2	10.21±0.66	0.022±0.004	0.262±0.018
386	100	8.2	22.05±0.56	0.068±0.006	0.270±0.024
579	100	8.2	31.89±0.79	0.082±0.009	0.378±0.034

4.4.3 Virus inactivation rates reduced following aggregation and uptake on flocs

Another control experiment was performed where free chlorine was externally added to viruses suspended in a 100mM NaCl solution without electrolysis (brown line in Figure 4.3). Even though chlorine concentrations were similar, viruses were extremely rapidly inactivated in this experiment compared to when chlorine was electrochemically generated along with $Al(OH)_{3(s)}$ (blue line in Figure 4.3) and when chlorine was externally added to viruses electrocoagulated in the absence of NaCl (purple line in Figure 4.3). The presence of solids (20mg/L Al) reduced the first order inactivation rate approximately by a factor of 18 (12.9 to 0.715 h^{-1}). Hence, viruses were more resistant to inactivation following aggregation and encapsulation in the flocs potentially due to (a) shielding from chlorine (Hejkal et al. 1979, Ohgaki and Mongkonsiri 1990) and (b) consumption and increase in time taken to reach viruses as chlorine diffuses through the porous flocs (Boardman and Sproul 1977, Cromeans et al. 2010, Dietrich et al. 2003). Lower rates of inactivation have also been reported for viruses in the presence of solids such as clay,

bacterial debris, and natural colloids (Sobsey et al. 1991, Stagg et al. 1977, Young and Sharp 1977) confirming our observations.

4.4.4 Oxidative transformations of virus proteins and nucleic acids

Chlorine is highly reactive with amino acids such as Cys, Met, Lys His, Trp, Tyr oxidizing them to form oxyacids (Deborde and von Gunten 2008), nitriles (Pereira et al. 1973), aldehydes (Hazell et al. 1994), and ketones (Hazell et al. 1994, Thomas et al. 1986). Since these amino acids constitute 7.7% of the coat protein and 11% of the A-protein of MS2, mid infra-red (1800-1500cm^{-1}) spectra of native and inactivated viruses were collected to obtain evidence for the formation of these products (Figure 4.4 and Table 7.2A). ATR-FTIR spectrum of the native MS2 was obtained after freeze drying 100mL of stock suspension. For destabilized viruses, the entire electrocoagulated suspension was centrifuged, the pellet dried at room temperature, and directly placed in the transmissive Ge window. Next, the spectrum of "pure" $Al(OH)_{3(s)}$ was obtained after electrolyzing pH-adjusted nanopure water. This spectrum was background subtracted from that of electrocoagulated viruses to obtain the spectrum of electrochemically inactivated MS2 phages (red line in Figure 4.4). Free viruses were also inactivated with an equivalent free chlorine dosage (~0.06mg/L) and its spectrum was obtained by placing them on a clean polished silicon wafer (green line in Figure 4.4).

Second derivative analysis qualitatively revealed the appearance of new peaks in the 1710-1760cm^{-1} regions for inactivated viruses (e.g., summarized in Table 4.2 at 1758 and 1767cm^{-1} in Figure 4.4), indicating the formation of oxyacids and aldehydes. Additionally, several peaks associated with aldehydes and ketones intensified in the spectrum of inactivated viruses with respect to the native phages as evidence for the chlorine-induced oxidation of capsid proteins (Pattison and Davies 2001).

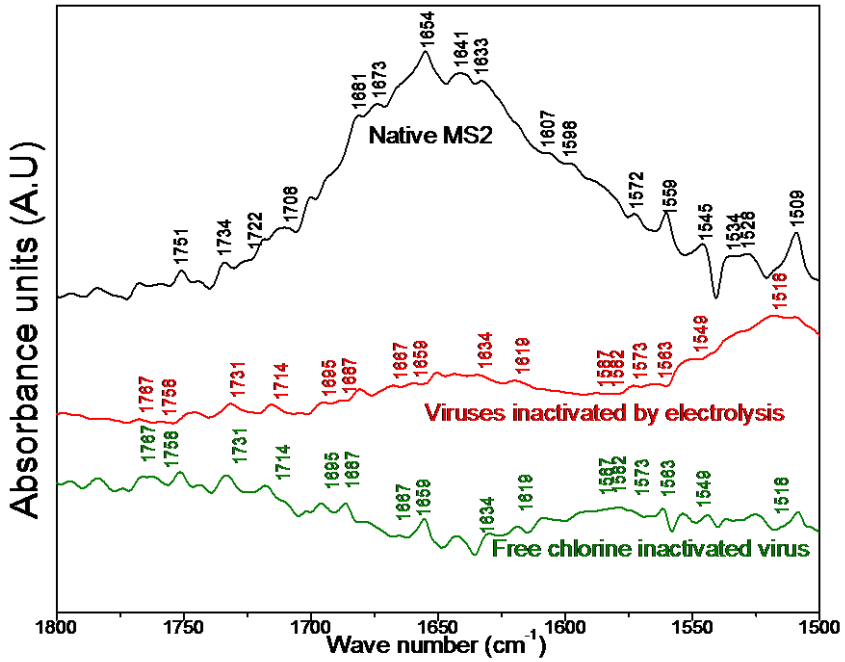

Figure 4.4. ATR-FTIR spectra of native and inactivated viruses.

Relative changes in peak areas in the amide I region (1700-1600 cm^{-1}) were used to deduce alterations to secondary structures (peak fits shown in Figure 7.21A). α and 3-turn helices, inter- and intra-molecular β structures, random coils, and amino acid side chains in inactivated viruses all decreased with respect to native viruses. Changes in helical and β-structures are consistent with chlorine reactions with α-amino acid side chains containing Lys (1626-1629cm^{-1}), Trp (1622cm^{-1}) and Tyr (1614-1621cm^{-1}) (Barth 2000, Pattison and Davies 2001) to form unstable chloramines and chlorotyrosine. The A-protein also appears to have been modified evidenced by changes in N-H stretching bands for Met (1615cm^{-1}), Cys (1677cm^{-1}-1650cm^{-1}), His (1631cm^{-1} and 1575 cm^{-1}), Tyr (1614-1621cm^{-1}), and Trp (1622 cm^{-1}) (Sigstam et al. 2013). Peak shifts and changes in peak areas in IR spectra indicate chlorine-induced morphological disordering and deformation of the capsid (Badireddy et al. 2012, Hotze et al. 2009, Kuzmanovic et al. 2006). Further, since chlorine can also oxidize RNA components, genomic degradation was investigated in detail using q-RT-PCR as discussed next.

Table 4.2. Change in peak areas of amide I and amide II bands of MS2 in mid infrared regions. This region specifically represents vibrational frequencies associated with protein secondary structures

Wave number (cm^{-1})	Contributors	Native viruses	Electrocoagulated viruses	Free chlorine inactivated viruses
1733-1710	Carbonyl groups, oxyacids, aldehydes and ketones	1.43	12.76	39.9
1690-1680	Turns and bends	8.96	3.25	11.5
1680-1660	Higher frequency of β structure	11.28	2.91	1.94
1666-1659, 1657-1648	'3-turn' and α-helix	8.9	4.9	4.2
1650-1645	Random coil	21.32	6.02	4.21
1640-1630 ,1680-1690	Intra-molecular β-structure	25.8	6.23	3.98
1625-1610, 1695-1670	Inter-molecular β-structure	11.34	8.64	8.64
1610-1600	amino acid side chain	25.5	Interpreted as peak shift	5.44
1550-1510	N-H Secondary amide, aldehydes, ketones	2.95	49.78	45.9

4.4.5 Genome damage also contributed to inactivation

Figure 4.5 summarizes changes in the MS2 genome following various electrolysis times (aluminum dosages) at different ionic strengths corresponding to different free chlorine concentrations. MS2 genomic damage occurred rapidly in the first hour in the chosen amplicon region and then started to tail as reported recently (Lim et al. 2010) and similar to animal viruses (Jin et al. 2013, Thurston-Enriquez et al. 2003) despite generation of only small amounts of free chlorine, and shielding by solids, and aggregation.

Initial faster kinetics of RNA degradation followed by slower rate at longer times suggests a shift in inactivation mechanisms. This behavior is attributed to reactions of RNA and nucleotides with free chlorine that generate stable organic chloramines, a much weaker disinfectant along with other compounds such as 5-chlorocytosine, 5-chlorouracil, 8-chloroadenine and 8-chloroguanosine (Gould et al. 1984, Hawkins and Davies 2002).

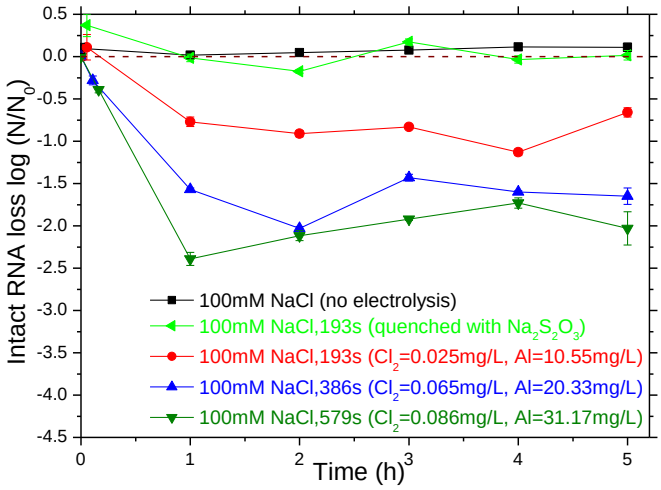

Figure 4.5. Comparison of genomic damage for different inactivation conditions (electrolysis time and aluminum/solids concentrations) at pH 6.2 ± 0.2.

As seen in Figure 4.2b and Figure 4.5, the plaque assay gave similar results to q-RT-PCR in the first hour for all three chlorine (aluminum) dosages, indicating that inactivation was accompanied by sufficient damage to the genome. In contrast, inactivation appears to have been dominated by damage/modifications to the capsid at longer exposures since loss of infectivity was greater than loss of intact RNA (e.g. at 3h RNA damage was only 1.5logs but inactivation was 2.5logs for 100mM NaCl and 386s electrolysis). Hence, after 1h a portion of inactive viruses possessed intact RNA and the inability to replicate only contributed partially to measured overall inactivation (Figure 4.2b) (Lim et al. 2010, Sigstam et al. 2013, Wigginton et al. 2012).

Electrolysis of model saline waters generated low but sufficient amounts of free chlorine to simultaneously coagulate and inactivate viruses in the absence of naturally occurring colloids or organic matter. Hence, microorganism control during electrocoagulation of seawater (Timmes et al. 2010), reverse osmosis concentrate brine (Bagastyo et al. 2013), and other feed waters (Gao et al. 2010), is expected to include contributions from both removal and inactivation. Findings from our laboratory need to be cautiously extrapolated to other natural and treated waters since natural organic matter tends to consume free chlorine (Korshin et al.

2007) even potentially forming disinfection by-products (Yan et al. 2014).

Chapter 5. Membrane Rejection of Nonspherical Particles: Modeling and Experiment

5.1 Background

This work is the result of collaboration between Clarkson University and University of Houston. Basavaraju Agasanapura a graduate student of Dr. Ruth E. Baltus at Clarkson University developed quantitative models for the convective transport of a rigid particle in a cylindrical pore using Computational Fluid Dynamics (CFD) and we at University of Houston performed microfiltration experiments to measure removals of viruses, bacteria and silica colloids. In this chapter only experimental data are included because the modeling results are included in Basavaraju Agasanapura's dissertation.

5.2 Introduction

Microfiltration and ultrafiltration processes are extensively employed in various fields such as clinical applications, dairy processing, biotechnological applications, water and wastewater treatment, and microelectronic applications (Zeman and Zydney 1996). Of particular relevance to environmental engineering applications is the prevention of waterborne disease such as the 1993 *Cryptosporidium* outbreak in Milwaukee, WI that caused over 400,000 illnesses, 1,000 hospitalizations, and 50 deaths (Kramer et al. 1996). Several literature reports indicate that microfiltration or ultrafiltration systems achieve complete separation of protozoa but not bacteria and viruses (Jacangelo et al. 1995, Madaeni et al. 1995, Mi et al. 2005, Sadr Ghayeni et al. 1999, Urase et al. 1996). While microbial retention can be increased by employing membranes with smaller pore sizes, such an approach also concomitantly increases capital and energy costs by necessitating larger membrane area and higher pressures. Developing a quantitative understanding of the factors determining bacteria and virus removal is the first step

towards optimizing the membrane pore size necessary to economically produce biologically stable water (Jornitz and Meltzer 2001).

Efforts to theoretically analyze retention of particles by a porous membrane date back several decades, with studies focused primarily on spheres (Anderson 1981, Anderson and Malone 1974, Anderson and Quinn 1974). Because pathogenic bacteria and viruses present in feed waters are often non-spherical, a comprehensive model of membrane separations for such biological colloids is needed in order to design efficient membrane systems that balance microbial removal with energy and economic considerations (Anderson 1981).

A general expression (Equation 1) for the filtration rejection coefficient, σ_f, includes both hydrodynamic particle-pore wall interactions and steric restrictions with a Boltzmann distribution to describe particle concentration:(Anderson 1981)

$$\sigma_f = 1 - \frac{\iint G(X,\psi)\, v(X)\, e^{\left(\frac{-E(X,\psi)}{kT}\right)}\, dX\, d\psi}{\int v(X)\, dX}. \quad (1)$$

Here, $G(X,\psi)$ is the local lag coefficient, which represents the hydrodynamic particle-pore wall interactions, $v(X)$ is the fluid velocity field when the particles are excluded from the pore region, $E(X,\psi)$ is the particle-pore wall interaction energy, $X(x,y)$ is the two dimensional position vector in the pore and ψ is the particle orientation angle with respect to the pore axis.

Early analyses of hindered transport were focused on uncharged spheres using a centerline approximation (*G(X) = G(0)*) (Anderson and Quinn 1974, Bungay and Brenner 1973). Brenner and Gaydos (Brenner and Gaydos 1977) developed an analytical expression for *G(X)* which is valid for relatively small spheres. Ennis et al. (Ennis et al. 1996) used a Padé approximation to combine the small particle expression developed by Brenner and Gaydos (Brenner and Gaydos 1977) with a large particle expression developed by Bungay and Brenner (Bungay and Brenner 1973). Numerical simulations were carried out by Higdon and Muldowney

(Higdon and Muldowney 1995) who also fit their results to provide an analytical expression for $G(X)$. Dechadilok and Deen (Dechadilok and Deen 2006) used this expression to determine radially averaged hindrance factors as a function of relative particle size which were in excellent agreement with the expression developed by Ennis et al. (Ennis et al. 1996).

Anderson (Anderson 1981) theoretically examined the transport of capsule shaped particles in a cylindrical pore by considering only configurational effects (i.e., $G(X,\psi) = 1$ was assumed for all particle positions and orientations). The reflection coefficient for a capsule - shaped particle was predicted to be larger (higher removals) than for a spherical particle with equivalent volume, with reflection coefficient increasing as particle aspect ratio increases.

In a recent paper (Baltus et al. 2009), we described results from short-term membrane rejection measurements that were performed to examine the removal of two Gram-negative bacteria (*Brevundimonas diminuta* and *Serratia marcescens*), two bacteriophages (PRD1 and T4), and several spherical silica particles. These (bio) colloids ranged from spherical to capsule shaped, with aspect ratio in the range 1 – 9. Track etch membranes with well-defined capillary pores with a tight pore size distribution were used for these measurements. In contrast to Anderson's predictions (Anderson 1981), similar reflection coefficient values were measured for particles of the same dimensionless size but with different aspect ratios. We speculated that this might be attributed to hydrodynamic particle-pore wall interactions which were neglected in the model.

The objective of the work reported here was to perform detailed theoretical analyses of the convective transport of a rigid capsule shaped particle in a cylindrical pore, yielding predictions of σ_f for these particles. Specifically, we have determined $G(X,\psi)$ using two different approaches. As a first approximation, the results of Higdon and Muldowny(Higdon and Muldowney 1995) describing $G(X)$ for spherical particles were incorporated into the Anderson

model (Anderson 1981) that considers the steric limitations for a capsule in a pore. Because only one size parameter characterizes the sphere geometry, we considered different size parameters when using the sphere model to quantify the hydrodynamic interactions for a capsule: the diameter of a sphere with volume equivalent to the capsule volume, the diameter of a sphere equal to the capsule length and the diameter of a sphere equal to the capsule diameter. To develop a more comprehensive model of this system, computational fluid dynamic (CFD) calculations based on a finite element model were used to determine $G(0,\psi)$ for a capsule shaped particle in a cylindrical pore. These values were used in equation 1, along with steric restrictions for a capsule to predict σ_f for particles with different size and aspect ratio. Modeling results were validated by short-term measurements of the removal of three rod-shaped bacteria (*B. diminuta, S. marcescens,* and *E. coli*) and two spherical bacterial viruses (MS2 and PRD1) by a number of track-etched membranes with near cylindrical pore geometry in a stirred cell before the onset of fouling.

5.3 Experimental Methods

5.3.1 Spherical colloids

The number-weighted hydrodynamic diameters of colloidal silica (SNOWTEX-OL Nissan Chemical Industries Ltd.) and two bacterial viruses (MS2 and PRD1) measured using dynamic light scattering (DLS, BI200SM, Brookhaven Instruments) are given in Table 5.1. Particle polydispersity is characterized using the degree of polydispersity, which is the normalized variance of the particle diffusion coefficients, as defined by Brown et al (Brown et al. 1975). In all cases, the degree of polydispersity was very low, demonstrating the narrow size distribution of these particles.

Silica concentration was measured using light extinction at 600 nm using a 5 cm path length cell (DR 6000, Hach Co.). The bacteriophages MS2 (ATCC 15597-B1) and PRD1 (provided by David Metge at the United States Geological Survey, Boulder, CO) were propagated with the double-top agar layer technique using their respective hosts *Escherichia coli* (ATCC 15597) and *Salmonella typhimurium* (ATCC 19585) as reported earlier by us (Tanneru and Chellam 2012). Virus stocks were further purified with two successive polyethylene glycol precipitations and chloroform extraction to increase monodispersity and reduce dissolved organic carbon carry over. For filtration experiments, 1mL of purified virus stock $O(10^{10} - 10^{11})$ Plaque Forming Units (PFU)/mL was added to 1L of feed water to obtain a feed concentration of O (10^{7}-10^{8}) PFU/mL.

5.3.2 Bacteria

Cultures of *E. coli, S. marcescens,* and *B. diminuta* were first grown in Tryptic Soy Broth (TSB; Difco) at 37, 26 and 30 °C respectively and then pelletized by centrifugation at 4 °C and 5000 g for 30 minutes. Bacteria were grown until early stationary phase after resuspending them in phosphate buffered saline (PBS; composition 137 mM NaCl, 2.7 mM KCl, 4.3 mM $Na_2HPO_4.7H_2O$, and 1.4 mM KH_2PO_4; pH 7.5), and immediately filtered. Feed concentrations for membrane rejection experiments were maintained in the range $O(10^{6}$-$10^{7})$ colony forming units (CFU) /mL. Bacteria were enumerated by serially diluting the samples, spreading on pre-solidified Trypticase Soy Agar petri dishes (TSA 1.5%, Difco), and counting 20-300 colonies after 24 h incubation. The length and diameter of bacteria were obtained by imaging them after fixing with 2.5% glutaraldehyde solution at 4 °C overnight. At least 100 cells were inspected. Prior to electron microscopy (LEO 1525, Carl Zeiss), samples were gently washed with ultrapure water, dehydrated using progressively increasing concentrations of ethanol, and sputter coated with a 10 nm layer of gold. Bacteria dimensions are listed in Table 5.1.

Table 5.1. Characteristics of spherical and rod shaped colloids used in the experiments

Colloid	Average size (nm)	Zeta potential charged-(mV)	Zeta potential uncharged-(mV)	Aspect ratio
ST-OL	47.78 ± 1.34	-46.08±1.48	-5.33± 1.26	1
MP 1040	101.1±0.42	-44.68±3.78	-4.53±2.22	1
MP 2010	199±4.46	-47.44±3.33	-3.67±1.98	1
MP 3040	318.24± 2.24	-49.52±2.33	-4.29±3.11	1
MS2	26.53±2.79	-18.5±0.615	-5.22±0.69	1
PRD1	80.72 ± 4.94	-15.57±2.13	-1.68±0.72	1
S. marcescens	1.67±0.44 (length) 0.76 ± 0.09 (diameter)	-25.54±3.62	-0.85±2.14	2.22 ± 0.577
B. dimunita	1.75±0.38 (length) 0.51±0.04 (diameter)	-29.84±3.04	-1.1±2.88	3.51±0.93
E. coli	2.42±0.50 (length) 0.5±0.06 (diameter)	-27.75±3.92	-2.83±1.96	4.93±1.2

5.3.3 Membranes

Pore sizes of polycarbonate hydrophilic track-etched membranes (Isopore, Millipore) were independently measured by image analysis and water permeability. Electron micrographs of membranes were digitally reversed using Image J software so that the background appeared as black and pores were white. The Farsight ToolKit was then used to measure the pore area in square pixels (at least 200 pores from different scale images were analyzed). The pore diameter was calculated by obtaining the pixel size from the scale bar and assuming a circular cross-section. Hydraulic equivalent pore diameters were calculated from measurements of pure water fluxes over the pressure range 2-15 psig assuming Poiseuille flow through individual pores and using average pore densities obtained from image analysis. Pore sizes determined using image analysis were used when comparing experimental and predicted membrane rejection.

5.3.4 Filtration Procedure

Suspensions were dead-end filtered at constant pressure in a cell with 4.1 cm^2 effective area (model 8010, Millipore) and very low hold up volume. The pressure (PX303-050G5V, Omega) and cumulative permeate volume (Ohaus Navigator, NIH110, Fisher Scientific) were

digitally monitored using LabView (National Instruments, v. 8.5). To reduce concentration polarization and fouling, the filtration cell was continuously stirred at ~3,000 rpm using a magnetic Teflon bar. First, 100 mL of PBS was passed through the membrane to rinse it before filtering the colloids. Short term experiments were performed before any fouling could be discerned and rejection was measured after filtering 5 mL of feed water. Biocolloid stocks were diluted in PBS to reduce their ζ potential to near neutral values (measured to be between -5 and +3 mV using electrophoretic light scattering, Nicomp 380 ZLS, Particle Sizing Systems), ensuring negligible electrostatic interactions during their passage across membranes. Biocolloid stocks were suspended in low ionic strength 1:1 electrolyte solutions to study the charge effects.

5.4 Results and Discussion

5.4.1 Spherical particles

A comparison of the experimentally measured membrane rejection coefficients for spherical silica colloids and the spherical virus particles PRD1 and MS2 to model predictions is shown in Figure 5.1. The model predictions were generated using the centerline approximation (*G(X) = G(0)*). Excellent agreement was observed between data and experiment for both virus and silica particles for the entire range of dimensionless particle sizes, confirming the validity of the pore size values and the experimental procedures used for the rejection measurements.

5.4.2 Bacteria

Experimental membrane rejection data for *S. marcescens* (ε = 2.22), *B. diminuta* (ε = 3.51) and *E. coli* (ε = 4.93) are compared in Figure 5.2. Experimental results were generated using membranes with different pore sizes, yielding results over a range of dimensionless particle sizes. The results generally follow the trends predicted from our model, with increasing rejection as aspect ratio increases at a fixed value of λ.

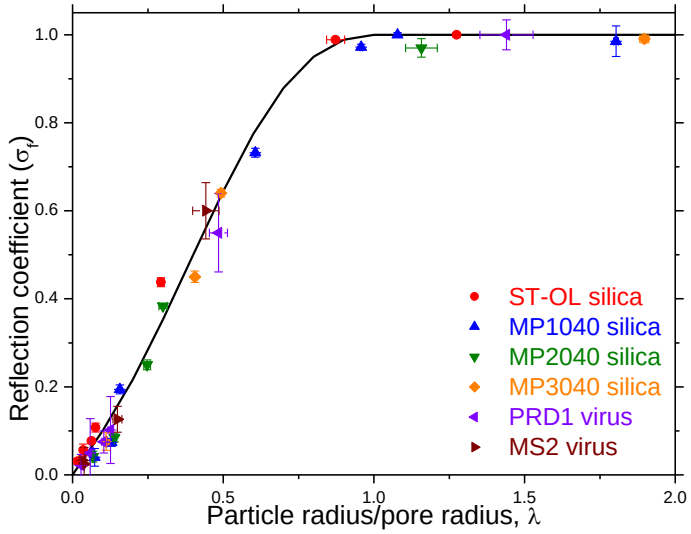

Figure 5.1. Comparison of experimental results for uncharged spherical particles with theoretical predictions of rejection coefficient. Model predictions were made using centerline model for the lag coefficient of a sphere.

In our earlier publication (Baltus et al. 2009), experimental results for four different non-spherical bacteria and viruses with aspect ratio ranging from 2.7 to 8.9 showed measured reflection coefficients that were generally independent of particle aspect ratio, results that are not consistent with those presented in Figure 5.2. In the previous work, the aspect ratio for three of the particles ranged from 2.7 to 4.0, differences that, according to our model, are not expected to yield significant differences in rejection. The fourth particle was a unique *B. diminuta* that, because of growth conditions had an aspect ratio of 8.9. This elongated particle may have become aligned with the flow in the pores, yielding lower rejections than predicted from both the steric restrictions model (G = 1) as well as the current CFD model that includes hydrodynamic resistances.

Comparisons of the experimentally measured membrane rejection coefficients to model predictions are shown in Figure 5.3 with comparisons for *S. marcescens* in Figure 5.3a, for *B. diminuta* in Figure 5.3b and for *E. coli* in Figure 5.3c. The theoretical predictions were obtained from our CFD calculations using the appropriate aspect ratio for each particle.

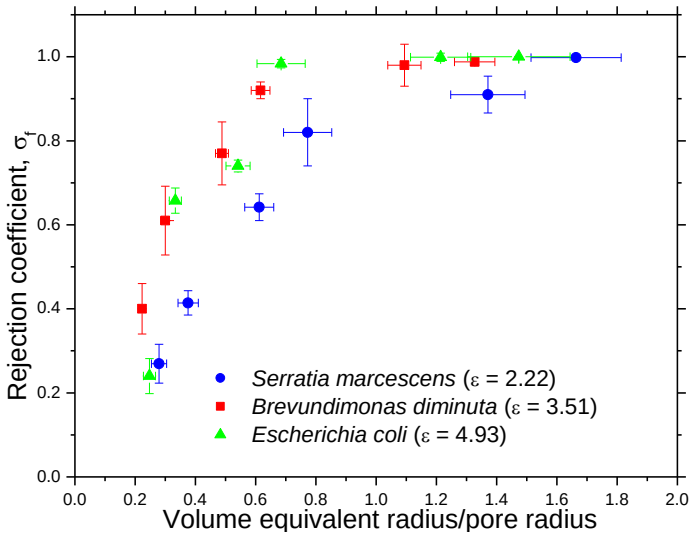

Figure 5.2. Experimental membrane rejections results for rod shaped bacteria, *S. marcescens* (ε = 2.22), *B. diminuta* (ε = 3.51) and *E. coli* (ε = 4.93).

The comparisons in Figure 5.3 show generally good agreement between experiment and theory for all systems. The increase in rejection observed as λ increases (i.e., decreasing pore size) follows the rate of increase predicted by the model. Complete rejection is observed for experiments with small pore membranes (λ > 1). Note that the volume equivalent sphere radius is used here to define λ. Therefore, with appropriate orientation, the particles could access the pore even when λ > 1, but do not to any significant extent, as predicted by the model.

The comparisons in Figure 5.3 also show that in all cases, measured rejection values were less than or equal to model predictions. There were no experimental rejection coefficients larger than predicted values. Particle alignment in the pores, which was neglected in the CFD calculations, may be responsible for this trend. Our current efforts are focused on a model that includes torque on the particles. Results from this revised model may help us to better understand these observations.

Long range particle – pore wall interactions were also neglected in the CFD model. Attractive particle – pore wall interactions could result in higher particle concentrations in the pore, yielding reduced membrane rejections relative to values predicted when only steric

interactions are considered.

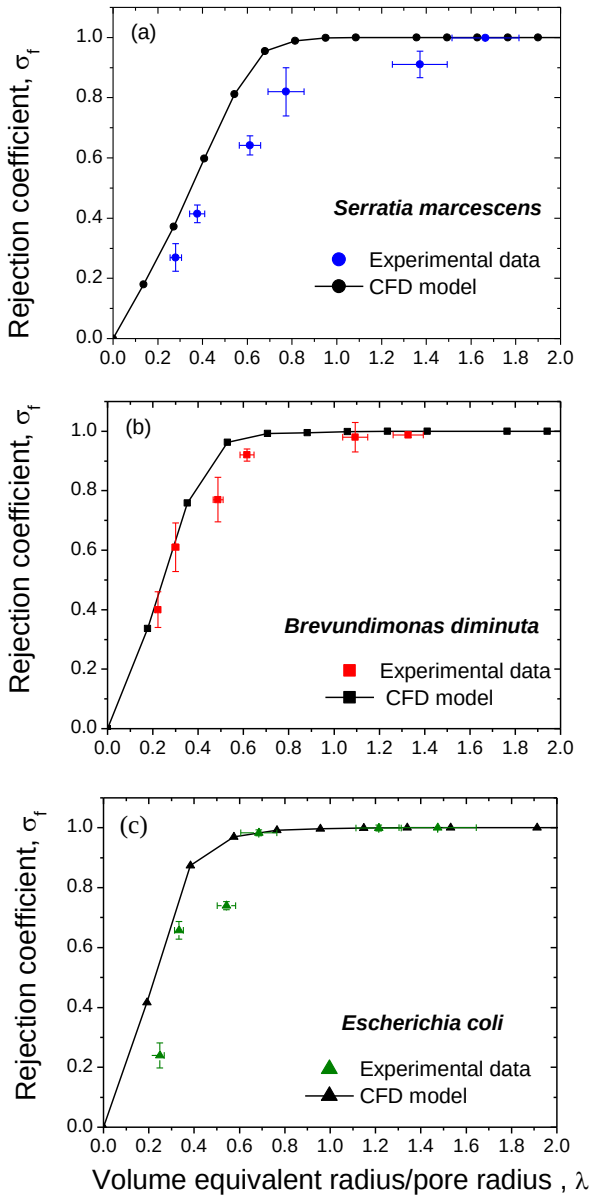

Figure 5.3. Comparison of experimental results with theoretical predictions (a) S. marcescens (ε = 2.22 compared to a model with ε = 2.0), (b) B. diminuta (ε = 3.51 compared to a model with ε = 3.5) and (c) E. coli (ε = 4.93 compared to ε = 5.0).

Experimentally, buffer conditions were established to keep particle ζ potential at near neutral conditions. Future experiments will examine rejection with different ionic strength buffers. Results from these measurements may also help us to better understand our

observations. A revised model that includes particle – pore wall electrostatic interactions is also being developed.

5.5 Summary and Conclusions

Experimental results collected from filtration experiments performed with track etch polycarbonate membranes and three for uncharged bacteria with aspect ratio ranging from 2.2 to 5 show generally good agreement between model predictions and experimentally observed membrane rejection coefficients.

Chapter 6. Summary, Conclusions and Recommendations for Future Work

Increasing the removal of bacteria and viruses is important to ensure biological stability of drinking water and to better protect public health. To this end, a novel electrochemical coagulation method was investigated for effective virus control. The effectiveness of membrane microfiltration for microorganism control was also quantitatively evaluated.

Iron electrocoagulation pretreatment to microfiltration significantly improved virus reductions only in the absence of NOM. Importantly, virus control in such an integrated system included both removal and inactivation only in synthetic water containing no NOM. Significantly lower removal and inactivation was measured in surface water containing moderate NOM concentrations. Hence, NOM appears to inhibit inactivation by decreasing oxidant generation rate, better scavenging potentially generated oxidants, and complexing with Fe^{2+} thereby reducing its interactions with capsid amino acids. Direct measurements of oxidants such as ROS need to be made to provide more conclusive evidence for inactivation mechanisms in during iron electrocoagulation.

During relatively long durations of aluminum electrolysis, a portion of the flocs migrated to the top of the water column, i.e., electroflotation. Both electrocoagulation and electroflotation with aluminum outperformed conventional alum coagulation as a highly effective and facile method to remove viruses. Enhancements in virus removal as progressively more aluminum was electrolyzed embodies contributions from (i) better encapsulation onto greater amounts of fresh $Al(OH)_3$ precipitates, (ii) increased adsorption capacity associated with higher available coagulant surface area, (iii) greater virus-floc binding affinity due to effective charge neutralization and hydrophobic interactions, and/or (iv) additional removal by a "dynamic membrane" if a thick cake layer of flocs is deposited.

Two important advantages of electroflotation over electrocoagulation are that it

inherently comprises an additional microbial barrier (floc flotation) without adding a separate unit process and it achieves higher MF flux. We are also working to simultaneously maximize removal of turbidity, microorganisms, as well as NOM and DBP precursors (similar to "enhanced coagulation"). An important impediment to widespread implementation of these technologies is passivation, which reduces Faradaic coagulant dissolution due to the accumulation of corrosion products and macromolecules on electrode surfaces or formation of an oxide film. On the other hand, pitting can lead to super Faradaic dissolution. In either case, unreliable coagulant dissolution is detrimental to electrochemical cell performance and necessitates system downtime for periodic electrode cleaning. Further, the kinetics of these phenomena cannot be predicted *a priori* during treatment of natural waters, which necessitates long-term site-specific evaluations.

Higher virus reductions were measured during aluminum electrolysis of saline solutions. Mechanisms of virus control in such feed waters that only contained NaCl included both uptake onto aluminum flocs and inactivation. Free chlorine produced by electrochemical oxidation of chloride ions inactivated MS2 viruses. Virus inactivation appears to be the result of alterations to the capsid protein and loss of genome structural integrity. Presence of solids and encapsulation within aluminum flocs shielded viruses from chlorine. Hence, inactivation was considerably slower and less effective compared to control experiments were the same concentration of free chlorine was added to virus suspensions in the absence of solids. Ongoing work is focused towards maximizing free chlorine generation using aluminum and different dimensionally stable electrodes as cathode to facilitate both coagulation and disinfection. In any case, experimentation using synthetic water alone is insufficient and virus removal/inactivation should be quantified directly with natural water before implementing electrocoagulation for drinking water treatment. In addition, larger-scale testing and engineering cost comparisons are

necessary before electrochemical processes can be recommended over conventional chemical coagulation for full-scale applications.

Finally, experimental results collected from filtration experiments performed with track-etch polycarbonate membranes and three different bacteria with aspect ratio ranging from 2.2 to 5 show generally good agreement between model predictions and experimentally observed membrane rejection coefficients. From a practical perspective, the current results indicate that selection of a pore size needed to achieve a desired level of rejection of capsule-shaped microorganisms is not particularly sensitive to whether or not hydrodynamic interactions are included in the model predictions, particularly for high rejection systems (σ_f > 0.5). Selection of pore size using a no lag model or a model based on a spherical approximation for the hydrodynamic lag coefficient provides a conservative estimate that should not have a significant impact on energy requirements for a given system.

The following ideas could potentially serve as new research directions:

In this research all experiments were performed with bacteriophages. To this end, we rigorously evaluated bacteriophage control with electrocoagulation. However, to our knowledge no data are available for animal viruses (e.g., adenovirus, echovirus, etc.) control in such systems. It is important to elucidate animal virus reduction mechanisms with integrated electrocoagulation-microfiltration.

During iron electrocoagulation we empirically demonstrated virus control by inactivation. We attributed it to reactive oxygen species (ROS) mediated inactivation based on literature information. Directly measuring ROS species and adding specific quenchers (to selectively inhibit individual ROS) to the electrochemical system will determine chemical intermediates responsible for disinfection.

Building on a recently established collaboration with Prof. Scott Husson of Clemson University, we are demonstrating virus adsorption mechanisms onto strong anion exchange membranes. We at the University of Houston are establishing adsorption isotherms for anion exchange membranes prepared by Dr. Husson's research group. Preliminary results are encouraging as seen in Figure 6.1. Negatively charged virus (øX174 at ~7.8) adsorbed strongly onto anion exchange membrane. Fluorescently tagging these and performing confocal microscopy will strongly establish adsorption mechanisms.

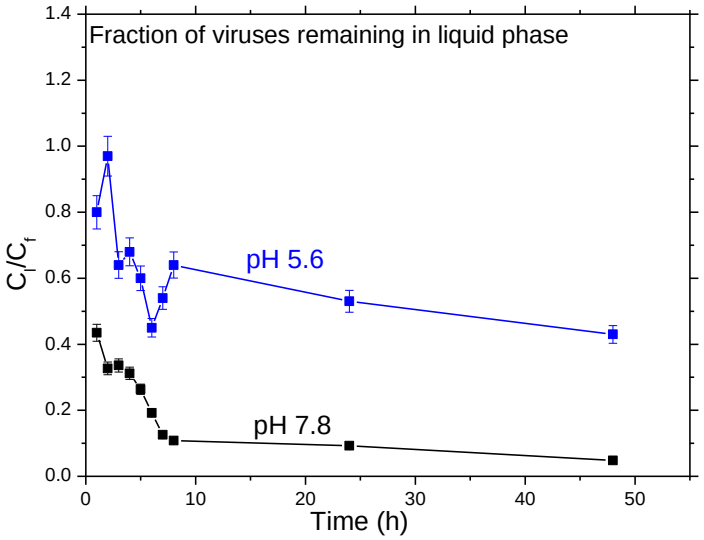

Figure 6.1. Fraction of viruses remaining in the liquid phase.

Finally, we are also experimentally evaluating electrostatic effects on the hindered transport of spherical microorganisms and silica colloids across track-etched membranes. Again, this collaborative effort is between our group (that generates laboratory data) and Prof. Baltus of Clarkson (who performs computational fluid dynamics modeling). Experimental results summarized in Figure 6.2 demonstrate that negatively charged colloids suspended in low ionic strength waters are removed to a greater extent than their well-destabilized counterparts (as seen in Figure 5.1) by negatively charged membranes. This suggests that public health would be better protected by taking advantage of electrostatic repulsion.

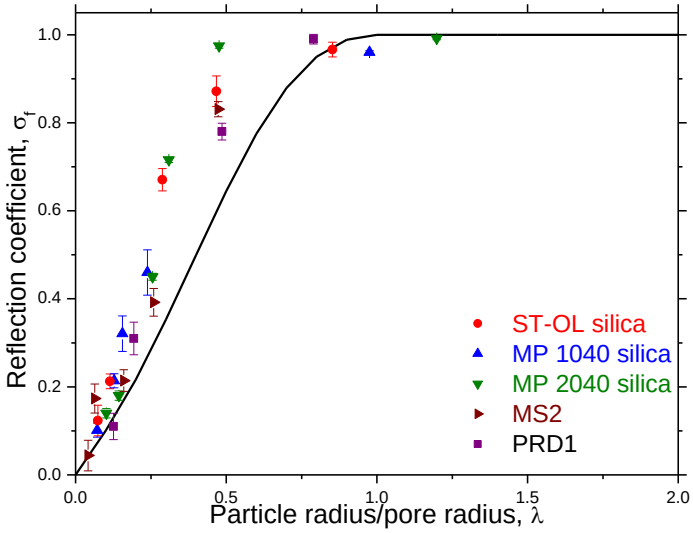

Figure 6.2. Comparison of experimental results for charged spherical particles with theoretical predictions of rejection coefficient. Model predictions were made using uncharged system and centerline model for the lag coefficient of a sphere. Uncharged data is shown in Figure 5.1.

References

Abbaszadegan, M., Mayer, B.K., Ryu, H. and Nwachuku, N. (2007) "Efficacy of removal of CCL viruses under enhanced coagulation conditions." *Environmental Science & Technology* 41(3), 971-977.

Agasanapura, B., Baltus, R.E., Tanneru, C. and Chellam, S. (2013) "Membrane Rejection of Nonspherical Particles: Modeling and Experiment." *Aiche Journal* 59(10), 3863-3873.

Anders, R. and Chrysikopoulos, C.V. (2006) "Evaluation of the factors controlling the time-dependent inactivation rate coefficients of bacteriophage MS2 and PRD1." *Environmental Science & Technology* 40(10), 3237-3242.

Anderson, J.L. (1981) "Configurational effect on the reflection coefficient for rigid solutes in capillary pores." *Journal of Theoretical Biology* 90(3), 405-426.

Anderson, J.L. and Malone, D.M. (1974) "Mechanism of osmotic flow in porous membranes." *Biophysical Journal* 14(12), 957-982.

Anderson, J.L. and Quinn, J.A. (1974) "Restricted transport in small pores : A model for steric exclusion and hindered particle motion." *Biophysical Journal* 14, 130-150.

Attinti, R., Wei, J., Kniel, K., Sims, J.T. and Jin, Y. (2010) "Virus' (MS2, phi X174, and Aichi) attachment on sand measured by atomic force microscopy and their transport through sand columns." *Environmental Science & Technology* 44(7), 2426-2432.

Badireddy, A.R., Budarz, J.F., Chellam, S. and Wiesner, M.R. (2012) "Bacteriophage inactivation by UV-A illuminated fullerenes: Role of nanoparticle-virus association and biological targets." *Environmental Science & Technology* 46(11), 5963-5970.

Baes, C.F. and Mesmer, R.E. (1976) The Hydrolysis of Cations, New York, N.Y., .

Bagastyo, A.Y., Batstone, D.J., Rabaey, K. and Radjenovic, J. (2013) "Electrochemical oxidation of electrodialysed reverse osmosis concentrate on Ti/Pt-IrO2, Ti/SnO2-Sb and boron-doped diamond electrodes." *Water Research* 47(1), 242-250.

Bagga, A., Chellam, S. and Clifford, D.A. (2008) "Evaluation of iron chemical coagulation and electrocoagulation pretreatment for surface water microfiltration." *Journal of Membrane Science* 309(1-2), 82-93.

Bakhshayeshi, M., Jackson, N., Kuriyel, R., Mehta, A., van Reis, R. and Zydney, A.L. (2011) "Use of confocal scanning laser microscopy to study virus retention during virus filtration." *Journal of Membrane Science* 379(1-2), 260-267.

Baltus, R.E., Badireddy, A.R., W, X. and Chellam, S. (2009) "Analysis of configurational effects on the hindrance convective non spherical bacteria and viruses across microfiltration membranes." *Industrial and Engineering Chemistry Research* 298, 193-210.

Barth, A. (2000) "The infrared absorption of amino acid side chains." *Progress in Biophysics & Molecular Biology* 74(3-5), 141-173.

Bayat, O., Kilic, O., Bayat, B., Anil, M., Akarsu, H. and Poole, C. (2006) "Electrokinetic dewatering of Turkish glass sand plant tailings." *Water Research* 40(1), 61-66.

Bellona, C., Marts, M. and Drewes, J.E. (2010) "The effect of organic membrane fouling on the properties and rejection characteristics of nanofiltration membranes." *Separation and Purification Technology* 74(1), 44-54.

Ben Sasson, M. and Adin, A. (2010) "Fouling mitigation by iron-based electroflocculation in microfiltration: Mechanisms and energy minimization." *Water Research* 44(13), 3973-3981.

Ben Sasson, M., Calmano, W. and Adin, A. (2009) "Iron-oxidation processes in an electroflocculation (electrocoagulation) cell." *Journal of Hazardous Materials* 171(1-3), 704-709.

Bensalah, N. and Abdel-Wahab, A. (2013) "Electrochemical inactivation of *P. Aeruginosa*, *A. hydrophila*, *L. pneumophila* using boron doped diamond anodes." *Journal of Advanced Oxidation Technologies* 16(1), 9-15.

Boardman, G.D. and Sproul, O.J. (1977) "Protection of viruses during disinfection by adsorption to particulate matter." *Journal Water Pollution Control Federation* 49(8), 1857-1861.

Brady-Estevez, A.S., Nguyen, T.H., Gutierrez, L. and Elimelech, M. (2010) "Impact of solution chemistry on viral removal by a single-walled carbon nanotube filter." *Water Research* 44(13), 3773-3780.

Brenner, H. and Gaydos, L.J. (1977) "The constrained brownian movement of spherical particles in cylindrical pores of comparable radius: Models of the diffusive and convective transport of solute molecules in membranes and porous Media." *Journal of Colloid and Interface Science* 58(2), 312-356.

Brown, J., Pusey, P.N. and Dietz, R. (1975) "Photon correlation study of polydisperse samples of polystyrene in cyclohexane." *The Journal of Chemical Physics* 62(3), 1136-1144.

Bungay, P.M. and Brenner, H. (1973) "The motion of a closely-fitting sphere in a fluid-filled tube." *International Journal of Multiphase Flow* 1(1), 25-56.

Cañizares, P., Jiménez, C., Martínez, F., Sáez, C. and Rodrigo, M.A. (2007) "Study of the electrocoagulation process using aluminum and iron electrodes." *Industrial & Engineering Chemistry Research* 46(19), 6189-6195.

Cañizares, P., Martinez, F., Jimenez, C., Lobato, J. and Rodrigo, M.A. (2006) "Coagulation and electrocoagulation of wastes polluted with dyes." *Environmental Science & Technology* 40(20), 6418-6424.

Chen, G.H. (2004) "Electrochemical technologies in wastewater treatment." *Separation and Purification Technology* 38(1), 11-41.

Chen, X.M., Chen, G.H. and Yue, P.L. (2002) "Novel electrode system for electroflotation of wastewater." *Environmental Science & Technology* 36(4), 778-783.

Choi, K.Y.J. and Dempsey, B.A. (2004) "In-line coagulation with low-pressure membrane filtration." *Water Research* 38(19), 4271-4281.

Choi, K.Y.J. and Dempsey, B.A. (2005) "Bench-scale evaluation of critical flux and TMP - in low-pressure membrane filtration." *Journal American Water Works Association* 97(7), 134-143.

Clesceri, L.S., Greenberg, A.E., Eaton, A.D. and Franson, M.A.H. (2005) Standard Methods for the Examination of Water and Wastewater 21st edition, American Public Health Association; American Water Works Association; Water Environment Federation, Washington, DC.

Cromeans, T.L., Kahler, A.M. and Hill, V.R. (2010) "Inactivation of adenoviruses, enteroviruses, and murine norovirus in water by free chlorine and monochloramine." *Applied and Environmental Microbiology* 76(4), 1028-1033.

Deborde, M. and von Gunten, U. (2008) "Reactions of chlorine with inorganic and organic compounds during water treatment - Kinetics and mechanisms: A critical review." *Water Research* 42(1-2), 13-51.

Dechadilok, P. and Deen, W.M. (2006) "Hindrance factors for diffusion and convection in pores." *Industrial & Engineering Chemistry Research* 45(21), 6953-6959.

Dietrich, J.P., Basagaoglu, H., Loge, F.J. and Ginn, T.R. (2003) "Preliminary assessment of transport processes influencing the penetration of chlorine into wastewater particles and the subsequent inactivation of particle-associated organisms." *Water Research* 37(1), 139-149.

Drees, K.P., Abbaszadegan, M. and Maier, R.M. (2003) "Comparative electrochemical inactivation of bacteria and bacteriophage." *Water Research* 37(10), 2291-2300.

Dubrawski, K.L. and Mohseni, M. (2013) "In-situ identification of iron electrocoagulation speciation and application for natural organic matter (NOM) removal." *Water Research* 47(14), 5371-5380.

Durante, C., Cuscov, M., Isse, A.A., Sandona, G. and Gennaro, A. (2011) "Advanced oxidation processes coupled with electrocoagulation for the exhaustive abatement of Cr-EDTA." *Water Research* 45(5), 2122-2130.

Engel, A. and Muller, D.J. (2000) "Observing single biomolecules at work with the atomic force microscope." *Nature Structural Biology* 7(9), 715-718.

Ennis, J., Zhang, H., Stevens, G., Perera, J., Scales, P. and Carnie, S. (1996) "Mobility of protein through a porous membrane." *Journal of Membrane Science* 119(1), 47-58.

Fiksdal, L. and Leiknes, T. (2006) "The effect of coagulation with MF/UF membrane filtration for the removal of virus in drinking water." *Journal of Membrane Science* 279(1-2), 364-371.

Gamage, N.P. and Chellam, S. (2011) "Aluminum electrocoagulation pretreatment reduces fouling during surface water microfiltration." *Journal of Membrane Science* 379(1-2), 97-105.

Gamage, N.P., Rimer, J.D. and Chellam, S. (2012) "Improvements in permeate flux by aluminum electroflotation pretreatment during microfiltration of surface water." *Journal of Membrane Science* 411, 45-53.

Gao, S., Du, M., Tian, J., Yang, J., Yang, J., Ma, F. and Nan, J. (2010) "Effects of chloride ions on electro-coagulation-flotation process with aluminum electrodes for algae removal." *Journal of Hazardous Materials* 182(1-3), 827-834.

Gould, J.P., Richards, J.T. and Miles, M.G. (1984) "The formation of stable organic chloramines during the aqueous chlorination of cytosine and 5-methylcytosine." *Water Research* 18(8), 991-999.

Grabow, W.O.K. (2007) In Human Viruses in Water. Bosch, A. (ed), pp. 1-26, Elsevier Science and Technology, Amsterdam.

Gutierrez, L. and Nguyen, T.H. (2012) "Interactions between rotavirus and suwannee river organic matter: aggregation, deposition, and adhesion force measurement." *Environmental Science & Technology* 46(16), 8705-8713.

Harrington, G.W., Xagoraraki, I., Assavasilavasukul, P. and Standridge, J.H. (2003) "Effect of filtration conditions on removal of emerging waterborne pathogens." *Journal American Water Works Association* 95(12), 95-104.

Havelaar, A.H., Vanolphen, M. and Drost, Y.C. (1993) "F-Specific RNA bacteriophages are adequate model organisms for enteric viruses in fresh-water." *Applied and Environmental Microbiology* 59(9), 2956-2962.

Hawkins, C.L. and Davies, M.J. (2002) "Hypochlorite-induced damage to DNA, RNA, and polynucleotides: Formation of chloramines and nitrogen-centered radicals." *Chemical Research in Toxicology* 15(1), 83-92.

Hazell, L.J., Vandenberg, J.J.M. and Stocker, R. (1994) "Oxidation of low-density-lipoprotein by hypochlorite causes aggregation that is mediated by modification of lysine residues rather than lipid oxidation." *Biochemical Journal* 302, 297-304.

Hejkal, T.W., Wellings, F.M., Larock, P.A. and Lewis, A.L. (1979) "Survival of poliovirus within organic-solids during chlorination." *Applied and Environmental Microbiology* 38(1), 114-118.

Hendricks, D.W., Clunie, W.F., Sturbaum, G.D., Klein, D.A., Champlin, T.L., Kugrens, P., Hirsch, J., McCourt, B., Nordby, G.R., Sobsey, M.D., Hunt, D.J. and Allen, M.J. (2005) "Filtration removals of microorganisms and particles." *Journal of Environmental Engineering-Asce* 131(12), 1621-1632.

Higdon, J.J.L. and Muldowney, G.P. (1995) "Resistance functions for spherical particles, droplets and bubbles in cylindrical tubes." *Journal of Fluid Mechanics* 298, 193-210.

Hill, V.R., Kahler, A.M., Jothikumar, N., Johnson, T.B., Hahn, D. and Cromeans, T.L. (2007) "Multistate evaluation of an ultrafiltration-based procedure for simultaneous recovery of enteric microbes in 100-liter tap water samples." *Applied and Environmental Microbiology* 73(13), 4218-4225.

Holt, P.K., Barton, G.W. and Mitchell, C.A. (2005) "The future for electrocoagulation as a localised water treatment technology." *Chemosphere* 59(3), 355-367.

Holt, P.K., Barton, G.W., Wark, M. and Mitchell, C.A. (2002) "A quantitative comparison between chemical dosing and electrocoagulation." *Colloids and Surfaces a-Physicochemical and Engineering Aspects* 211(2-3), 233-248.

Hotze, E.M., Badireddy, A.R., Chellam, S. and Wiesner, M.R. (2009) "Mechanisms of bacteriophage inactivation via singlet oxygen generation in UV illuminated fullerol suspensions." *Environmental Science & Technology* 43(17), 6639-6645.

Jacangelo, J.G., Adham, S.S. and Laine, J.M. (1995) "Mechanism of *Cryptosporidium, Giardia*, and MS2 virus removal by Mf and Uf." *Journal American Water Works Association* 87(9), 107-121.

Jeong, J., Kim, C. and Yoon, J. (2009) "The effect of electrode material on the generation of oxidants and microbial inactivation in the electrochemical disinfection processes." *Water Research* 43(4), 895-901.

Jeong, J., Kim, J.Y. and Yoon, J. (2006) "The role of reactive oxygen species in the electrochemical inactivation of microorganisms." *Environmental Science & Technology* 40(19), 6117-6122.

Jiang, J.Q., Graham, N., Andre, C., Kelsall, G.H. and Brandon, N. (2002) "Laboratory study of electro-coagulation-flotation for water treatment." *Water Research* 36(16), 4064-4078.

Jin, M., Shan, J., Chen, Z., Guo, X., Shen, Z., Qiu, Z., Xue, B., Wang, Y., Zhu, D., Wang, X. and Li, J. (2013) "Chlorine dioxide inactivation of enterovirus 71 in water and its impact on genomic targets." *Environmental Science & Technology* 47(9), 4590-4597.

Johnson, I. and Spence, M.T.Z. (2010) The Molecular Probes handbook. A guide to fluorescent probes and labeling technologies, Invitrogen Corporation.

Jornitz, M.W. and Meltzer, T.H. (2001) Sterile filtration: A practical approach, Informa Healthcare.

Kim, J.Y., Lee, C., Love, D.C., Sedlak, D.l., Yoon, J. and Nelson, K.L. (2011) "Inactivation of MS2 coliphage by ferrous ion and zero-valent iron nanoparticles." *Environmental Science & Technology*.

Kim, J.Y., Lee, C., Sedlak, D.L., Yoon, J. and Nelson, K.L. (2010) "Inactivation of MS2 coliphage by Fenton's reagent." *Water Research* 44(8), 2647-2653.

Kitajima, M., Tohya, Y., Matsubara, K., Haramoto, E., Utagawa, E. and Katayama, H. (2010) "Chlorine inactivation of human norovirus, murine norovirus and poliovirus in drinking water." *Letters in Applied Microbiology* 51(1), 119-121.

Korshin, G.V., Benjamin, M.M., Chang, H.-S. and Gallard, H. (2007) "Examination of NOM chlorination reactions by conventional and stop-flow differential absorbance spectroscopy." *Environmental Science & Technology* 41(8), 2776-2781.

Kramer, M.H., Herwaldt, B.L., Craun, G.F., Calderon, R.L. and Juranek, D.D. (1996) "Waterborne disease: 1993 and 1994." *AWWA* 88(3), 66-80.

Kuzmanovic, D.A., Elashvili, I., Wick, C., O'Connell, C. and Krueger, S. (2006) "The MS2 coat protein shell is likely assembled under tension: A novel role for the MS2 bacteriophage A protein as revealed by small-angle neutron scattering." *Journal of Molecular Biology* 355(5), 1095-1111.

Lahoussine-Turcaud, V.r., Wiesner, M.R. and Bottero, J.-Y. (1990) "Fouling in tangential-flow ultrafiltration: The effect of colloid size and coagulation pretreatment." *Journal of Membrane Science* 52(2), 173-190.

Laine, J.M., Clark, M.M. and Mallevialle, J. (1990) "Ultrafiltration of lake water - effect of pretreatment on the partitioning of organics, THMFP, and flux." *Journal American Water Works Association* 82(12), 82-87.

Lakshmanan, D., Clifford, D.A. and Samanta, G. (2009) "Ferrous and Ferric ion generation during iron electrocoagulation." *Environmental Science & Technology* 43(10), 3853-3859.

Lakshmanan, D., Clifford, D.A. and Samanta, G. (2010) "Comparative study of arsenic removal by iron using electrocoagulation and chemical coagulation." *Water Research* 44(19), 5641-5652.

Langlet, J., Ogorzaly, L., Schrotter, J.C., Machinal, C., Gaboriaud, F., Duval, J.F.L. and Gantzer, C. (2009) "Efficiency of MS2 phage and Q beta phage removal by membrane filtration in water treatment: Applicability of real-time RT-PCR method." *Journal of Membrane Science* 326(1), 111-116.

Lee, G.U., Chrisey, L.A. and Colton, R.J. (1994) "Direct measurement of the forces between complementary strands of DNA." *Science* 266(5186), 771-773.

Lee, S.-Y., Lim, J.S., Culver, J.N. and Harris, M.T. (2008) "Coagulation of tobacco mosaic virus in alcohol-water-LiCl solutions." *Journal of Colloid and Interface Science* 324(1-2), 92-98.

Li, L., van Genuchten, C.M., Addy, S.E.A., Yao, J., Gao, N. and Gadgil, A.J. (2012) "Modeling As(III) oxidation and removal with iron electrocoagulation in groundwater." *Environmental Science & Technology* 46(21), 12038-12045.

Lim, M.Y., Kim, J.-M. and Ko, G. (2010) "Disinfection kinetics of murine norovirus using chlorine and chlorine dioxide." *Water Research* 44(10), 3243-3251.

Lindsey, M.E. and Tarr, M.A. (2000) "Inhibited hydroxyl radical degradation of aromatic hydrocarbons in the presence of dissolved fulvic acid." *Water Research* 34(8), 2385-2389.

Liu, W.K., Brown, M.R.W. and Elliott, T.S.J. (1997) "Mechanisms of the bactericidal activity of low amperage electric current (DC)." *Journal of Antimicrobial Chemotherapy* 39(6), 687-695.

Madaeni, S.S. (1999) "The application of membrane technology for water disinfection." *Water Research* 33(2), 301-308.

Madaeni, S.S., Fane, A.G. and Grohmann, G.S. (1995) "Virus removal from water and wastewater using membranes." *Journal of Membrane Science* 102(0), 65-75.

Mansouri, K., Hannachi, A., Abdel-Wahab, A. and Bensalah, N. (2012) "Electrochemically dissolved aluminum coagulants for the removal of natural organic matter from synthetic and real industrial wastewaters." *Industrial & Engineering Chemistry Research* 51(5), 2428-2437.

Matsui, Y., Matsushita, T., Sakuma, S., Mamiya, T., Suzuoki, H. and Inoue, T. (2003) "Virus inactivation during coagulation with aluminum coagulants." *Environmental Science & Technology* 37(22), 5175-5180.

Matsushita, T., Shirasaki, N., Matsui, Y. and Ohn, K. (2011) "Virus inactivation during coagulation with aluminum coagulants." *Chemosphere* 85(4), 571-576.

Mavrov, V., Stamenov, S., Todorova, E., Chmiel, H. and Erwe, T. (2006) "New hybrid electrocoagulation membrane process for removing selenium from industrial wastewater." *Desalination* 201(1-3), 290-296.

Mayer, B.K., Ryu, H. and Abbaszadegan, M. (2008) "Treatability of US environmental protection agency contaminant candidate list viruses: Removal of coxsackievirus and echovirus using enhanced coagulation." *Environmental Science & Technology* 42(18), 6890-6896.

Meyn, T., Leiknes, T.O. and Koenig, A. (2012) "MS2 removal from high NOM content surface water by coagulation - ceramic microfiltration, for potable water production." *Aiche Journal* 58(7), 2270-2281.

Mi, B., Mariñas, B.J., Curl, J., Sethi, S., Crozes, G. and Hugaboom, D. (2005) "Microbial passage in low pressure membrane elements with compromised Integrity." *Environmental Science & Technology* 39(11), 4270-4279.

Mollah, M.Y.A., Morkovsky, P., Gomes, J.A.G., Kesmez, M., Parga, J. and Cocke, D.L. (2004) "Fundamentals, present and future perspectives of electrocoagulation." *Journal of Hazardous Materials* 114(1-3), 199-210.

Moreno C, H.A., Cocke, D.L., Gomes, J.A.G., Morkovsky, P., Parga, J.R., Peterson, E. and Garcia, C. (2009) "Electrochemical reactions for electrocoagulation using iron electrodes." *Industrial & Engineering Chemistry Research* 48(4), 2275-2282.

Morgan, B. and Lahav, O. (2007) "The effect of pH on the kinetics of spontaneous Fe(II) oxidation by O-2 in aqueous solution - basic principles and a simple heuristic description." *Chemosphere* 68(11), 2080-2084.

Mouedhen, G., Feki, M., Wery, M.D.P. and Ayedi, H.F. (2008) "Behavior of aluminum electrodes in electrocoagulation process." *Journal of Hazardous Materials* 150(1), 124-135.

O'Connell, K.P., Bucher, J.R., Anderson, P.E., Cao, C.J., Khan, A.S., Gostomski, M.V. and Valdes, J.J. (2006) "Real-time fluorogenic reverse transcription-PCR assays for detection of bacteriophage MS2." *Applied and Environmental Microbiology* 72(1), 478-483.

O'Melia (1972). Weber, W.J., Ed. Wiley-Interscience (ed), pp. 61-109, New Yor.

Ohgaki, S. and Mongkonsiri, P. (1990) Chemical Water and Wastewater Treatment. Hahn, H. and Klute, R. (eds), pp. 75-84, Springer Berlin Heidelberg.

Oroudjev, E., Soares, J., Arcdiacono, S., Thompson, J.B., Fossey, S.A. and Hansma, H.G. (2002) "Segmented nanofibers of spider dragline silk: Atomic force microscopy and single-molecule force spectroscopy." *Proceedings of the National Academy of Sciences of the United States of America* 99, 6460-6465.

Pattison, D.I. and Davies, M.J. (2001) "Absolute rate constants for the reaction of hypochlorous acid with protein side chains and peptide bonds." *Chemical Research in Toxicology* 14(10), 1453-1464.

Pereira, W.E., Hoyano, Y., Summons, R.E., Bacon, V.A. and Duffield, A.M. (1973) "Chlorination studies II. Reaction of aqueous hypochlorous acid with a amino-acids and dipeptides." *Biochimica Et Biophysica Acta* 313(1), 170-180.

Pontius, F.W., Amy, G.L. and Hernandez, M.T. (2009) "Fluorescent microspheres as virion surrogates in low-pressure membrane studies." *Journal of Membrane Science* 335(1-2), 43-50.

Ramani, S. and Kang, G. (2009) "Viruses causing childhood diarrhoea in the developing world." *Current Opinion in Infectious Diseases* 22(5), 477-482.

Ricordel, C., Darchen, A. and Hadjiev, D. (2010) "Electrocoagulation-electroflotation as a surface water treatment for industrial uses." *Separation and Purification Technology* 74(3), 342-347.

Sadr Ghayeni, S.B., Beatson, P.J., Fane, A.J. and Schneider, R.P. (1999) "Bacterial passage through microfiltration membranes in wastewater applications." *Journal of Membrane Science* 153(1), 71-82.

Sano, D., Pinto, R.M., Omura, T. and Bosch, A. (2010) "Detection of oxidative damages on viral capsid protein for evaluating structural integrity and infectivity of human norovirus." *Environmental Science & Technology* 44(2), 808-812.

Schafer, A.I., Fane, A.G. and Waite, T.D. (2001) "Cost factors and chemical pretreatment effects in the membrane filtration of waters containing natural organic matter." *Water Research* 35(6), 1509-1517.

Shen, C., Phanikumar, M.S., Fong, T.T., Aslam, I., McElmurry, S.P., Molloy, S.L. and Rose, J.B. (2008) "Evaluating bacteriophage P22 as a tracer in a complex surface water system: The Grand River, Michigan." *Environmental Science & Technology* 42(7), 2426-2431.

Shirasaki, N., Matsushita, T., Kobuke, M. and Ohno, K. (2009) "Comparison of removal performance of two surrogates for pathogenic waterborne viruses, bacteriophage Qβ and MS2, in a coagulation–ceramic microfiltration system " *Journal of Membrane Science* 326(2), 564-571.

Shirasaki, N., Matsushita, T., Matsui, Y. and Ohno, K. (2008) "Effects of reversible and irreversible membrane fouling on virus removal by a coagulation-microfiltration system." *Journal of Water Supply Research and Technology-Aqua* 57(7), 501-506.

Sigstam, T., Gannon, G., Cascella, M., Pecson, B.M., Wigginton, K.R. and Kohn, T. (2013) "Subtle differences in virus composition affect disinfection kinetics and mechanisms." *Applied and Environmental Microbiology* 79(11), 3455-3467.

Singer, P.C. and Reckhow, D.A. (1999) Chemical Oxidation. Water Quality and Treatment: A Handbook of Community Water Supplies., McGraw Hill, New York.

Sobsey, M.D., Fuji, T. and Hall, R.M. (1991) "Inactivation of cell-associated and dispersed Hepatitis-A virus in water." *Journal American Water Works Association* 83(11), 64-67.

Staehelin, J. and Hoigne, J. (1985) "Decomposition of ozone in water in the presence of organic solutes acting as promoters and inhibitors of radical chain reactions." *Environmental Science & Technology* 19(12), 1206-1213.

Stagg, C.H., Wallis, C. and Ward, C.H. (1977) "Inactivation of clay-associated bacteriophage MS2 by chorine." *Applied and Environmental Microbiology* 33(2), 385-391.

Stumm, W. and Morgan, J.J. (eds) (1996) Aquatic Chemistry, John Wiley & Sons, New York.

Tanneru, C.T. and Chellam, S. (2012) "Mechanisms of virus control during iron electrocoagulation - Microfiltration of surface water." *Water Research* 46(7), 2111-2120.

Tanneru, C.T., Rimer, J.D. and Chellam, S. (2013) "Sweep flocculation and adsorption of viruses on aluminum flocs during electrochemical treatment prior to surface water microfiltration." *Environmental Science & Technology* 47(9), 4612-4618.

Theis, T.L. and Singer, P.C. (1974) "Complexation of iron(II) by organic-matter and its effect on iron(II) oxygenation." *Environmental Science & Technology* 8(6), 569-573.

Thomas, E.L., Grisham, M.B. and Jefferson, M.M. (1986) "Preparation and characterization of chloramines." *Methods in enzymology* 132, 569-585.

Thurston-Enriquez, J.A., Haas, C.N., Jacangelo, J. and Gerba, C.P. (2003) "Chlorine inactivation of adenovirus type 40 and feline calicivirus." *Applied and Environmental Microbiology* 69(7), 3979-3985.

Timmes, T.C., Kim, H.-C. and Dempsey, B.A. (2010) "Electrocoagulation pretreatment of seawater prior to ultrafiltration: Pilot-scale applications for military water purification systems." *Desalination* 250(1), 6-13.

Urase, T., Yamamoto, K. and Ohgaki, S. (1996) "Effect of pore structure of membranes and module configuration on virus retention." *Journal of Membrane Science* 115(1), 21-29.

USEPA (2006) National Primary Drinking Water Regulations: Ground Water Rule; Final Rule, Federal Register,40 CFR Parts 9, 141, and 142, pp. 65574-65660.

van Voorthuizen, E.M., Ashbolt, N.J. and Schafer, A.I. (2001) "Role of hydrophobic and electrostatic interactions for initial enteric virus retention by MF membranes." *Journal of Membrane Science* 194(1), 69-79.

Vinckier, A., Gervasoni, P., Zaugg, F., Ziegler, U., Lindner, P., Groscurth, P., Pluckthun, A. and Semenza, G. (1998) "Atomic force microscopy detects changes in the interaction forces between GroEL and substrate proteins." *Biophysical Journal* 74(6), 3256-3263.

Wan, W., Pepping, T.J., Banerji, T., Chaudhari, S. and Giammar, D.E. (2011) "Effects of water chemistry on arsenic removal from drinking water by electrocoagulation." *Water Research* 45(1), 384-392.

White, G.C. (2010) White's handbook of chlorination and alternative disinfectants, John Wiley & Sons, Hoboken, N.J., .

White, M.C., Thompson, J.D., Harrington, G.W. and Singer, P.C. (1997) "Evaluating criteria for enhanced coagulation compliance." *Journal American Water Works Association* 89(5), 64-77.

Wigginton, K.R., Pecson, B.M., Sigstam, T., Bosshard, F. and Kohn, T. (2012) "Virus inactivation mechanisms: Impact of disinfectants on virus function and structural integrity." *Environmental Science & Technology* 46(21), 12069-12078.

Yan, M., Korshin, G.V. and Chang, H.-S. (2014) "Examination of disinfection by-product (DBP) formation in source waters: A study using log-transformed differential spectra." *Water Research* 50(0), 179-188.

Young, D.C. and Sharp, D.G. (1977) "Poliovirus aggregates and their survival in water." *Applied and Environmental Microbiology* 33(1), 168-177.

Zeman, L.J. and Zydney, A.L. (1996) Microfiltraction and ultrafiltraction: Principles and application, Dekker, New York.

Zhu, B.T., Clifford, D.A. and Chellam, S. (2005a) "Comparison of electrocoagulation and chemical coagulation pretreatment for enhanced virus removal using microfiltration membranes." *Water Research* 39(13), 3098-3108.

Zhu, B.T., Clifford, D.A. and Chellam, S. (2005b) "Virus removal by iron coagulation-microfiltration." *Water Research* 39(20), 5153-5161.

Appendix

A.1 Supporting information from chapter 3

Quality assurance.

All virus removal experiments were repeated at least two times. Additionally, approximately 25% of the associated measurements (e.g., zeta potential, floc dissolution, fluorescence quantitation, and adhesion force) at different coagulant dosages were repeated. Paired t-tests conducted on virus log removal values and AFM force curves from duplicate experiments showed no statistical differences at the 95% confidence level. Therefore, all laboratory protocols related to electro-and chemical coagulation, microfiltration, and virus enumeration were highly reproducible (see Figure 7.1A). In addition, water quality parameters (alkalinity, calcium and total hardness, pH, turbidity, DOC, UV_{254}, and conductivity) monitored over the entire duration of study showed coefficients of variation ≤ 5% allowing the quantitative comparison of experiments performed over the 9-month period of this study.

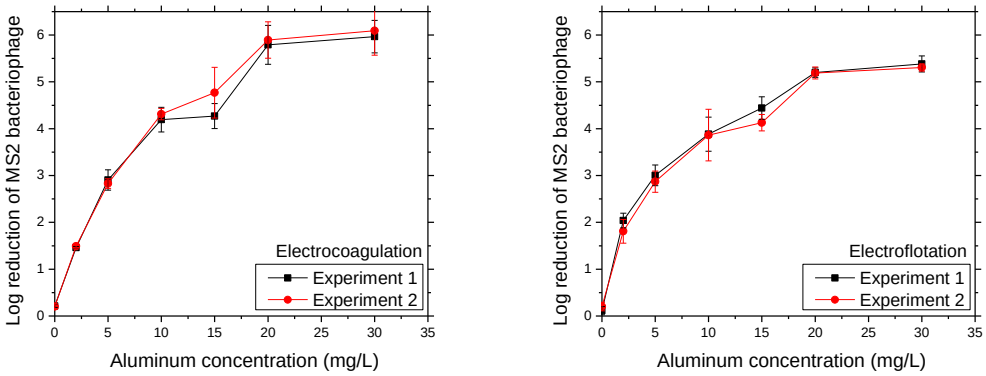

Figure 7.1A. Excellent reproducibility of virus removals from duplicate experiments at different aluminum dosages for electrocoagulation (left) and electroflotation (right) experiments.

Electrochemical treatment.

As shown in Figure 7.2A, electrochemical dissolution of aluminum generated Al^{3+} with nearly 100 % efficiency. Aluminum concentrations were measured by atomic absorption spectroscopy (Flame AA-Analyst 300, Perkin-Elmer) and compared with theoretical predictions

from Faraday's law ($m = \frac{26.98It}{zF}$), where *m* is dose of Al generated at a current I (0.25 A, ampere) for a stipulated time t (s), 26.98 $g.mol^{-1}$ is the atomic weight of Al, z (3 for Al) is number electrons transferred per Al atom, and F (96,486 C eq^{-1}) is Faraday's constant**.**

In our experiments, current density was maintained constant (20 mA/cm^2) and time was changed to generate required aluminum dosage. Lake Houston water (450 mL) spiked with MS2 (to obtain a feed concentration of $O(10^8)$ PFU/mL) at pH 6.4 was used for each experiment. During aluminum generation the electrochemical suspension was vigorously stirred in the cell to simulate rapid mixing and under open atmospheric conditions with dissolved oxygen content near saturation (~ 9 mg/L). The entire suspension was then slowly mixed for 2 minutes to facilitate flocculation. In electrocoagulation experiments, the entire electrochemically treated suspension was transferred to a feed tank to perform microfiltration. During electroflotation, the floating flocs were not sent to microfiltration by draining the treated water from the bottom of electrolysis cell. The 3-electron transfer is consistent with the electrochemical reactions listed below. Similarly, aluminum concentrations measured in jar tests were also very close to those calculated simply by dilution (data not shown). This demonstrates the accuracy of our stock concentration and dosing into respective jars.

Anode: $Al^0_{(S)} \rightarrow Al^{3+} + 3e^-$

Hydrolysis: $Al^{3+} + 3H_2O \rightarrow Al(OH)_{3(s)} + 3H^+$

Cathode: $3H_2O + 3e^- \rightarrow 3OH^- + 1.5\ H_2$

Overall reaction: $Al^0_{(S)} + 3H_2O \rightarrow Al(OH)_{3(s)} + 1.5\ H_2$

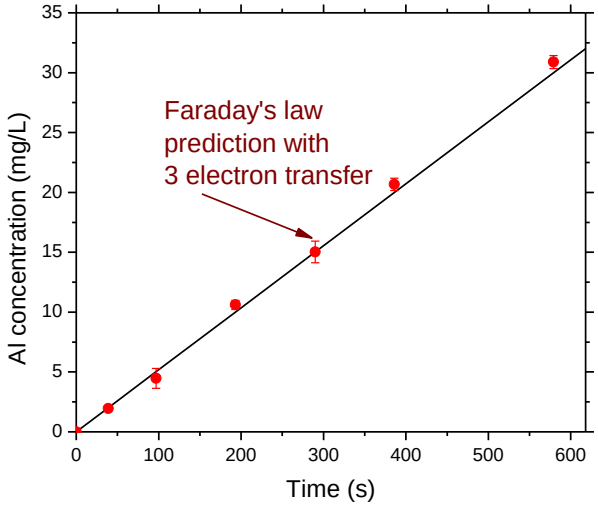

Figure 7.2A. Aluminum concentrations generated during electrochemical pretreatment measured by atomic absorption spectroscopy agree quantitatively with theoretical predictions with 3-electron transfer using Faraday's law.

MS2 propagation and enumeration.

MS2 (ATCC 15597-B1) and its host *Escherichia coli* (ATCC 15597) stocks were bought from American Type Culture Collection (ATCC). The double-top agar layer technique was used to propagate MS2 and the stock titer was expressed in terms of Plaque Forming Units/mL (PFU/mL). Overnight culture of *E. coli* grown in Tryptic Soy Broth (TSB; Difco) at 37 °C was batch transferred to fresh TSB and grown to a mid-log phase for 3-6 hours also at 37 °C. Serial dilutions of MS2 stock were performed in Phosphate Buffered Saline (PBS; composition 137 mM NaCl, 2.7 mM KCl, 4.3 mM $Na_2HPO_4.7H_2O$, and 1.4mM KH_2PO_4; pH 7.5). Quantities of 0.1 mL serially diluted stock and 0.9 mL *E. coli* suspension were mixed in ~3mL of 0.5% soft overlay agar and poured onto pre-solidified Trypticase Soy Agar petri dishes (TSA 1.5%, Difco). The plates were incubated at 37 °C for 24 h. Plaques numbering between 20-300 were counted and MS2 concentrations were determined.

Viruses were monodispersed after two successive PEG precipitations.

After two successive PEG purifications, MS2 size and monodispersity were quantitatively analyzed using dynamic light scattering (DLS, Brookhaven BI-200SM). As shown in the Figure 7.3A (left), the MS2 mean hydrodynamic diameter was 27 ± 3 nm. A polydispersity index (PDI) of 0.19 ± 0.08 was obtained from the second moment of diffusion coefficient distribution (method of cumulants). Near horizontal behavior (Figure 7.3A, right) obtained by plotting Γ/q^2 versus q^2 depicts the independence of diffusion coefficient on scattering angle. Low PDI and no rotational motion (inferred from the level Γ/q^2 vs q^2 plot) confirm that MS2 viruses were fairly monodispersed.

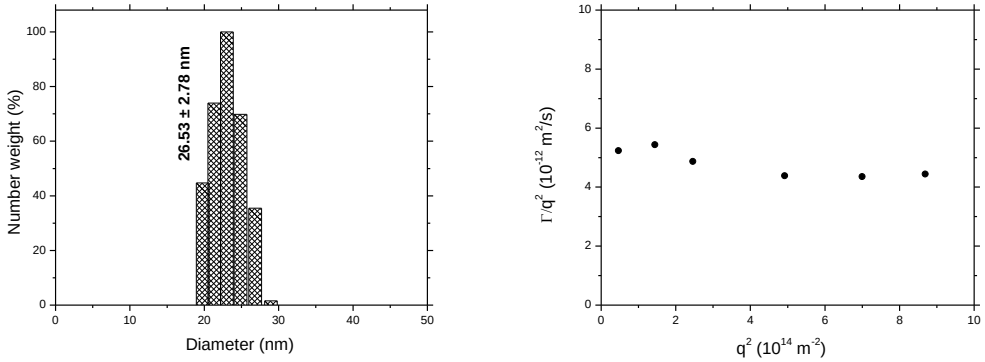

Figure 7.3A. (left) Number weighted size distribution of MS2 obtained by DLS at a scattering angle of 90° reveals a monodisperse population of particles. (Right) Plot of Γ/q2 vs q2 for MS2 revealed nearly horizontal behavior, which is indicative of monodispersity.

Negligible MS2 inactivation during electrochemical and chemical coagulation.

After selected experiments, coagulated suspensions were gently mixed (32 s^{-1}) to keep them suspended for an extended duration of 5h and sampled hourly. Flocs were separated by centrifugation (10,000 g for 20 minutes) and dissolved in 6% beef extract after elevating the pH to 9.5 using NaOH. Free and coagulated viruses in the feed water, corresponding to the respective supernatant and dissolved pellet in the previous step, were enumerated next. Figure 7.4A shows that total virus concentrations remained relatively constant over the entire period for a representative dosage of 10 mg/L. Therefore, unlike electrolysis using (i) iron, Cu/Pt, and

boron doped diamond electrodes, (ii) chemical addition of prehydrolyzed aluminum salts (eg: PACl), or (iii) Ferrous ion/zero valent iron, viruses were not inactivated by aluminum electrolysis and aluminum sulfate addition. As such, reductions in virus concentrations measured in our experiments (e.g., Figure 3.1) were solely due to *removal* and not *inactivation*. It is emphasized that our findings are consistent with concentration of viruses from water samples by removing them onto aluminum hydroxide precipitates without inactivation, which is the basis of Standard Method 9510 D.

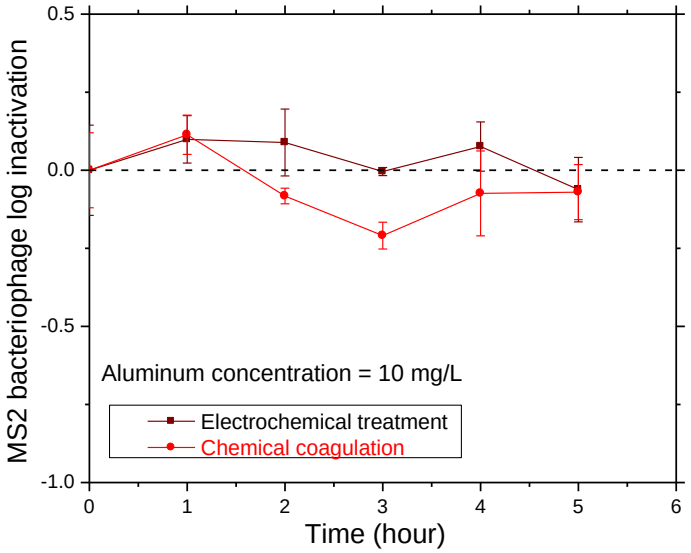

Figure 7.4A. Negligible inactivation of MS2 viruses was observed during both electrochemical (brown squares) and chemical coagulation (red circles) pretreatment.

AFM adhesion force measurements.

Adhesion forces were measured between MS2 virus coated AFM tips and the surfaces of aluminum precipitates generated (at different Al dosages) during pretreatment. Solid precipitates were concentrated by filtering the pretreated water using a 0.22 µm filter (i.e. the same type used for filtration experiments). The adhesion force was measured in a fluid cell using a solution with similar Al dose to ensure similar experimental interactions between virus (immobilized on the AFM tip) and the aluminum precipitate (substrate). The adhesion force was

calculated using Hooke's law, F = *Kd* where *K* is the calibrated cantilever spring constant and *d* is the maximum tip deflection obtained from the average of multiple pull-off curves.

Control experiments were performed to confirm the successful virus attachment to the tip. The average adhesion force was measured between electrochemically generated Al precipitates using a clean (unmodified) tip and AFM tips modified with silane (APTES). Representative pull-off curves from these experiments (Figure 7.5A a and b) show the force profiles measured upon the approach and retraction of AFM tips from a contacting surface. Measurements with the bare tip (Figure 7.5A a) resulted in single peaks (typical of nonspecific binding). Silane-coated tips showed primarily single peaks and a small population of pull-off curves exhibiting multiple peaks (as illustrated in Figure 7.5A b), which are most likely due to a minor fraction of APTES polymers on the tip surface. The number and frequency of multiple peaks in the force pull-off curves dramatically increased when AFM tips were covalently modified with virus (Figure 7.5A c). A negatively-charged PVDF membrane surface (0.22 µm Durapore, GVWP02500, Millipore) was used as substrate for these calibration tests. The average adhesion force between the negatively-charged membrane surface and the virus-coated AFM tip was ca. 70 pN (see the representative pull-off curve in Figure 7.5A d). These force curves also depict a repulsive profile upon tip approach to and retraction from the membrane surface. This general profile suggests purely electrostatic repulsive interactions between negatively-charged virus (AFM tip) and the negatively-charged membrane surface. It should also be noted that there are no hydrophobic interactions in these AFM force spectroscopy measurements since the membrane used was hydrophilic in nature. In a separate study, AFM tips were functionalized with MS2 virus that was labeled with FITC. The tip was imaged using a fluorescence microscope (Olympus BX 51) at 100x magnification after 250 ms exposure. The fluorescence image of the AFM tip in Figure 7.6A confirms virus immobilization on the cantilever surface.

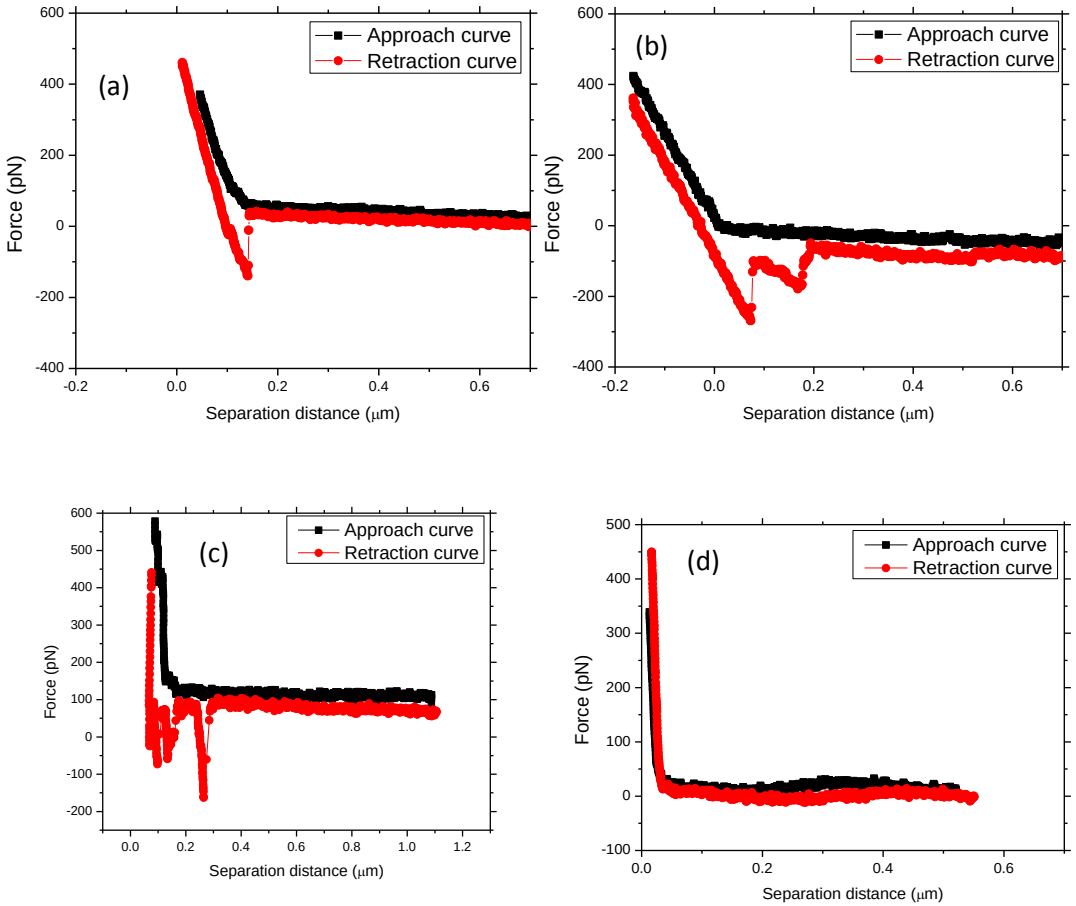

Figure 7.5A. Representative approach and retraction pull-off curves for AFM tips interacting with aluminum precipitate (a) bare tip, (b) silane modified tip (APTES), and (c) virus-coated tip. (d) Measurement of a virus-coated AFM tip with a hydrophilic membrane.

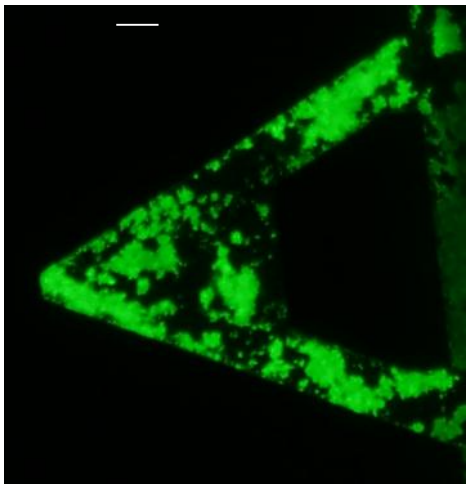

Figure 7.6A. Fluorescence image of an AFM tip modified with MS2 virus (labeled with FITC). The labeled virus was covalently immobilized on an APTES-functionalized silicon nitride AFM tip. The scale bar equals 10 µm.

Statistical distributions of the adhesion force between MS2-modified AFM tips and aluminum precipitates prepared using aluminum concentrations of 0, 5, 10, 30 mg/L are shown in Figure 7.7A. Histograms of experimental adhesion force data were fitted with a log-normal distribution using MATLAB.

Fits of the experimental data with the log-normal density function revealed that the adhesion force profile followed a log-normal distribution in many but not all cases. Table 7.1A reports the average adhesion force obtained from the experimental arithmetic mean compared to values calculated using the log-normal distribution. The adhesion force at each aluminum dose (shown in Figure 3.5f of the manuscript) is the average of all the individual forces within each histogram.

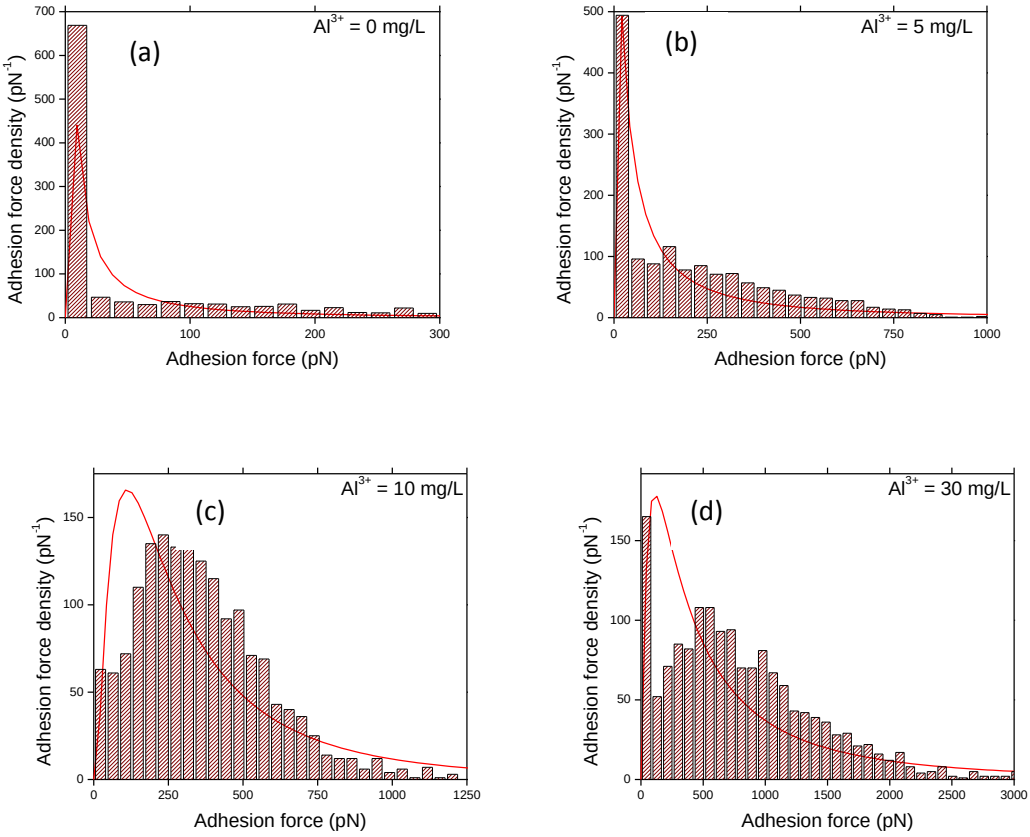

Figure 7.7A. Histograms of adhesion force profiles and fitted log-normal distributions for virus-coated AFM tips interacting with surfaces of Al precipitates that were prepared from solutions with (a) 0 mg/L, (b) 5 mg/L, (c) 10 mg/L, and (d) 30 mg/L Al dosage.

Table 7.1A. Average virus(tip)-aluminum precipitation adhesion force for solid precipitates prepared at varying Al dosage

Aluminum dosage (mg/L)	Average and standard deviation of adhesion force (pN)	
	Arithmetic mean	Log normal distribution
0	63±22	95±2
2	65±53	88±68
5	195±42	265±25
10	345±57	375±85
20	694±88	805±283
30	789±144	934±233

FITC-labeling did not change adhesion force between viruses and aluminum precipitates.

One control experiment was performed with AFM force spectroscopy to assess any possible effect of fluorescence labeling on the adhesion force between viruses and aluminum precipitates. In this experiment, an aluminum concentration of 10 mg/L was used and the average force of adhesion between AFM tips immobilized with FITC-tagged MS2 virus and the surface of aluminum precipitate was compared with those using untagged viruses. Figure 7.8A shows the average adhesion force data (using the arithmetic mean). As seen, FITC-tagged viruses and untagged viruses exhibited similar adhesion force. This result is qualitatively consistent with a previous report that FITC-tagged MS2 and untagged MS2 exhibited similar behavior during coagulation and media filtration. Also, the virus modified tips (both labeled and unlabeled viruses) interacted more strongly with the aluminum flocs suggesting APTES functionalization covalently bonded viruses.

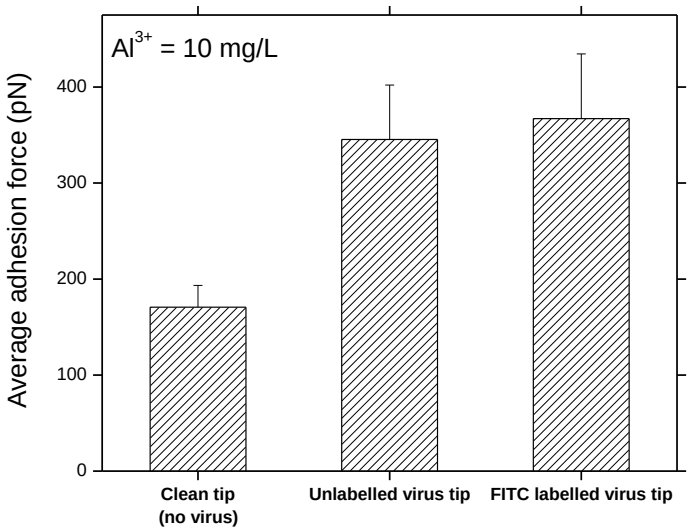

Figure 7.8A. Average adhesion force between aluminum precipitates and a clean Si3N4 AFM tip, a tip modified with unlabelled viruses, and a tip modified with FITC-labeled virus. Standard deviations correspond to two measurements (ca. 2500 pull-off curves).

Fluorescence microscopy.

Three controls experiments were performed to ensure efficient FITC conjugation with MS2 and to validate our tagging procedure. These experiments show that the entire fluorescence signal that has been collected by the detector is only due to the virus encapsulation in aluminum precipitates. All control experiments were performed with a preselected aluminum dose of 10 mg/L. These controls confirmed that all fluorescence signal in our experiments was obtained from FITC conjugated MS2 viruses encapsulated in the aluminum solid precipitates. It is also noted that in all of our experiments some inherent low fluorescence.

An experiment was performed without adding any tagged viruses to source water. Flocs were generated through electrochemical treatment at 10 mg/L Al. Figure 7.9A shows detectable but negligible fluorescence signal from flocs even in the absence of any tagged viruses.

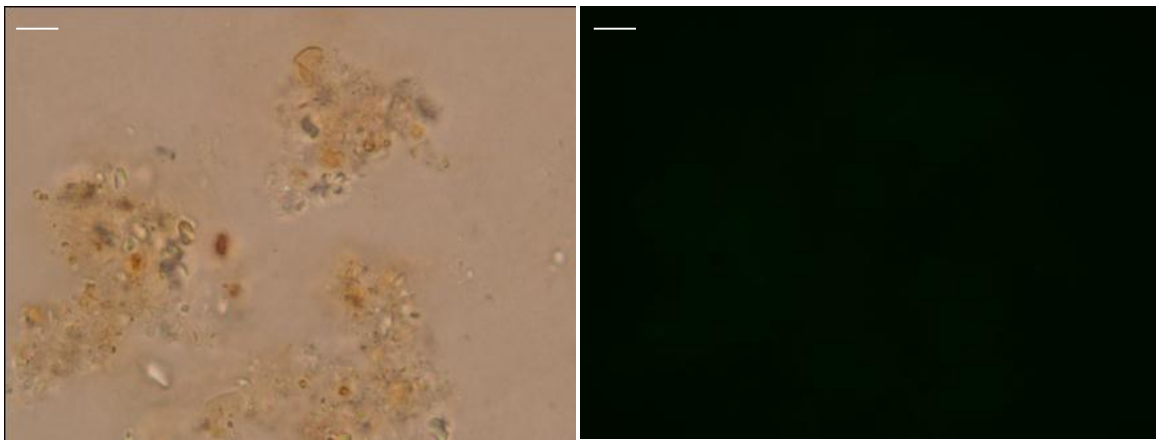

Figure 7.9A. Electrochemical treatment at 10 mg/L aluminum with unlabeled viruses.

A second control experiment was performed by adding the free dye to electrocoagulation treatment at 10 mg/L Al. FITC was added to the dialysis bag without any viruses and the free dye was obtained at the end of the dialysis procedure. This control experiment was performed to determine whether any of the free dye remaining in the dialysis bag was captured by Al precipitates. As seen in Figure 7.10A, there was virtually no (or significantly weak) signal, which suggests that the free dye was not captured by the precipitates.

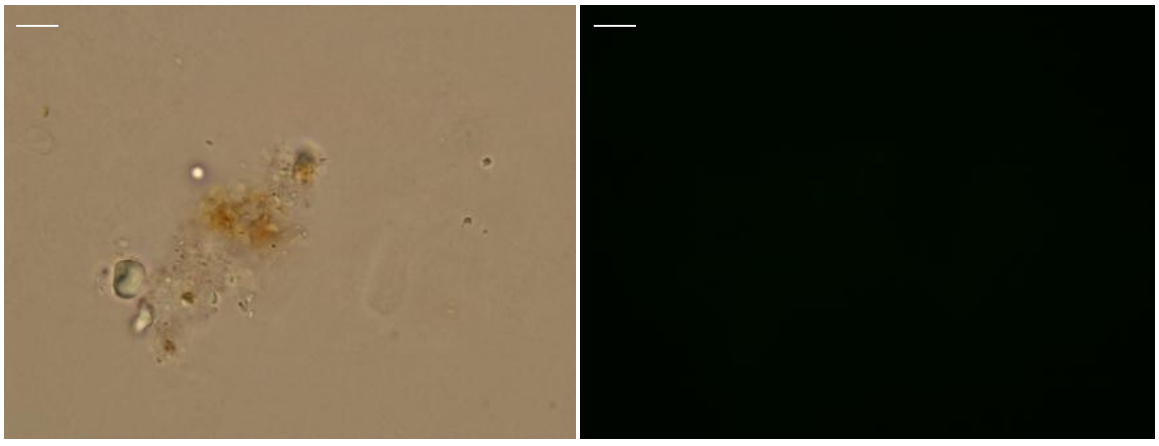

Figure 7.10A. Electrochemical treatment with free FITC dye alone at 10 mg/L aluminum.

To ensure that nearly all the FITC was conjugated to MS2 and that the free dye concentration in the suspension was negligible, two successive PEG precipitations were performed with the end product of dialysis. All the tagged viruses were concentrated in the precipitates and most of the free dye was removed through supernatant. Electrochemical

pretreatment performed with the supernatant from second PEG precipitation in Figure 7.11A resulted in low fluorescence signal. This demonstrates that there were negligible amounts of free dye in the supernatant.

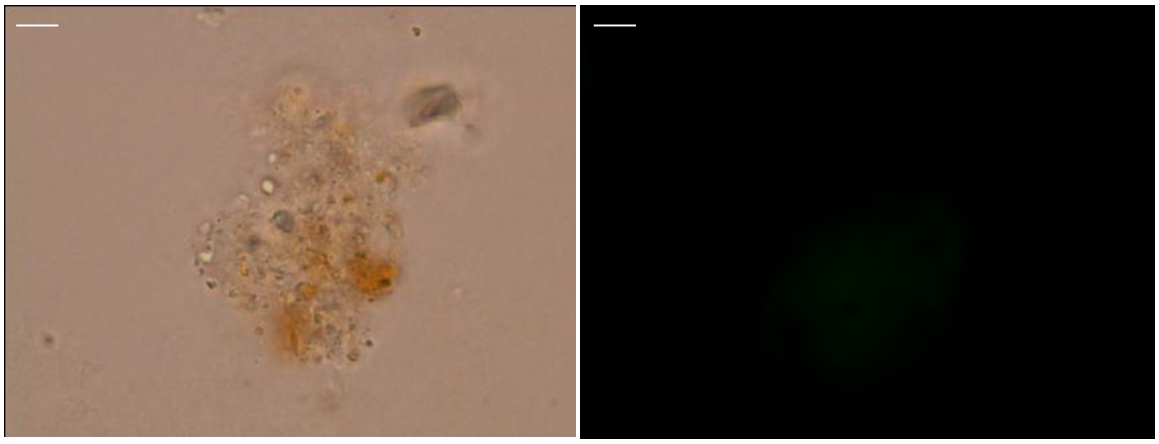

Figure 7.11A. Electrochemical treatment with PEG supernatant alone at 10 mg/L aluminum.

Virus removals obtained in Figure 3.1 of the main manuscript were semi-quantitatively compared with these fluorescence images. Average fluorescence intensity over the entire imaged area was obtained (using Image J) for each fluorescence image and for all samples at different dosages. As shown in the Figure 7.12A, the increasing fluorescence intensity can be quantitatively compared with the removal of MS2 viruses since it monotonically increased with increased aluminum dosage. Hence, fluorescence measurements quantitatively show that virus capture was higher when more and more aluminum was precipitated.

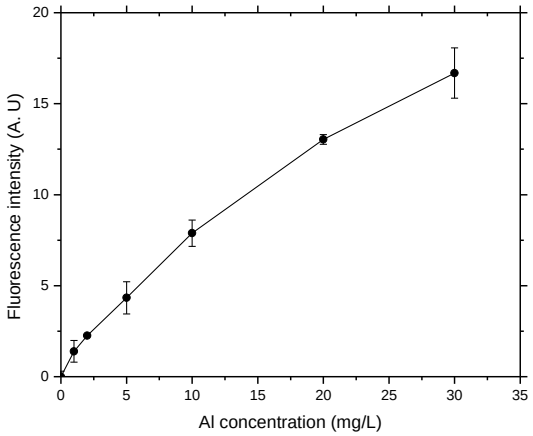

Figure 7.12A. Fluorescence intensity of labeled viruses captured over a range of aluminum dosages.

Complete set of fluorescence images.

The entire set of microscope images for aluminum concentrations in the range 0 – 30 mg/L are shown below in Figure 7.13A. As described in the main text of the manuscript, this demonstrates increasing virus capture with aluminum electrocoagulant dosage

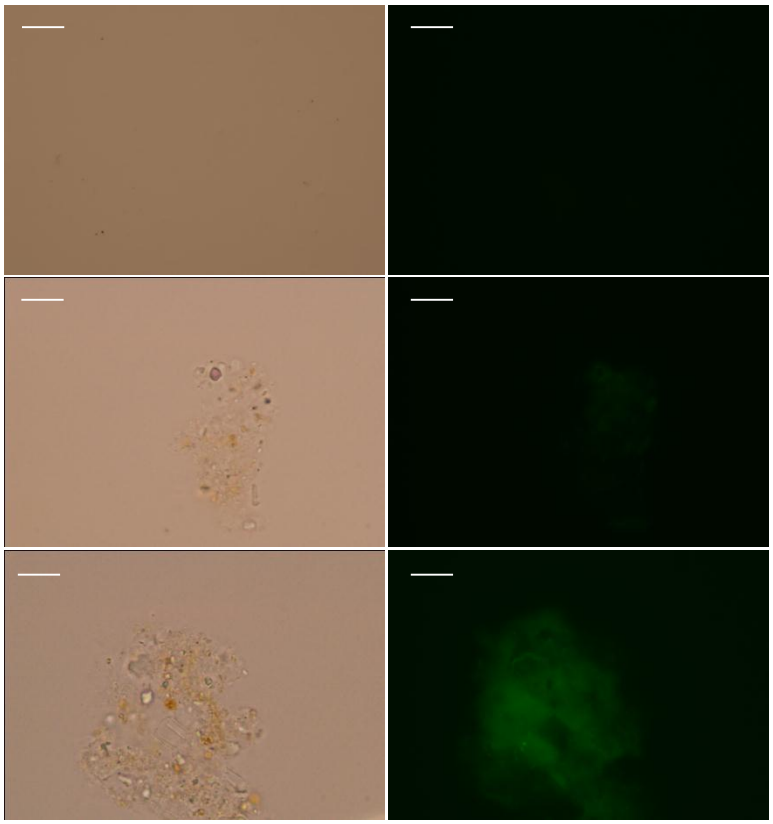

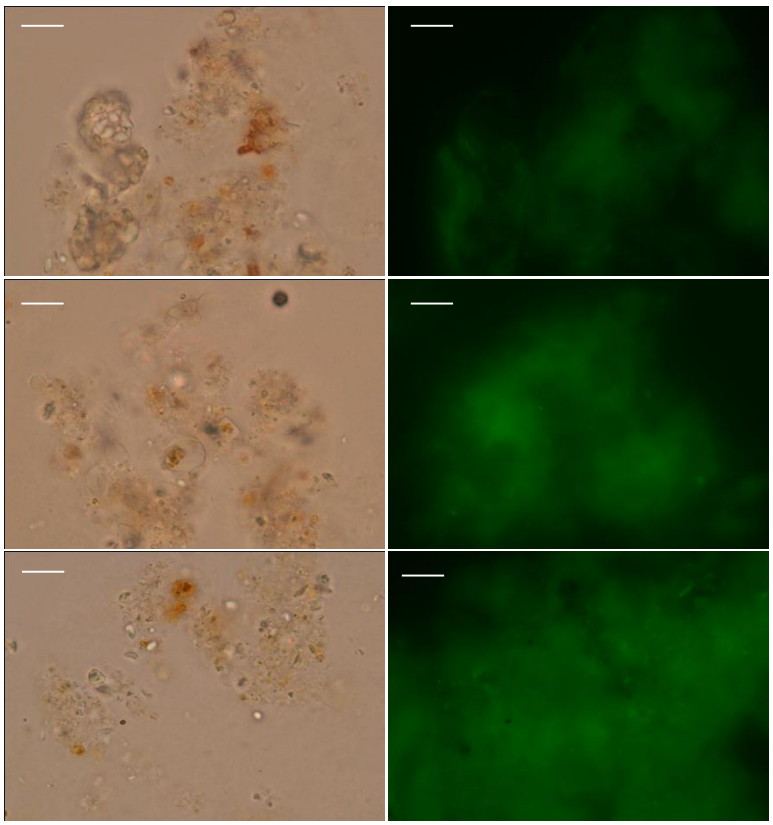

Figure 7.13A. Bright field (left column) and epifluorescence images (right column) of flocs incorporating FITC tagged viruses. Electrocoagulant dosages from top to bottom are 0, 2, 5, 10, 20, and 30 mg/L Al, respectively. The scale bar equals 10 µm.

A.2 Supporting information for chapter 4

Electrochemical treatment.

As shown in Figure 7.14A, electrochemical dissolution of aluminum generated Al^{3+} with nearly 100% efficiency. Aluminum concentrations were measured by atomic absorption spectroscopy (Flame AA-Analyst 300, Perkin-Elmer) and compared with theoretical predictions from Faraday's law ($m = \frac{26.98It}{zF}$), where *m* is dose of Al generated at a current I (0.25 A, ampere) for a stipulated time t (s), 26.98 $g.mol^{-1}$ is the atomic weight of Al, z (3 for Al) is number electrons transferred per Al atom, and F (96,486 C eq^{-1}) is Faraday's constant.

In our experiments, current density was maintained constant (20 mA/cm^2) and time was changed to generate required aluminum dosage. Lake Houston water (450 mL) spiked with MS2 (to obtain a feed concentration of $O(10^8)$ PFU/mL) at pH 6.4 was used for each experiment. During aluminum generation the electrochemical suspension was vigorously stirred in the cell to simulate rapid mixing. The entire suspension was then slowly mixed for 5h to facilitate flocculation. The 3-electron transfer is consistent with the electrochemical reactions listed below. This demonstrates the accuracy of our stock concentration and dosing into respective jars.

Anode: $Al^0_{(S)} \rightarrow Al^{3+} + 3e^-$

Hydrolysis: $Al^{3+} + 3H_2O \rightarrow Al(OH)_{3\,(s)} + 3H^+$

Cathode: $3H_2O + 3e^- \rightarrow 3OH^- + 1.5\,H_2$

Overall reaction: $Al^0_{(S)} + 3H_2O \rightarrow Al(OH)_{3\,(s)} + 1.5\,H_2$

Above reactions are also accompanied by oxidation of chloride ions to generate free chlorine species

$2Cl^- \rightarrow Cl_2 + 2e^-$

$Cl_2 + H_2O \rightarrow HOCl + H^+Cl^-$

$HOCl \rightarrow H^+ + OCl^-$

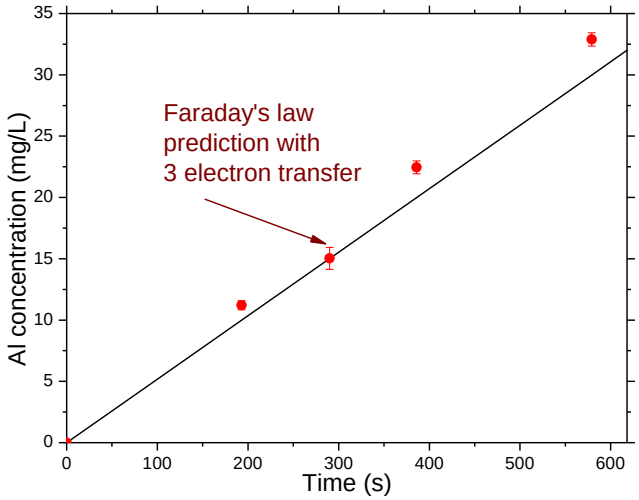

Figure 7.14A. Aluminum concentrations generated during electrochemical pretreatment measured by atomic absorption spectroscopy agree quantitatively with theoretical predictions with 3-electron transfer using Faraday's law.

MS2 propagation and enumeration.

MS2 (ATCC 15597-B1) and its host *Escherichia coli* (ATCC 15597) stocks were bought from American Type Culture Collection (ATCC). The double-top agar layer technique was used to propagate MS2 and the stock titer was expressed in terms of Plaque Forming Units/mL (PFU/mL). Overnight culture of *E. coli* grown in Tryptic Soy Broth (TSB; Difco) at 37 °C was batch transferred to fresh TSB and grown to a mid-log phase for 3-6 hours also at 37 °C. Serial dilutions of MS2 stock were performed in model NaCl saline solutions (100 mM). Quantities of 0.1 mL serially diluted stock and 0.9 mL *E. coli* suspension were mixed in ~3mL of 0.5% soft overlay agar and poured onto pre-solidified Trypticase Soy Agar petri dishes (TSA 1.5%, Difco). The plates were incubated at 37 °C for 24 h. Plaques numbering between 20-300 were counted and MS2 concentrations were determined.

Quality control.

All virus reduction (inactivation/removal) experiments were repeated at least two times. Additionally, approximately 25% of the associated measurements (e.g. zeta potential, floc dissolution, ATR-FTIR, q-RT-PCR) at different coagulant dosages were repeated.

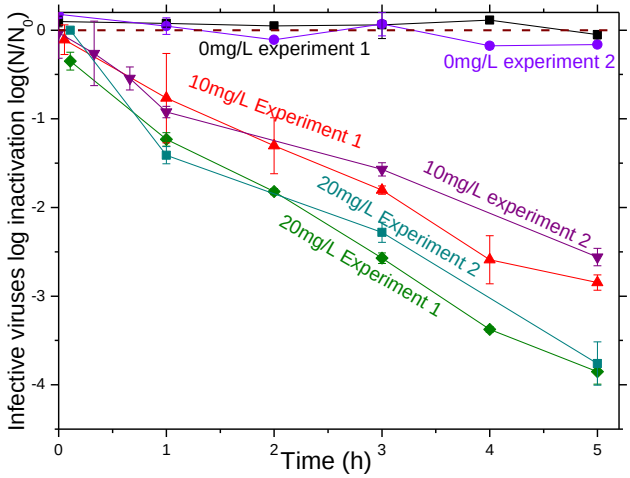

Figure 7.15A. Excellent reproducibility of virus removals from duplicate experiments at different aluminum dosages for electrocoagulation.

Virus reductions at pH 8.2.

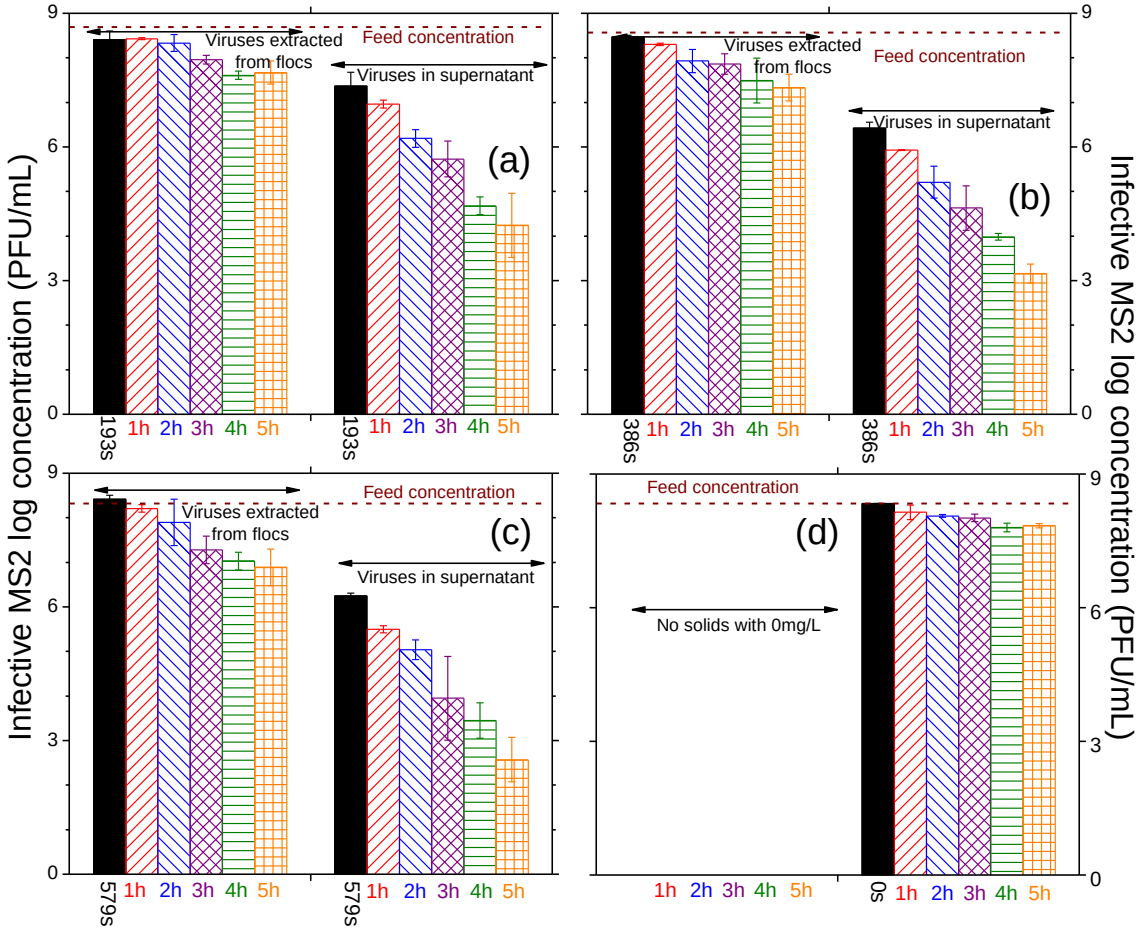

Figure 7.16A. Infective viruses extracted from the flocs and supernatant after centrifugation at different aluminum dosages after electrolysis; (a) 10mg/L (b) 20mg/L (c) 30mg/L (d) no electrolysis (0mg/L). The error bars correspond to standard deviation.

Effect of ionic strength on virus inactivation.

To probe further into effect of chlorine generation on virus inactivation, few experiments were performed at varying NaCl concentrations. As seen Figure 7.17A, virus inactivation increased when the NaCl concentration is increased suggesting that higher chlorine concentrations further inactivated viruses over a period of 5h.

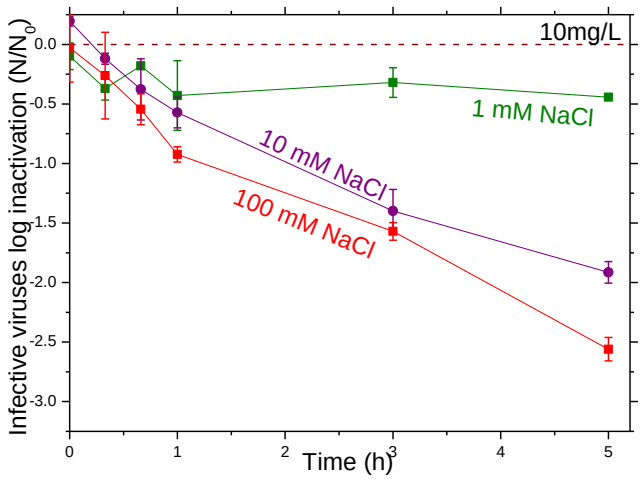

Figure 7.17A. Effect of ionic strength on virus inactivation. Electrolysis was performed at 10mg/L aluminum concentration and at different NaCl concentrations.

Electrophoretic mobility measurements

An electrophoretic light scattering technique (Nicomp 380 ZLS, Particle Sizing Systems, Santa Barbara, CA) was used to measure the electrophoretic mobility of colloids in coagulated suspensions. A He-Ne laser of 632.8 nm wavelength, 0.4 cm electrode spacing, and 4 V/cm field strength were employed for all measurements. The Smoluchowski equation was used to convert electrophoretic mobility to zeta potential. Each sample was run in triplicate each for 180 s duration. Progressive charge neutralization with increasing Al dosage was consistent with adsorption of $Al(OH)_2^+$, the predominant hydrolysis product at pH 6.2 and $Al(OH)_4^-$ at pH 8.2 during our experiments. As seen in Figure 7.18A the ζ potential (or approximate surface charge) of viruses and flocs effectively approached 0 near 10 mg/L limited restabilization was observed even when more aluminum was electrolyzed.

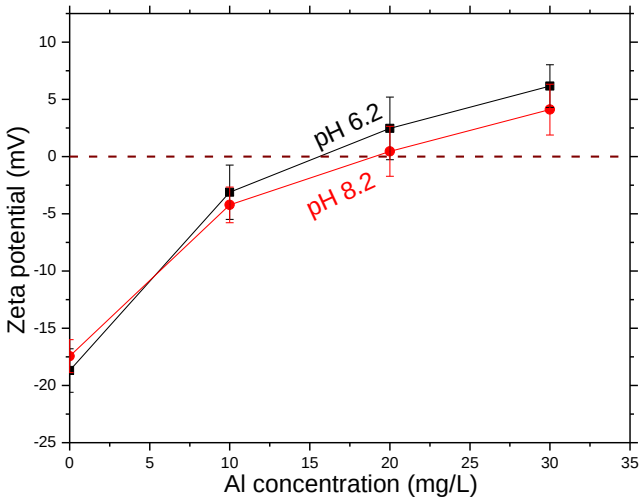

Figure 7.18A. Progressive neutralization of MS2 surface charge (ζ potential → 0) with aluminum addition.

Microscopy.

Scanning electron micrographs (SEM) of the clean (new) and used aluminum rod (after experiments) were obtained using field emission scanning electron microscope (LEO 1525, Carl Zeiss). Also, Following electrolysis of saline water samples spiked with viruses, 25 µL of suspension was placed on a glass slide and imaged (Olympus BX51) at 100x magnification. Flocs ($Al(OH)_{3(s)}$) generated during electrolysis were visually observed.

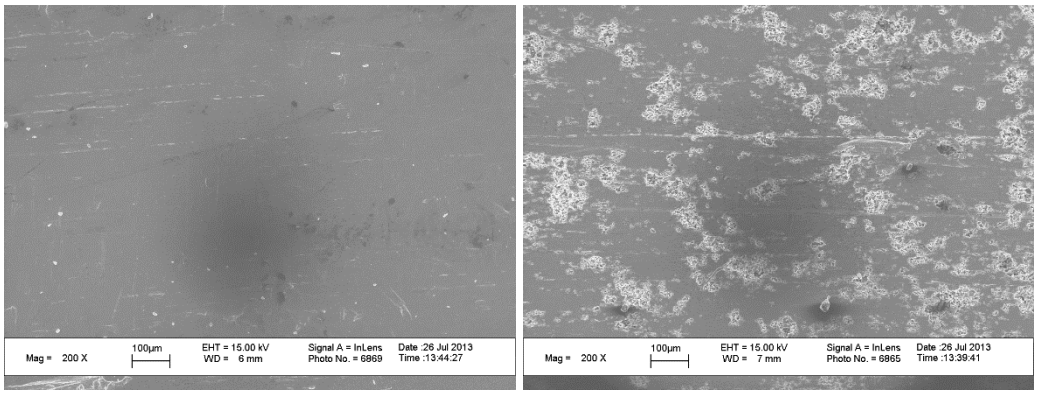

Figure 7.19A. Scanning electron micrographs of clean (unused) and used aluminum rod. Scale bar printed in the micrograph represents 100µm.

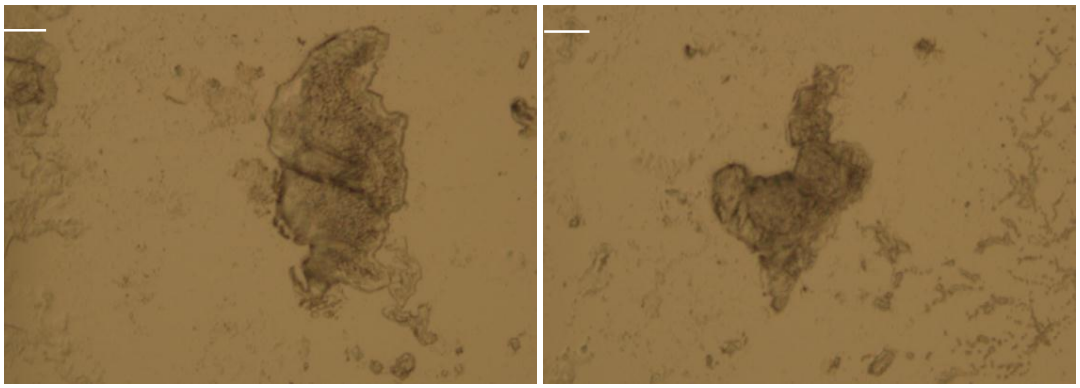

Figure 7.20A. Phase contrast images of $Al(OH)_{3(s)}$ flocs generated during electrolysis. Scale bar represents 10µm.

ATR-FTIR peak assignments.

Table 7.2A. Infrared frequencies and associated band assignments for MS2 virus

Wave number (cm^{-1})	Contributer
1750-1733	C=O carbonyl groups, aldehydes
1710	Glu, ν(C=O)
1690-1680	Turns and bends
1680-1660	Higher frequency of βstructure
1666-1659	'3-turn' helix
1657-1648	α-helix
1650-1645	Random coil
1640-1630	Intramolecular β-structure
1625-1610	Intermolecular β-structure
1610-1600	Amino acid side chain
1580	Gln
1573	HisH, ν(C=C); Asp, νas(COO-)
1550-1510	N-H, secondary amide,aldehydes, ketones, nitrile
1504	C=C, aromatic

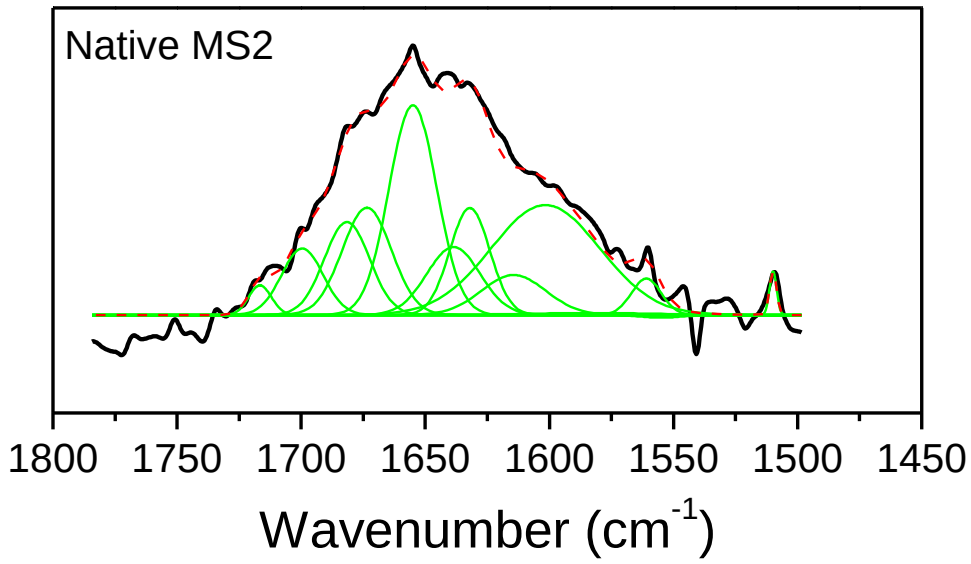

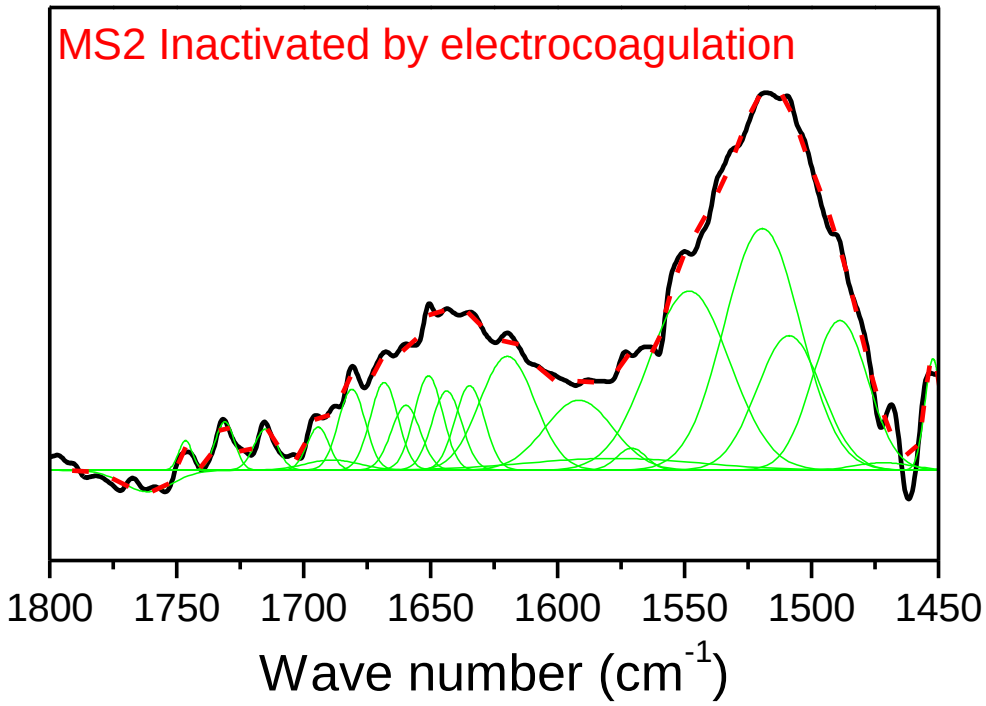

Figure 7.21A. Representative peak fits for of native and inactivated MS2 virus in the mid-infra region depicting protein secondary structures.

Table 7.3A. CT $_{99.99}$ values from various literature reports

Water/Buffer	Experimental pH	Temperature	$CT_{99.99}$	Cl concentration (mg/L)
ODF buffer	7.2	5 and 20 ° C	0.688 and 0.258	0.174
CDF buffer	6	5	0.333	1
Dilution buffer	7.4	Not mentioned Room temperature	1	1
ODF buffer	7	Room temperature	0.9	0.6
Phosphate buffer	6.5	7	0.4	0.28
CDF (Qβ)	6	5 15 25 35	0.666 0.333 0.25 0.166	0.5
100 mM Nacl 10 mM $NaHCO_3$	6.3	Room temperature	**0.822**	**0.052**